Journal of
Materials Chemistry C

REVIEW

View Article Online
View Journal | View Issue

Published on 14 April 2016. Downloaded by Fail Open on 7/23/2025 9:06:09 AM.

Cite this: J. Mater. Chem. C, 2016, 4, 5154

Received 10th February 2016,
Accepted 14th April 2016

DOI: 10.1039/c6tc00605a

www.rsc.org/MaterialsC

Optical chemosensors for water sample analysis

Hemant Sharma,[a] Navneet Kaur,[b] Amanpreet Singh,[a] Anil Kuwar*[c] and Narinder Singh*[a]

Molecular recognition is an emerging field of Supramolecular Chemistry. The major challenge for supramolecular chemists is detection in an aqueous medium. However, most biological and environmental processes happen in an aqueous medium; therefore, chemosensors that can operate in water are highly demanded. This review mainly focuses on the recognition of analytes (metal, anion and biomolecules) in an aqueous medium (≥90% water) and demonstrates that sensing in an aqueous medium can be achieved without compromising the selectivity and sensitivity. The detail discussion on the design of chemosensors and the mechanism of action for detection of metal ions, anions and biomolecules in an aqueous medium has been provided, reported in the period of 2001–2015.

1. Introduction

Sensors are generally understood to be devices that detect or measure a physical or chemical property and record, indicate or otherwise respond to it.[1] A chemical sensor achieves this goal by responding to particular analytes and converting the chemical stimuli into a signal which can be measured or recorded.[2] The chemosensors bind to particular guest analytes through non-covalent interactions, so called host–guest chemistry or supramolecular chemistry. Generally, a chemical sensor has three parts: a receptor, a signal transducer and a read-out mechanism as shown in Fig. 1.

The receptor is a moiety that interacts directly with the analyte and capable to converting the changes in the chemical composition of the molecular environment into a change in the physical or chemical properties like a change in the electron distribution energy of frontier orbitals, redox potential *etc.*[3] The key feature of a receptor is selectivity so that it interacts/binds with a particular analyte irrespective to other interfering molecules. The transducer transforms and amplifies the chemical changes into an observable analytical signal output like a change in the optical signal, electrochemical behavior or something else.[3] The read-out moiety is responsible for reporting the recognition event and processing the signal from the transducer.[4]

1.1 Need for chemosensors

Metal ions/anions/biomolecules play a significant role in various biological and environmental processes.[5–8] Calcium is one of the main constituent in building strong bones and teeth.[9,10] It also

[a] Department of Chemistry, Indian Institute of Technology Ropar (IIT Ropar), Rupnagar, Punjab, 140001, India. E-mail: nsingh@iitrpr.ac.in
[b] Department of Chemistry, Panjab University, Chandigarh, 160014, India
[c] School of Chemical Sciences, North Maharashtra University, Jalgaon, India. E-mail: kuwaras@gmail.com

Hemant Sharma

Dr Hemant Sharma was born in Punjab, India in 1985. He completed his PhD in 2015 with Dr Narinder Singh at the Indian Institute of Technology, Ropar. Currently, he is working as a Postdoctoral Fellow at the University of Sherbrooke. His area of research includes the study of photophysical, electrochemical and biological applications of imine linked and nanoparticle based receptors in aqueous medium and biosensors.

Navneet Kaur

Dr Navneet Kaur received her PhD from the National Institute of Pharmaceutical Education and Research (NIPER) Mohali. Currently, she is an Associate Professor of Nanoscience & Nanotechnology at Panjab University, Chandigarh. Her research interests include Medicinal and Materials Chemistry. She has published more than 70 research papers in reputed international journals.

This journal is © The Royal Society of Chemistry 2016

Published on 14 April 2016. Downloaded by Fail Open on 7/23/2025 9:06:09 AM.

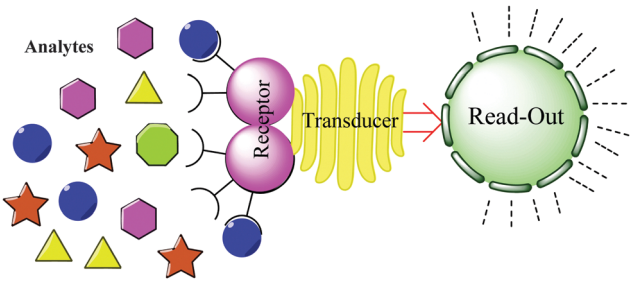

Fig. 1 A cartoon representation of molecular recognition.

helps to quell muscle cramps and initiate several reactions in the human body.[11] Likewise, Zn^{2+}, Ca^{2+} and Mg^{2+} prevent cytotoxicity and antagonize Cd-induced carcinogenesis *in vivo*.[12] Iron deficiency is common in cancer patients;[13] abnormality in K^{+} level leads to hypertension, stroke and seizures.[14] Deficiency of Cr^{3+} causes diabetes and cardiovascular diseases and an excess intake of Cr^{3+} leads to genotoxic effects.[15] More than 70% of our body's iron is found in hemoglobin and myoglobin, essential for transporting oxygen in the human body.[16] The ferrous/ferric couple (Fe^{2+}/Fe^{3+}) is an important redox couple involved in electron transport in the respiratory chain system.[17,18] Co^{2+} is an integral part of vitamin B_{12} and abnormality in Co^{2+} levels can lead to heart attacks, thyroid enlargement, anaemia *etc.*[19–21] Furthermore, Hg^{2+}, Cd^{2+}, Pb^{2+}, As^{2+} and Al^{3+} are most toxic metals that lack any involvement in physiological processes or beneficial effects. Accumulation of these metal ions in the human body can lead to serious disorders.[6,22–24]

Selective recognition of anions/biomolecules with artificial receptors has gained considerable attention over the past few years due to their vital role in biological systems.[25–28] Anions play a significant role in several biological processes like pyrophosphate ($P_2O_7^{4-}$, PPi) and adenosine triphosphate (ATP) is involved in energy transduction in organisms and controls metabolic processes by participating in enzymatic reactions.[29,30] Several biological processes such as DNA polymerization and the synthesis of cyclic adenosine monophosphate (AMP) require ATP hydrolysis with the concomitant release of PPi.[31] The iodide anion actively participates in many neurological activities and thyroid functions. Its deficiency causes physiological disorders, which leads to growth and maturation of the organ system.[32] Chloride anions regulate many cellular processes like membrane potential, neurotransmission, cell volume *etc.*[33–35] Moreover, some toxic anions like cyanide bind heme proteins and inhibit the terminal respiratory chain enzyme cytochrome *c* oxidase, which leads to fatal consequences.[36–38] Therefore, the recognition and sensing of these analytes in aqueous medium is an essential and challenging goal for the scientific community.

Several techniques like high-performance liquid chromatography, inductively coupled plasma atomic emission spectrometry, mass spectrometry and atomic absorption spectrometry have been developed to achieve sensing. However, these techniques are laborious, require several hours for detection, a pretreatment of the samples, sophisticated machinery and state-of-the-art clean room facilities for analysis. Fluorogenic chemosensors are a better and preferable approach for the recognition and sensing of these analytes because they offer a low detection limit, high selectivity and sensitivity, small response time and on-site detection.[39,40]

Amanpreet Singh

Amanpreet Singh is currently a PhD student with Dr Narinder Singh at the Indian Institute of Technology, Ropar, India. He has completed his master from the Dr B. R. Ambedkar National Institute of Technology, Jalandhar, India. His current main research is the design of fluorescent probes for biomolecules.

Anil Kuwar

Dr Anil S. Kuwar is currently working as an Assistant Professor at North Maharashtra University, Jalgaon, India. He has completed his PhD from North Maharashtra University. He has completed his postdoctoral research in Sunchon National University, Sunchon, South Korea and University of Utsunomiya, Utsunomiya, Japan (three years). His current main research is supramolecular chemistry, organic light emitting diode and bioinorganic chemistry.

Narinder Singh

Dr Narinder Singh obtained his PhD degree from Guru Nanak Dev University, Amritsar. After spending 3 years as a Postdoctoral fellow, he joined the Indian Institute of Technology, Ropar (IIT Ropar) as an Assistant Professor of Inorganic Chemistry. Currently, he is working as an Associate Professor, Chemistry Department of Indian Institute of Technology, Ropar. He has published more than 150 research papers in international peer reviewed journals. His area of research includes supramolecular and Materials Chemistry.

Published on 14 April 2016. Downloaded by Fail Open on 7/23/2025 9:06:09 AM.

1.2 Guidelines for chemosensors

The design of the receptor or binding site is an essential step for the development of chemosensors. Chemosensors are synthesized according to requirements like anion chemosensors that have binding sites or receptors enriched with N–H or O–H groups for hydrogen binding. Therefore, anion chemosensors must have moiety which can participate in H-bonding, such as amides, pyrrole, urea, thiourea, squaramide *etc.*[41] However, the detection of anions under aqueous conditions is a challenging task because water molecules give a tough competition to anions for binding sites.[42] Receptors based on H-bonding are not suitable under aqueous conditions. To achieve this target, metal complex based receptors have been employed. Two different strategies have been employed under this scheme. These two strategies are a metal displacement approach and electrostatic interaction between the metal complex and the anion. In the metal displacement approach, the anion binds to the metal complex through the metal atom and simultaneously the interaction between the metal atom and the compound is weakened. The metal atom came out from the coordination sphere of the complex and forms a new complex with the anion. As a consequence of this, the optical properties of the complex have been changed and a shift in the signals was observed. In another approach, the anion binds to the metal complex through electrostatic interactions between the anion and the metal. The metal atom remains in the complex, but this interaction changes the flow of the electron in the complex, which results in a shift in the spectra upon binding the anion. Recently, nanoparticle based anion chemosensors have been reported.[43–45] For detection, nanoparticles are coated with different capping agents (citrate, melamine and heptadentate macrocyclic Eu(III) cyclen) and these nanoparticles showed aggregation and disaggregation in the presence of a particular anion, which in turn change in color or fluorescence. In this review, all above mentioned strategies for the detection of anions in aqueous conditions have been discussed with suitable examples, which will be helpful to increase the selectivity and sensitivity of chemosensors.

In case of cation/metal ion chemosensors, the analyte binds to the receptor through electrostatic interactions.[46] Therefore, the receptor contains electron donating groups that are commonly employed in the design of metal detecting chemosensors. Mostly receptors enriched with O, N and S atoms are used. Metal ions have vacant orbitals and accept the electron density from the electron donating groups. This interaction changes the electronic structure of the molecule, which leads to a change in the intensity or wavelength of the absorption or emission spectra. In some cases, the binding of the metal ion caused irreversible change in the structure of the chemosensor, so called chemodosimeter. This change in the structure can alter the distance between the donor and acceptor, which results in a change in the photophysical properties of the molecule. Several clever approaches have been invested to design platforms for the detection of metal ions in aqueous medium. For example, polymers, small organic fluorophores, gels, material surfaces (quantum dots, glass or gold surfaces, and carbon nanotubes) and mesoporous materials are commonly employed. The most important point for detection in aqueous medium is the solubility of the chemosensor. A sensor should not be precipitated or aggregated in aqueous medium. Therefore, a sensor must have more electronegative groups for H-bonding with water molecules. It makes a molecule more hydrophilic. Moreover, nanoparticle- and aptamer-based chemosensors were investigated for the detection of metal ions under aqueous conditions. However, fluorescent organic nanoparticles (FONPs), due to their diverse molecular structures and optical properties, have become the subject of ever-increasing attention in recent years. The molecule selection is a crucial step for the formation of FONPs. All above techniques and designs will be discussed in this review with suitable examples. Moreover, there are some general parameters for a chemosensor. To be an effective chemosensor, it has to satisfy the following parameters.

1.2.1 Sensitivity. The sensor should be sensitive to a particular analyte. A small change in the concentration of the analyte should produce a huge change in the photophysical properties. The sensitivity depends upon the origination of the binding sites or receptors. A better organized binding site has good sensitivity. The influence of environmental interferences on sensitivity should be negligible. Swager and coworkers developed an approach to enhance the selectivity of chemosensors.[47,48] In this approach, chemosensors are wired in single series, which results into signal amplification compared to a single molecule (Scheme 1a).

This approach is known as the ''molecular wire effect''. These molecular wires or conducting polymers are conductive upon oxidation or reduction, and otherwise act as insulators in the neutral state. The conjugated polymers have a natural tendency to transmit the energy over longer distances. The main advantage of conjugated polymers over small molecules is the sensitivity to minor concentrations of analyte. The concept of conjugated polymers as chemosensors was further developed by the Huang and Kaner research group.[49–52] They developed various ultra-sensitive highly selective chemosensors through oxidative oligomerization. For example, oligofluoranthene (OFA) was synthesized through one-step chemical oxidative oligomerization of fluoranthene in nitromethane using $FeCl_3$ (oxidant).[50] The OFA structure prevents self-quenching, which results in enhanced fluorescence emission and maximum quenching amplification (Scheme 1b). OFA showed high selectivity for Fe^{3+} ion even under real environmental conditions. Using the same synthetic strategy, oligotriphenylene nanofibers were prepared from triphenylene monomers (Scheme 1c). These nanofibers have good thermal stability, high fluorescence quantum yield and stable fluorescence. Moreover, these blue light emitting nanofibers have selectivity for nitro based explosives like nitromethane, nitrobenzene and 2,4,6-trinitrophenol as well as the Fe^{3+} ion.[49]

Another fluorescent conjugated polymer, polyfluoranthene, was synthesized *via* interfacial chemical oxidative polymerization in a dynamic interface between *n*-hexane and nitromethane containing fluoranthene and $FeCl_3$.[51] The fluorescent polymer detected Fe^{3+} ions through π-conjugated electrons, and acts as both the fluorophore and receptor units (Scheme 1d). Furthermore,

 This journal is © The Royal Society of Chemistry 2016

Published on 14 April 2016. Downloaded by Fail Open on 7/23/2025 9:06:09 AM.

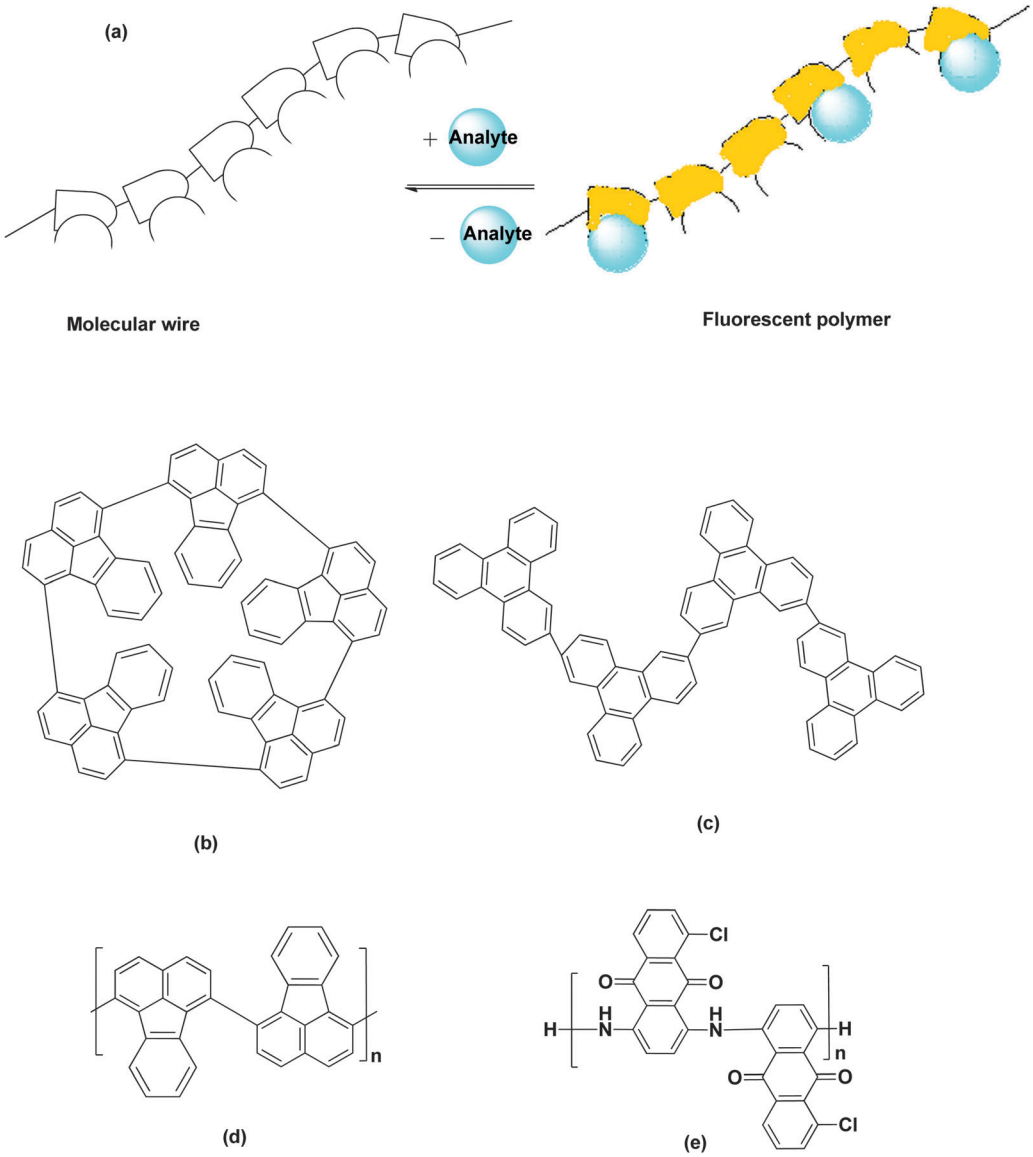

Scheme 1

poly(1-amino-5-chloroanthraquinone) was prepared *via* chemically oxidative interfacial polymerization.[52] This fluorescent polymer showed high selectivity for the Fe^{3+} ion in semi-aqueous medium (DMF/H_2O (9 : 1, v/v)) with a detection limit of 2.0×10^{-11} M (Scheme 1e). Upon binding with the Fe^{3+} ion, it formed a non-fluorescent complex, which results in quenching in the emission profile. The conjugated polymer also utilized for the detection of anions like F^- in non-aqueous medium.[53,54] Therefore, a conjugated polymer is a promising strategy to increase the selectivity of chemosensors.

1.2.2 Selectivity. The sensor should be highly selective toward a particular analyte. The binding interaction between the receptor and a particular analyte should not be affected by other competing molecules. The strength of the binding forces and solvent molecules are the main deciding factors for selectivity. For practical or real applications, a sensor should be highly selective for a particular analyte even in the presence of other competing molecules.

1.2.3 Binding constant, detection limit and response time. The ideal sensor should have a high binding constant, low detection limit and low response time. The binding constant is dependent upon the strength of non-covalent interactions between the host and guest. The sensor should respond to minute concentrations of the analyte over short durations.

1.2.4 Water solubility. All biological and environmental processes occur in aqueous medium.[55] To trace the anions/metal ions/biomolecules, a sensor should be soluble in water. In the case of optical chemosensors, the polarity of the solvent plays a significant role in the output signal of the sensor. Water is a highly polar protic solvent. It can stabilize or destabilize the ground state or the excited state of a molecule, depending upon the organic moiety. This interaction between the solvent and the organic molecule lead to bathochromic shift, hypsochromic shift, hyperchromic shift, hypochromic shift, quenching, enhancement, shift in the absorption or emission maxima. For example,

Published on 14 April 2016. Downloaded by Fail Open on 7/23/2025 9:06:09 AM.

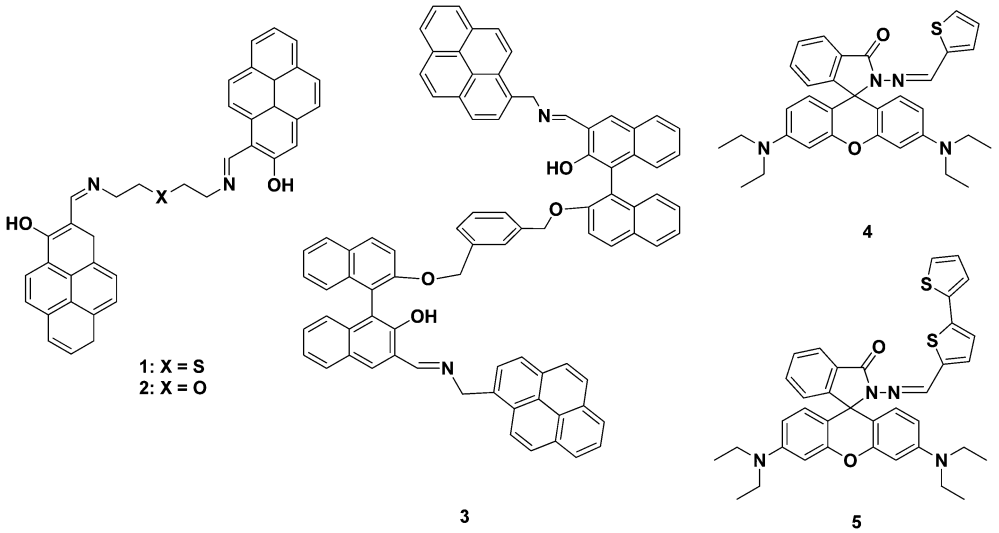

Fig. 2 Structure of (**1–5**).

electron donating groups like amines, alkylamines or dialkylamines at the 4-position of 1,8-naphthalimide in ethanol–water mixture showed bathochromic and bathofluoric shifts in absorption and emission spectroscopy.[56]

In the case of fluorescence spectroscopy, it is very hard to understand the effect of the solvent on the spectra. There are numbers of theories, which explain this effect in different opinions. Generally, the energy of the excited state decreases with an increase of the solvent polarity. Therefore, a polar solvent like water shifts the emission maxima to a higher wavelength. Usually, a fluorophore has a large dipole moment in the excited state (μ_E) compared to in ground state (μ_G).[57] In the excited state, the solvent dipole tends to reorganize around (μ_E), which lowers the energy of the excited state. This effect is more pronounced with an increase of solvent polarity. Moreover, this effect also depends upon the nature of the fluorophore; non-polar molecules have less sensitivity to solvent polarity. Therefore, the selection of the fluorophore for detection in aqueous medium is a crucial step for the development of good chemosensors. Most of the reported chemosensors are soluble in organic solvents. Recently, few chemosensors were reported in the literature, and could operate in some fraction of water.[46,58]

In the case of metal ions, Yoon and coworkers reported pyrene based fluorescent probe (**1** and **2**) for the detection of the Zn^{2+} ion in semi-aqueous medium DMSO–H_2O (1 : 1, v/v) as shown in Fig. 2.[59] Similarly, a binaphthyl-pyrene based chemosensor (**3**) was employed for the selective detection of the Zn^{2+} ion in DMSO–HEPES (9 : 1, v/v) using fluorescence and CD spectroscopy (Fig. 2).[60] Yoon *et al.*, in 2013, designed a rhodamine based chemosensor (**4** and **5**) for the selective detection of the Hg^{2+} ion in the EtOH–H_2O (1 : 1, v/v) solvent system (Fig. 2).[61]

Likewise, some extent of success for anion recognition in partial aqueous medium has been achieved by some research groups. Kuwar and coworkers reported a dipodal Zn^{2+} complex (**6**) for the selective detection of the HSO_4^- ion in the DMSO–H_2O (50 : 50, v/v) solvent system (Fig. 3).[62]

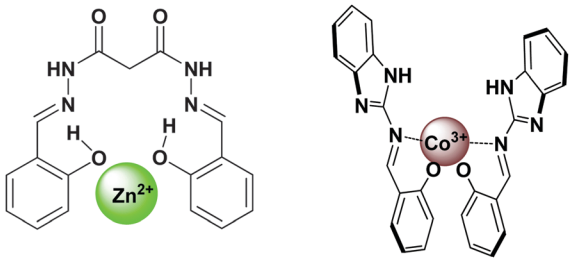

Fig. 3 Structure of (**6**) and (**7**).

Jang and coworkers reported a benzimidazole-based Co^{3+} complex (**7**) for the detection of the I^- and HSO_4^- ions in the MeOH–H_2O (8 : 2, v/v) solvent system as shown in Fig. 3.[42] Tsukube and coworkers reported a lanthanide complex for the detection of amino acids in the H_2O–CH_3CN (1/99, v/v) solvent system.[63] Kubik and coworkers reported several cyclopeptide based chemosensors (**8–14**) for the selective detection of anions in semi-aqueous medium (Fig. 4).[64–68]

A large number of reviews have been published in recent years.[5,31,69–71] However, a review focused on the detection of analytes under aqueous conditions is still in demand. Most biological and environmental processes are operated in aqueous systems. This review is focused on a compilation of sensors operated in aqueous medium ($\geq$90).

2. Sensors for H^+ ions

Most physiological processes are pH dependent and a deviation from normal values leads to fatal consequences like cancer, premature aging, cardiovascular damage and kidney stones.[72–74] Therefore, an extensive study has been carried out to find out a suitable pH sensor for aqueous media, and fluorescent chemosensors gained significant appreciation in this field.[75–78] Tan *et al.* designed a benzimidazole based (**15**) fluorescent pH sensor for

 This journal is © The Royal Society of Chemistry 2016

Published on 14 April 2016. Downloaded by Fail Open on 7/23/2025 9:06:09 AM.

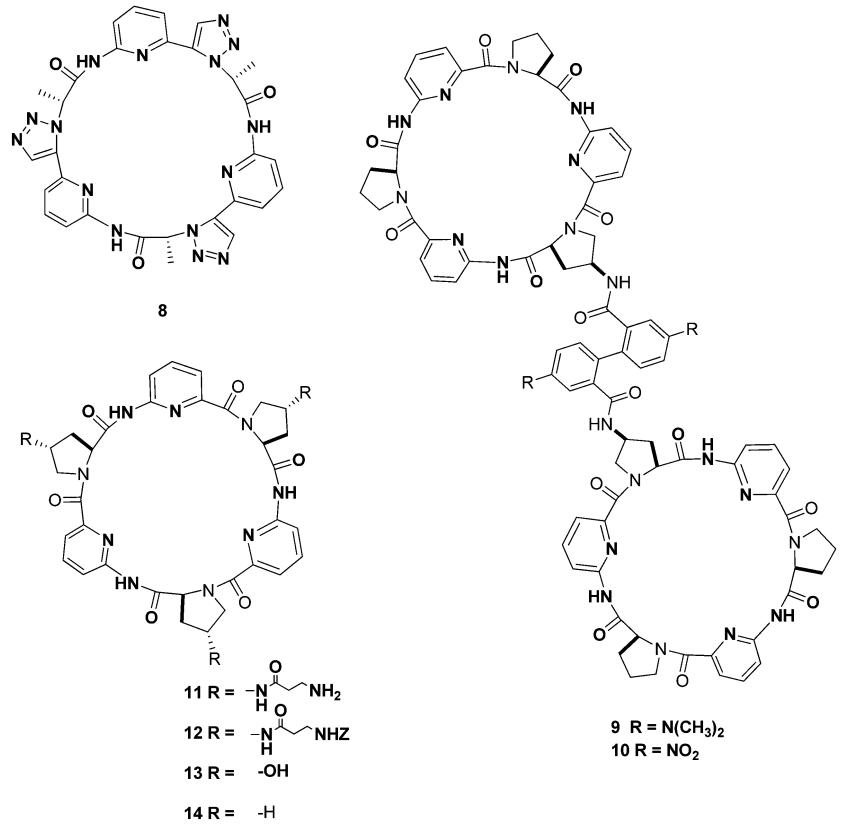

Fig. 4 Cyclopeptide based chemosensors (**8–14**) for the detection of anions.

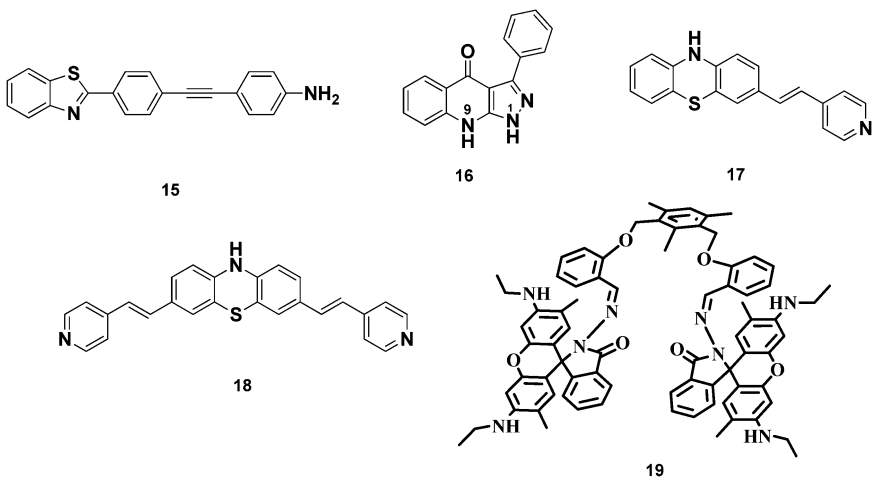

Fig. 5 Structure of (**15–19**).

strongly acidic conditions (Fig. 5).[79] The fluorescent probe (**15**) was based on the intramolecular charge transfer (ICT) effect and had high stability, sensitivity and selectivity to detect acidity within the pH range 0.5–2.5. To enhance the selectivity and sensitivity of the probe, an amino group and benzothiazole were introduced at two opposite ends (Fig. 5). The fluorescence behavior of (**15**) in aqueous solution is highly depending upon the pH of the solution; with a decrease of the pH, the intensity of (**15**) increases, which indicates the involvement of a PET mechanism.

Su *et al.* synthesized the quinolin-4-one (**16**) based fluorescent probe for extreme pH measurement (Fig. 5).[80] To avoid interference from common metal ions, the amino groups were introduced in the framework of the molecule. The receptor (**16**) has three nitrogen atoms and one oxygen atom to obtain a broad pH response range as shown in Fig. 5. The pH titration of (**16**) gave two pK_a values of 2.61 and 12.44, which corresponds to the protonation of two nitrogen atoms N9 and N1 of the receptor (**16**) respectively. It means that only two of the electronegative atoms

Published on 14 April 2016. Downloaded by Fail Open on 7/23/2025 9:06:09 AM.

exhibit pH-sensitivity, however the basicity of the other two (one N and one O) is sufficiently reduced due to the participation of a lone pair in conjugation. Therefore, receptor (**16**) is able to detect the extreme pH values over the two pH ranges 1.8–3.4 and 11.6–13.3. Lin *et al.* prepared pH dependent fluorescent organic nanoparticles (FONPs) of 3- or 3,7-divinyl substituted 10*H*-phenothiazines (**17**, **18**) as shown in Fig. 5.[81] The fluorescent organic nanoparticles have been used as biomarkers in cell biology. These receptors showed aggregation-induced enhanced emission (AIEE) properties for *in vitro* spectral studies and cellular staining.

Singh *et al.* designed a rhodamine-based dipodal framework (**19**) and preceded it into FONPs using a reprecipitation method (Fig. 5).[82] To optimize the conditions, pH titration was performed on both a fluorescence and absorption spectrophotometer. The receptor (**19**) showed high sensitivity toward an extreme acidic pH range (3.7–1.92). With the pH decreasing (below 3.7), a new band was raised in the emission and absorbance spectra at 555 and 538 nm respectively. Furthermore, a decrease of the pH led to enhancement in the fluorescence as well as absorption intensity of (**19**). The opening of the spirolactam ring is a possible reason behind this enhancement.

Similarly, Singh *et al.* designed tripodal ligand based fluorescent organic nanoparticles (FONPs) (**20**) for the detection of extreme acidic pH ranges (3 to 1.92) as shown in Fig. 6.[83] The emission intensity of (**20**) decreased with an increase of the acidity (below pH 3). The decrease of the pH led to the formation of large aggregates, which results into quenching the emission intensity due to aggregation caused quenching. Yang *et al.* presented the Tb(III) and Eu(III) complexes of the tripodal substituted salicylic ligand (H_3BSA, **21**) as potential pH sensors (Fig. 6).[84] Among these, Tb(III) complex BSA·Tb exhibited high sensitivity in the physiological pH range of 3.5–8.0 *via* a fluorescence "off–on–off" mechanism in aqueous medium. Salicylic acid acted as an antenna chromophore and the *para*-Br groups facilitated intersystem crossing owing to the heavy-atom effect, which results into enhancing the lanthanide-centered luminescence properties. It was observed that an increase of the pH value from 2.0 to 5.9, led to an enhancement in the fluorescence intensity of (BSA·Tb) at 496 nm (17 fold) and at 550 nm (50 fold). However, both bands showed quenching in the pH range of 6.5 to 9.9, which led to the conclusion that it was an off–on–off type fluorescent probe of pH. Furthermore, complex (BSA·Tb) has been investigated accurately for sensing the pH within HeLa cells. Noh *et al.* reported a Schiff base (**22**) between triaminoguanidinium and furfural.[85] Upon complexation with the Cu^{2+} ion, resultant complex (**22**)–Cu^{2+} behaves as an excellent pH sensor in the range of 2 to 5 as shown in Fig. 6. Complex (**22**)–Cu^{2+} begun to change color at pH 5.4 and with an increase of the pH, the absorption maximum at 325 nm significantly decreased; simultaneously, a new band at 425 nm appeared with an isosbestic point at 350 nm. The possible mechanism proposed for the color change was the protonation of the imine moieties of (**22**) a shown in Fig. 6. At low pH, protonation of the nitrogen atoms of the three imine moiety of (**22**) led to the exclusion of the Cu^{2+} ion from the binding cavity and produced a colorless solution of (**22**).

Yin *et al.* published a polymeric fluorescent pH probe (**23**) for lysosome imaging as shown in Fig. 7.[86] The basic strategy was the combination of a pH-responsive fluorescent dye [2-(6-(4-(2-hydroxyethyl)piperazin-1-yl)-1,3-dioxo-1*H*-benzo[*de*]isoquinolin-2(*3H*)-yl)ethyl methacrylate] with a thermo-responsive polymer (*N*-isopropylacrylamide), which responds to both pH and temperature in aqueous medium. The receptor (**23**) exhibited pH sensitivity in the range of 4.0 to 10.0 at 25 °C. The decrease in pH produced enhancement in the fluorescence intensity up to pH 4 and further decrease in pH did not cause any change. Similarly, quenching was observed upon increasing the pH up to 10. Under acidic conditions, the amino group of piperazine gets protonated, which cancels the Photo-induced Electron Transfer (PET) process from the amino group to the 1,8-naphthalimide fluorophore. Confocal fluorescence microscopy indicated bright green fluorescence in the HeLa cells upon incubation with (**23**) at 37 °C for 30 min. Possibly, the receptor (**23**) with a diameter of 50 nm (TEM) may be endocytosed and lysosomes have an acidic medium (pH 4.5 to 5.0), which results into green fluorescence.

Uchiyama *et al.* reported digital-type fluorescent pH sensors (**24**) through the incorporation of a water-sensitive fluorophore into a pH-responsive polymer (Fig. 8).[87] These polymeric pH sensors showed a change in the emission intensity in a narrow pH range and their response (working pH range and switching direction) can be controlled through modifications in the structure of the proton receptor. The digital fluorescent pH sensor (**24**) was prepared *via* random copolymerization of *N*-isopropylacrylamide (NIPAM),

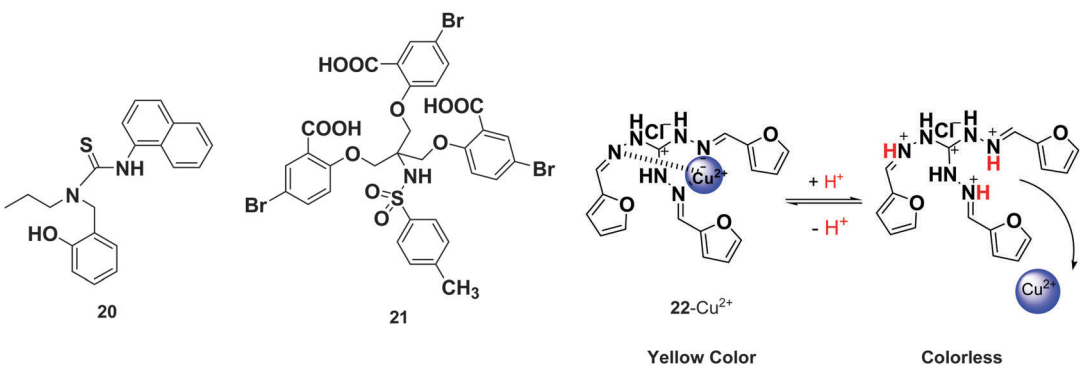

Fig. 6 Structure of (**20–21**) and mechanism of the pH response upon protonation and deprotonation of **22**–Cu^{2+}.

 This journal is © The Royal Society of Chemistry 2016

Published on 14 April 2016. Downloaded by Fail Open on 7/23/2025 9:06:09 AM.

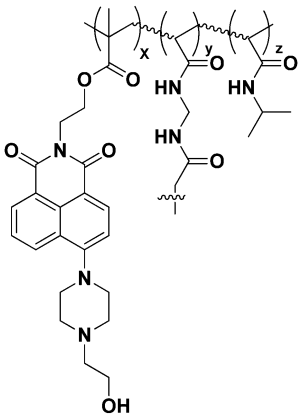

23

Fig. 7 Structure of the polymeric fluorescent pH probe (**23**).

N,*N*-dimethylaminopropylacrylamide (DMAPAM) having an amino group as the proton receptor, and fluorescent *N*-{2-[(7-*N*,*N*-dimethylaminosulfonyl)-2,1,3-benzoxadiazol-4-yl]-(methyl)-amino}ethyl-*N*-methylacrylamide (DBD-AA) as shown in Fig. 8. It was observed that sensor (**24**) has stronger fluorescence under basic conditions (pH > 9) than under acidic conditions (pH < 8) at 50 °C. The high hydrophilicity of the protonated DMAPAM units in acidic medium produced a hydrated open form of (**24**), which results into the interaction of the solvent water molecules to DBD-AA units and quenched the emission intensity.

In contrast, the dehydrated globular form of (**24**) was dominating in basic solution because of hydrophobic interactions between the NIPAM and deprotonated DMAPAM units; this led to an enhancement in the fluorescence intensity of (**24**). The fluorescence behavior of (**24**) is strongly dependent upon the temperature at 20 °C; however emission profile remains same in pH range 2 to 12. The proposed hypothesis for temperature dependency is that hydration by solvent molecules is dominating under basic conditions. Furthermore, the pH response of (**24**) can be tuned through chemical modification in the structure of ionizable units. For example, when the *N*-(3-morpholin-4-ylpropyl)acrylamide (MPAM) unit was employed as a weak proton receptor instead of DMAPAM units, the functional pH range of the resultant polymer (**25**) was shifted towards the acidic region (Fig. 8). The stronger proton receptor unit *N*-[3-(diethylamino)propyl]acrylamide (DEAPAM) as in copolymer (**26**) favored the basic pH range (Fig. 8). However, incorporation of acrylic acid as in copolymer (**27**) reversed the functional pH behavior from that of (**24**); an enhancement in emission intensity was observed under acidic conditions.

Li *et al.* designed squarylium indocyanine dye based OH^- ion sensors (**28** and **29**) as shown in Fig. 9.[88] These dyes have a ratiometric response towards extreme basic conditions (pH 13). In extreme basic conditions, the absorbance and emission intensities of these dyes (**28** and **29**) were quenched.

They showed reverse behavior upon addition of acid to the solution. The NMR analysis confirmed that the hydroxide ion attacks the N heterocycle through intramolecular nucleophilic addition. The addition of OH^- led to a decrease in the absorbance maxima at 637 nm and emission maxima at 647 nm; simultaneously, a new band appeared at 396 nm and 500 nm in the absorbance and emission spectra, respectively. These new

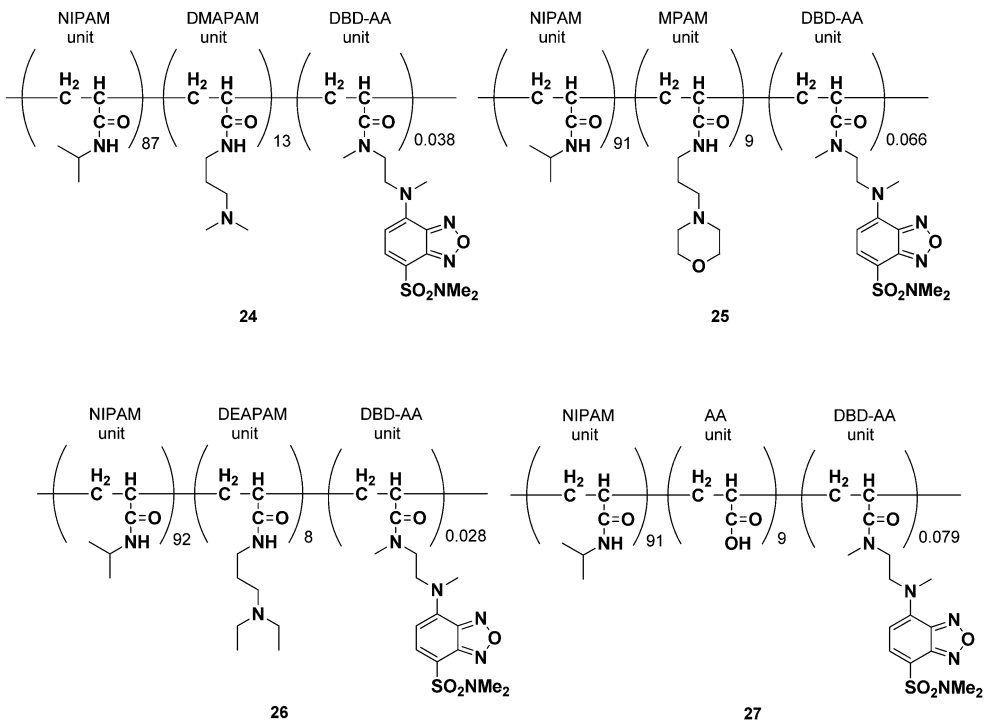

Fig. 8 Structure of (**24–27**).

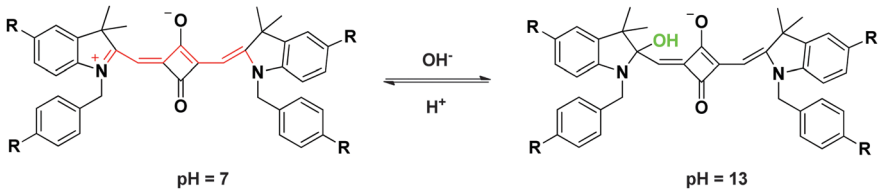

Fig. 9 A mechanism of action of squarylium cyanine dyes (**28**) and (**29**) under extremely basic conditions.

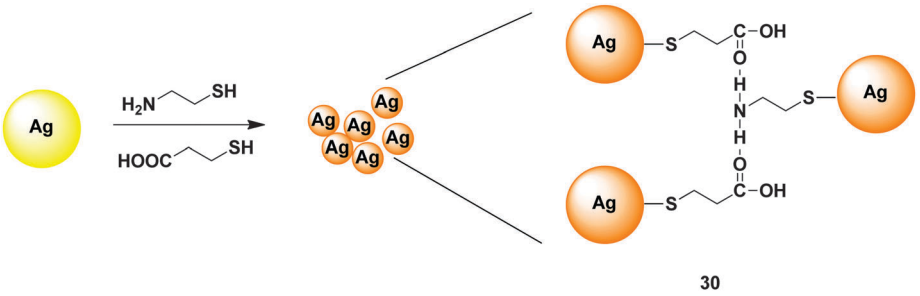

Fig. 10 Capped silver nanoparticles (**30**) for colorimetric pH sensing.

peaks were observed in the visible region and gave a colorimetric response to hydroxide ion concentration.

Chen *et al.* utilized capped silver nanoparticles for colorimetric sensing of pH.[89] The resultant sensor (**30**) was synthesized through capping of mercaptoacetic acid and 2-aminoethanethiol on the surface of silver nanoparticles through Ag–S bonds (Fig. 10). It was observed that a solution of (**30**) has a purple color at a pH = 1 and the color changed to pink upon increasing the pH to 7. The further increase in pH to 13 gave a bright yellow color to the solution. Chen *et al.* rationalized that the plot between ($A_{534nm/403nm}$) and the pH of the solution did not show a linear relationship. The non-linear increase was observed in the absorbance ratio at a high pH range (11 to 13); however, the absorbance ratio showed a linear decrease in the pH range 10 to 6 with a higher slope and from pH 6 to 1 with a lower slope. The possible cause behind it was the formation of aggregates with a change of pH due to the formation of various hydrogen bonds. These non-covalent interactions were confirmed through IR and TEM results.

3. Sensors for Na^+ ions

The recognition and sensing of the physiologically important Na^+ ion has gained considerable attention in the field of supramolecular chemistry.[90–92] All animal cells maintain equilibrium in intra and extra cellular Na^+ ion concentration.[93] It is involved in several physiological processes like action potentials, synaptic potentials in excitable cells, maintain cell volume and secondary active transport processes (Na^+/H^+ exchange and Na^+/Ca^{2+} exchange).[94] Mercato *et al.* fabricated microcapsules incorporated with sodium-binding benzofuran isophthalate (SBFI) for the detection of Na^+ ion as shown in Fig. 11.[95]

The blue-green fluorescence of SBFI is mainly responsive to the concentration of Na^+ ions in solution. Dy647 has been employed for red fluorescence and its first order intensity does not depend on the concentration of the Na^+ ion. To increase the sensitivity, dextran was conjugated with a fluorophore followed by encapsulation of the dye–dextran moiety. The positive charge of the amino-dextran repelled Na^+ ion in the local environment, which results in a less prominent fluorescence signal of dye–dextran than free dyes. The complete sensor has dextran conjugated to both SBFI and Dy647 and green QD barcodes in their outer walls. Mercato *et al.* successfully detected H^+ and K^+ ions using the same probe though substitution of ion-sensitive dyes (fluorescein 5(6)-isothiocyanate, FITC and potassium-binding benzofuran isophthalate, PBFI respectively). The three distinct excitation wavelengths were employed for the QDs, red fluorescence dyes and ion-sensitive dyes. It was observed that SBFI and PBFI filled capsules showed crosstalk with pH.

At high pH 9, SBFI dyes can distinguish between low and high concentrations of the Na^+ and K^+ ions (5 mM/140 mM). However, errors due to crosstalk between the Na^+ and K^+ ions are not much significant, which gave multiplexed measurement of H^+, Na^+ and K^+ in parallel.

He *et al.* reported an optical sensor for the detection of the Na^+ ion in aqueous medium. The probe was successfully utilized for detection of the Na^+ ion in whole blood, serum or plasma.[96] The basic concept was covalent immobilization of a new fluoroionophore (**31**) onto an amino-functionalized hydrophilic polymer as shown in Fig. 11. Due to the significant photophysical properties of 4-amino-1,8-naphthalimide was chosen as the fluorophore. While *N*-(*o*-methoxyphenyl)aza-15-crown-5 was employed as the ionophore because of its high affinity towards sodium ions regardless of environmental factors. The ionophore is attached at the 4-amino position of the fluorophore

Published on 14 April 2016. Downloaded by Fail Open on 7/23/2025 9:06:09 AM.

 This journal is © The Royal Society of Chemistry 2016

Published on 14 April 2016. Downloaded by Fail Open on 7/23/2025 9:06:09 AM.

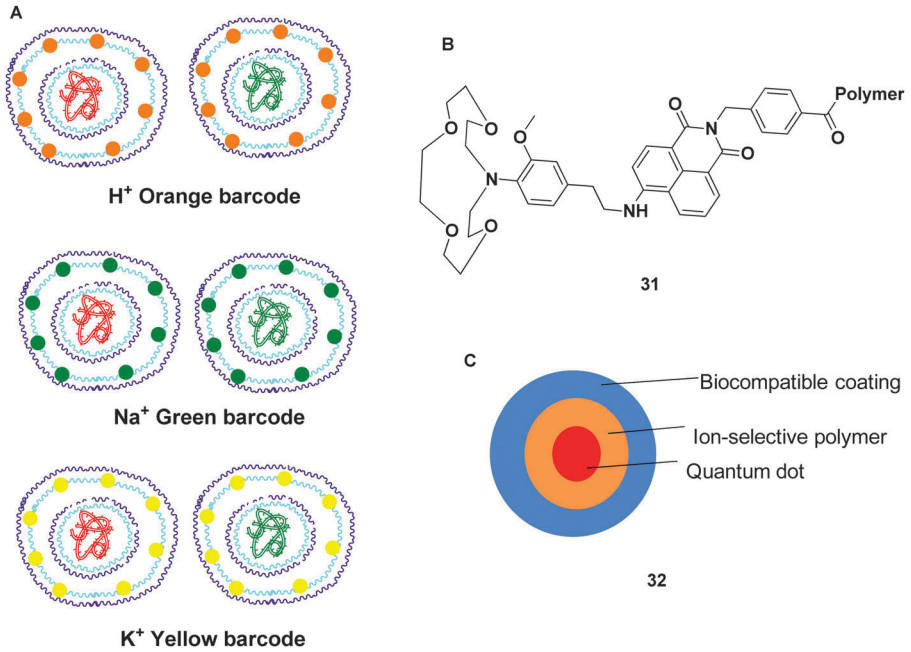

Fig. 11 (A) Three different types of capsules coloaded with dextran modified FITC, SBFI and PBFI and with dextran modified Dy647 in their cavities have been synthesized. They showed sensitivity to pH, Na^+, and K^+. These capsules were labeled with a quantum dot on their outermost surface; (B) structure of (**31**) and (C) structure of (**32**).

and the benzoic acid moiety coupled to the imide was suitable for covalent immobilization to amino-containing polymers. It was noticed that the emission intensity increased linearly with the concentration of the Na^+ ion. Upon coordinating with the Na^+ ion, fluorescence quenching due to the anisidine moiety was inhibited, which resulted into an enhancement in the emission spectrum. A Na^+ ion binds with an azacrown ether and there is no direct interaction between the Na^+ ion and the fluorophore. PET is the responsible phenomenon behind this enhancement.

Dubach *et al.* fabricated an ion-selective polymer based sensor (**32**) for estimation of Na^+ ions.[97] The sensor consists of three components: a quantum dot, an ion-selective polymer matrix and a biocompatible coating (Fig. 11). The polymer matrix has a light absorbing pH indicator (chromoionophore) in conjunction with a non-absorbing ion-binding molecule (ionophore). The ionophore has high selectivity for sodium ion and extracts the ion from the solution into the polymer. During extraction of the ions, the polymer matrix released H^+ ions into solution and as a result the pH and color of solution changed. The fluorescence intensity of the sensor increased with the concentration of Na^+ ions and has a dynamic range of 1 mM to 1 M. The sensor showed high selectivity for Na^+ ions even in the presence of potassium ions.

4. Sensors for K^+ ions

Potassium ions play a significant role in biological processes *e.g.* regulation of extracellular osmolarity and maintaining the concentration of other ions in living cells.[14,98–101] Imbalance in the concentration of K^+ ions may lead to the arrhythmia disease.[102] Lin *et al.* reported the determination of K^+ ions through 15-crown-5 functionalized gold nanoparticles (**33**) in aqueous system as shown in Fig. 12.[103] In the presence of K^+ ions, the red color solution of 15-crown-5 functionalized gold nanoparticles turns into blue. The probe (**33**) recognized K^+ ions even in the presence of Na^+ ions (Fig. 12). TEM images showed the formation of aggregates upon binding with K^+ ions. Therefore, aggregates are responsible for the colorimetric response and these aggregates are induced by the 2 : 1 sandwich complex between the 15-crown-5 moiety and K^+ ions.

The absorption spectrum of probe (**33**) has a maximum at 528 nm which decreases drastically along with a new band at 710 nm upon addition of K^+ ions. The new band (710 nm) is attributed to the coupled plasmon absorbance of nanoparticles in close contact. It is observed that a change in the solution color and the degree of the red shift depends upon the size of the aggregated nanoparticles. The system can be reversed upon addition of dichloromethane and 18-crown-6. In the absence of K^+ ions, crown ethers can exhibit either an entirely hydrophilic or hydrophobic exterior due to flexible oxygen atoms. However, binding with K^+ ions leads to the involvement of a lone-pair of oxygen atoms and non-polar ethylene chains exposed to solvent. The complex has an outer hydrophobic surface and inner hydrophilic cavity for encapsulation of K^+ ions. This phase separation prevents the reassociation of K^+ ions with nanoparticles and cause dissolution of the precipitant.

Chen *et al.* reported the synthesis of 15-crown-5 functionalized CdSe/ZnS QDs (**34**) for the detection of K^+ ions in aqueous solution as shown in Fig. 13.[104] The titration was performed between CdSe/ZnS (3.2/0.9 nm) or CdSe/ZnS (5.6/0.8 nm) QDs

Published on 14 April 2016. Downloaded by Fail Open on 7/23/2025 9:06:09 AM.

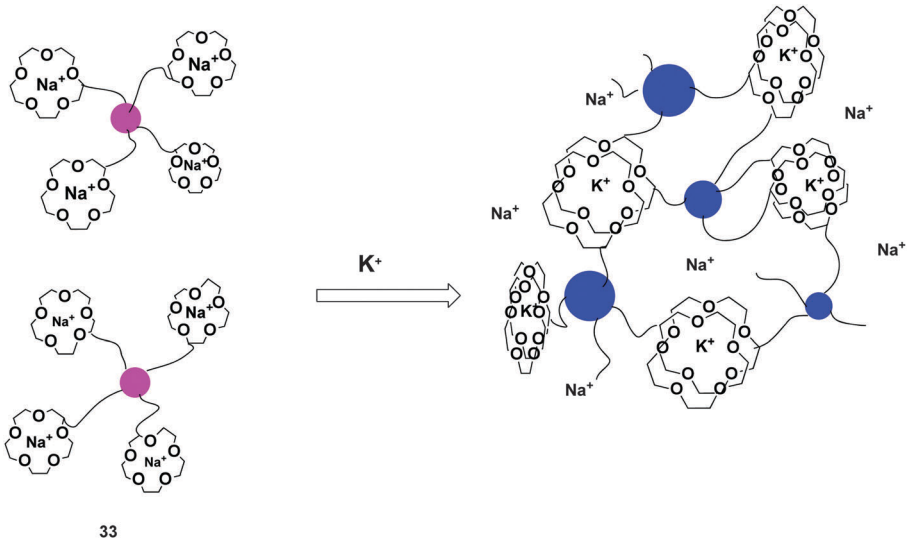

Fig. 12 Proposed binding mechanism of K^+ recognition using nanoparticle-networking through sandwich complexes.

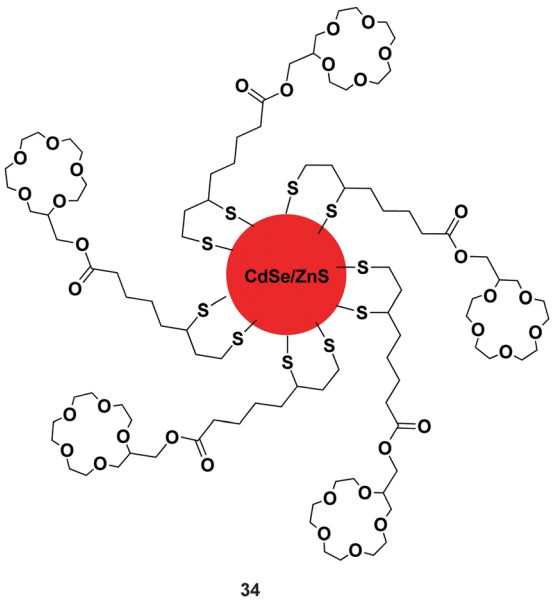

Fig. 13 Structure of 15-crown-5-capped CdSe/ZnS QDs.

and $KClO_4$ in water. To avoid pH interference, all studies have been performed at pH 7.1 using Tris-HCl buffer solution and term green (545 nm) and red QDs (635 nm) were employed to represent CdSe/ZnS (3.2/0.9 nm) and CdSe/ZnS (5.6/0.8 nm) respectively. It was observed that the absorption spectrum remained unchanged during K^+ ion titration. However, the emission spectrum of probe (**34**) has two peaks centered at 545 nm and 635 nm (λ_{max} = 430 nm). There is no interaction between the prepared green and red QDs; the quantum yields for the green and red QDs were measured to be 0.15 and 0.21, respectively. The addition of $KClO_4$ caused a decrease in the emission intensity at 545 nm and a simultaneous increases in intensity at 635 nm.

Chen *et al.* also executed a controlled experiment taking only green (or red) 15-crown-5 QDs and titrated with K^+ ions.[104] A negligible change in the emission intensity was seen in the controlled experiments. Therefore, there is an energy transfer interaction in the mixed 15-crown-5 capped QDs (green and red). The aggregates were observed in solution beyond a 5 mM concentration of K^+ ion. However, the energy transfer and aggregation effect was not observed upon adding Na^+ ions. The 15-crown-5/K^+/15-crown-5 sandwich type of complexation is responsible for the recognition of K^+ ions. Semi-empirical calculations concluded that a Föster type of energy transfer is operative upon binding of K^+ ions. According to the calculations, the distance between two K^+ bridged QDs (inter-particle model) was about ~26 Å, which increases the possibility of a Föster type of energy transfer. The response of probe (**34**) for K^+ ions remained the same even in the presence of numerous physiological important cations such as Li^+, Cs^+, Mg^{2+}, Ca^{2+} and Ba^{2+} and no aggregation was observed except for K^+ ions, which shows the high selectivity of probe (**34**) for K^+ ions.

Huang *et al.* reported a fluorescent probe (**35**) to signal aptamer–K^+ binding using an ATP-binding aptamer (dACCTGG GGGAGTATTGCGGAGGAAGGT) and OliGreen (OG) as shown in Fig. 14.[105] Upon interacting with ssDNA, OG showed significant fluorescence emission at 520 nm. OG formed a complex with a random-coil (ss) ATP-binding aptamer (Apt). The addition of K^+ ions lead to a change in the conformation of Apt from random coil to two stacked G-quadruplexes and two short double-helix stems as shown in Fig. 14. Due to conformational changes, the OG–Apt complex was dissociated to some extent and caused a decrease in fluorescence. To confirm the dissociation, centrifugal filters (molecular weight cut-off: 1000 Da) have been employed to separate the dissociated OG from the OG·Apt complex. It was estimated that 27% of the OG units had dissociated upon binding with 10 μM of K^+. Furthermore, binding between Apt and K^+ has been confirmed through a control DNA strand (ACGTTAGCTACTATTCCGTACGAACCT) that does not form a G-quadruplex structure to have a strong interaction with K^+ ions. The emission profile of a mixture of OG and control DNA did not

 This journal is © The Royal Society of Chemistry 2016

Published on 14 April 2016. Downloaded by Fail Open on 7/23/2025 9:06:09 AM.

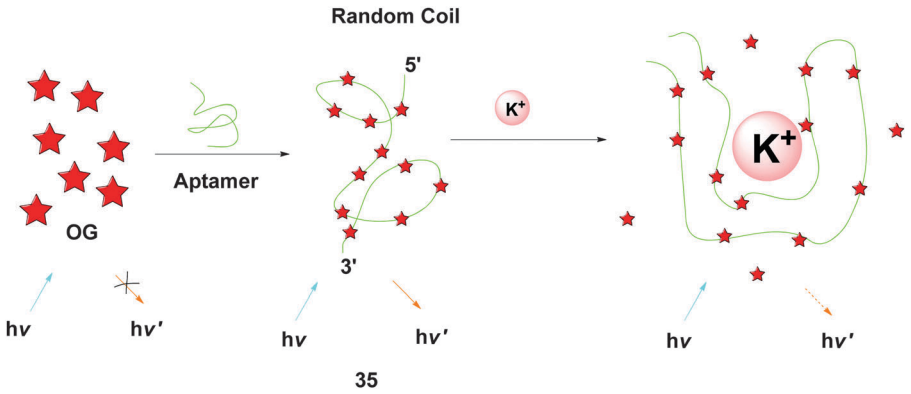

Fig. 14 Proposed mechanism of K^+ sensing using (**35**): an ATP-binding aptamer (dACCTGGGGGAGTATTGCGGAGGAAGGT) and OliGreen (OG).

produce a significant change. Capillary electrophoresis confirmed both the kinetic and thermodynamic stability of the G-quadruplex OG·Apt complex. The fluorescence intensity of the OG·Apt complex decrease linearly upon increase of the K^+ concentration from 100 to 1000 nM and has a detection limit of about 75 nM. The OG·Apt probe (**35**) shows high selectivity even in the presence of other competing ions like Na^+, Li^+, NH_4^+, Mg^{2+} and Ca^{2+}.

Ueyama *et al.* published the novel potassium sensing oligonucleotide PSO (**36**) to detect K^+ ions in aqueous medium (Fig. 15).[106] The four GGG sequence sites of oligonucleotide formed a binding cavity in the intramolecular tetraplex folding to form a guanine quartet. The quinine quartet is the part of the tetraplex structure of DNA and tetraplex formation is promoted by the presence of monovalent cations. The guanine quartet is especially stable with K^+ ions due to the complementary size of the K^+ ion with the cavity created between two guanine quartets (Fig. 15).

PSO (**36**) has two fluorophores 6-carboxyfluorescein (6-FAM) and 6-carboxytetramethylrhodamine (6-TAMRA), at the 5′- and 3′-termini of the oligonucleotide as the donor and acceptor, respectively. In the presence of K^+ ions, the oligonucleotide can form a tetraplex structure and two chromophores come adjacent to each other, which results into FRET as shown in Fig. 15. The emission spectrum of PSO has two bands at 515 nm and 581 nm, which correspond to 6-FAM and 6-TAMRA, respectively. The addition of K^+ ions gave a ratiometric response through a decrease in intensity at 515 nm and an increase in intensity at

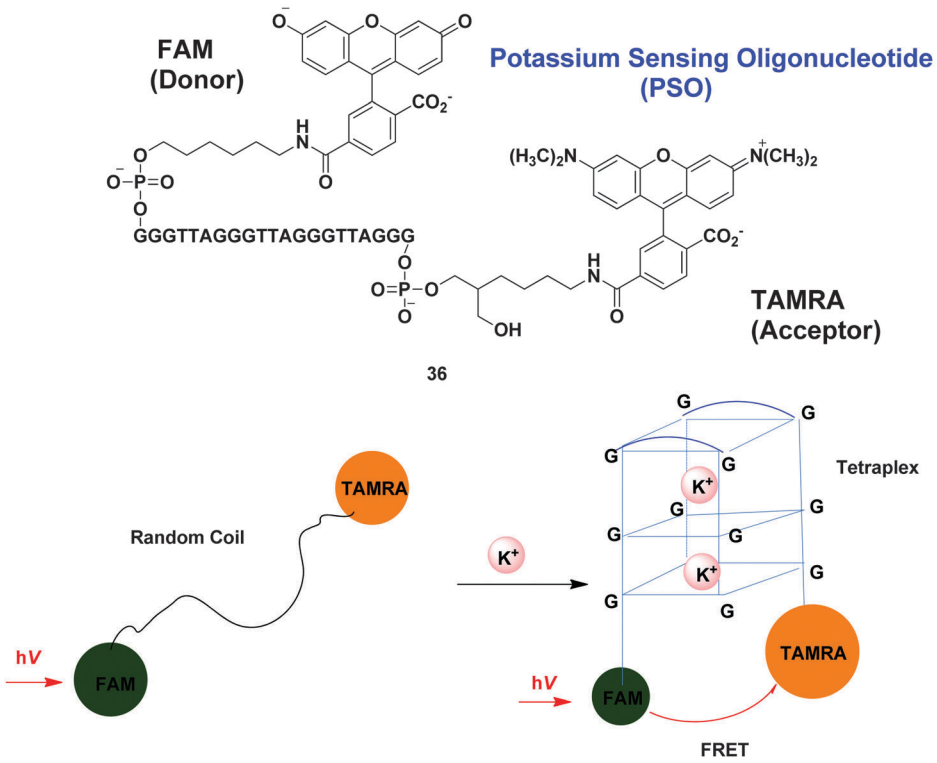

Fig. 15 Structure of PSO (**36**) and proposed binding mechanism for the detection of K^+ ions.

Published on 14 April 2016. Downloaded by Fail Open on 7/23/2025 9:06:09 AM.

581 nm with an isoemissive point at 565 nm. The titration experiment revealed that K^+ ions shift the equilibrium toward the tetraplex form, which is also confirmed through the circular dichroism (CD) spectrum of PSO. The probe (**36**) has high selectivity for K^+ ions even in the presence of Na^+, Li^+, Cs^+ and NH_4^+ ions.

He *et al.* synthesized a new photoinduced electron transfer (PET) based fluorophore (**37**) for extracellular detection of K^+ ions.[107] The probe (**37**) consists of cryptand (binding site), *o*-alkoxyaniline (PET donor), 4-aminonapthalimide (fluorophore) and benzoic acid (linker to solid support) as shown in Fig. 16. The binding of K^+ ions to cryptand results into cancellation of PET and enhancement in the emission and excitation spectra is observed.

The fluorophore does not directly interact sterically or electronically with the cation. Therefore, the excitation and emission maxima are nearly invariant to the K^+ ion concentration, which indicated the PET phenomenon. The sensor has high selectivity for K^+ ions even in the presence or absence of interfering Na^+ and Ca^{2+} ions.

He *et al.* utilized guanine quadruplex–DNA coupled with cationic conjugated polymers (CCP) for the selective detection of potassium ions in water as shown in Fig. 16.[108] The poly(9,9-bis(6′-*N*,*N*,*N*-trimethylammonium)hexyl)fluorenylene phenylene (PF) is employed as CCP. Fluorescein labeled G-rich single stranded DNA was employed for detection and has a random coil conformation in the absence of K^+ ions. Due to weak electrostatic interactions between ssDNA-FI and CCP, fluorescein remains far away from CCP. However, the addition of K^+ ions escalates the formation of G-quadruplex and increases the magnitude of the electrostatic interaction in G-quadruplex–DNA/PF. As a consequence of a strong electrostatic interaction, CCP residues come in vicinity to fluorescein and efficient FRET from CCP to fluorescein is observed. The addition of NaCl (50 mM) did not produce a G-quadruplex structure, which authenticates the specificity of the method. The value of the FRET ratio (I_{527}/I) for K^+ ion 16 times higher than for Na^+, Li^+ and NH_4^+ and 6 times higher than for Ca^{2+} and Mg^{2+} ions.

5. Sensors for Mg^{2+} ions

Magnesium ions are present either in the free or bound state in cells. They bind with a large variety of negatively charged molecules like nucleic acids, ATP, proteins and phospholipids.[109,110] Therefore, magnesium is involved in various biological events such as hormone release, muscle contraction and cell proliferation.[111] Recently, it was found that the knockdown of genes encoding for magnesium transporters leads to cell death.[112–114] Kim *et al.* synthesized a probe (**38**) with high selectivity for the intracellular free Mg^{2+} ion as shown in Fig. 17.[115] The probe (**38**) has high photostability, no Ca^{2+} ion interference, little background emission, increased water solubility and optimal cell permeability. The probe (**38**) has β-keto acid for the binding of Mg^{2+} ions (Fig. 17). The addition of Mg^{2+} ions produced a bathochromic shift in the absorbance maxima of (**38**) from 413 to 443 nm in aqueous micellar solution. The possible reason behind this shift was the increased acceptor strength of the β-keto acid moiety upon binding with an Mg^{2+} ion. A micellar solution offered the hydrophobic environment to facilitate metal binding. It was observed that the binding constant between (**38**) and Mg^{2+} ions remained unaffected above the critical micellar concentration and Job's plot depicted a 1:1 stoichiometry between (**38**) and Mg^{2+} ions. The probe (**38**) can measure the

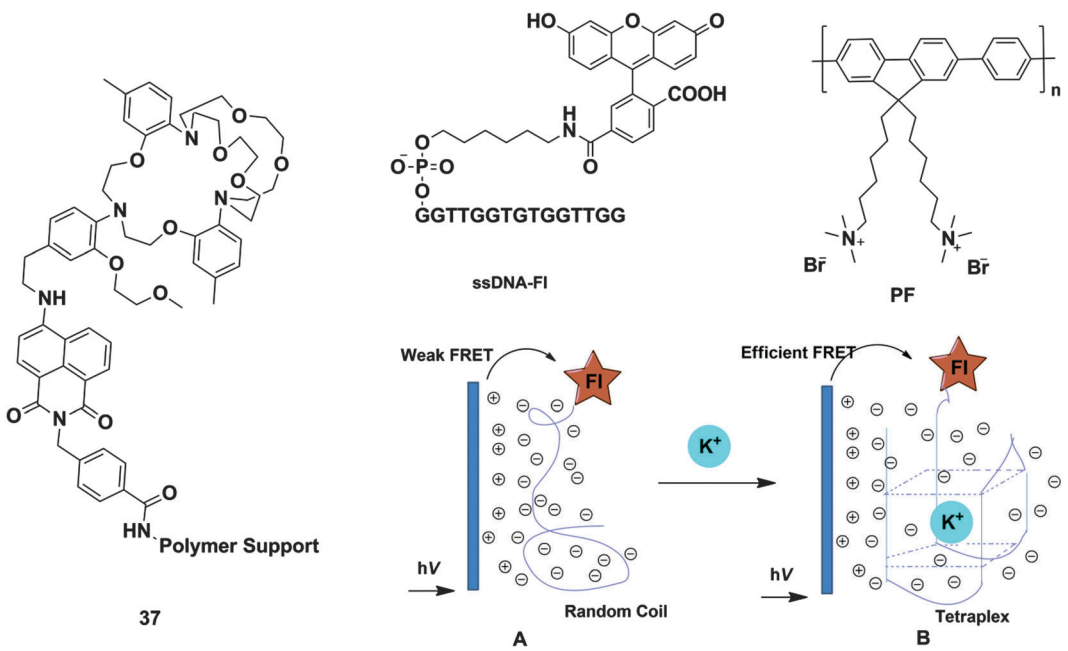

Fig. 16 Chemical structure of (**37**), PF and schematic representation of K^+ recognition using guanine quadruplex–DNA coupled with cationic conjugated polymers.

 This journal is © The Royal Society of Chemistry 2016

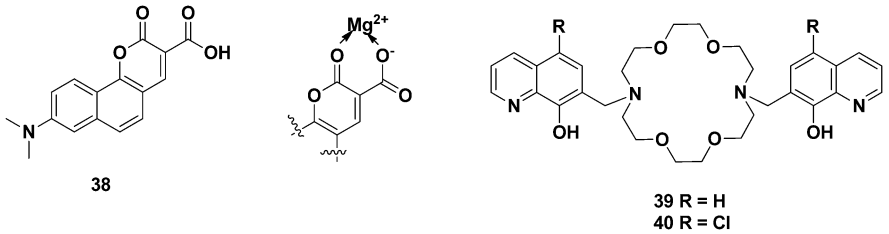

Fig. 17 Chemical structure of (**38**) and proposed binding mode with a Mg^{2+} ion and structure of the diaza-18-crown-6-hydroxyquinoline based chemosensor (**39** and **40**) of Mg^{2+} ions.

Published on 14 April 2016. Downloaded by Fail Open on 7/23/2025 9:06:09 AM.

intracellular free Mg^{2+} ion concentration without interference through Ca^{2+} ions. The binding of Mg^{2+} ions also influenced the emission intensity of probe (**38**) and enhancement was observed in the presence of Mg^{2+} ions. The emission properties of (**38**) and (**38**)·Mg^{2+} are nearly constant above pH 6.5, which means that the probe is pH-sensitive in the biologically relevant pH range in SDS solution.

Farruggia *et al.* reported two diaza-18-crown-6-hydroxyquinoline derivatives (DCHQ) (**39** and **40**) for intracellular detection of Mg^{2+} ions as shown in Fig. 17.[116] The 8-hydroxyquinoline (HQ) group is responsible for the absorption and emission bands. The probes (**39**) and (**40**) have almost similar absorption spectra, a sharp intense band in the region of 230–250 nm correspond to π–π* transition and less intense as well as broader band at 360 nm due to charge transfer from the oxygen atom to the quinoline moiety of the chromophore. The emission spectra of (**39**) and (**40**) have a band in the range of 360–520 nm, which strongly depends on the nature of the solvent. The addition of Mg^{2+} ion significantly changes the absorption and emission profiles of both (**39**) and (**40**). The probe (**40**) showed a red shift in the absorption peak, while the shift was not much prominent in the case of (**39**). The red shift in the absorbance maximum is attributed to the deprotonation of the hydroxyl groups of HQ followed by complexation with an Mg^{2+} ion. The addition of Mg^{2+} ions caused an enhancement in the emission intensity of probes (**39**) and (**40**), due to cancellation of the photoinduced proton transfer (PPT) and photoinduced electron transfer (PET) processes. These probes (**39** and **40**) also have high selectivity towards Mg^{2+} ions even in the presence of other competing alkali and alkaline earth metal ions.

Suzuki *et al.* synthesized coumarin based fluorophores (**41** and **42**) for the detection of Mg^{2+} ions (Fig. 18).[117] These coumarin derivatives (**41** and **42**) have a β-hydroxy carboxylic acid group for binding with Mg^{2+} ions and an aromatic amine group connected through a conjugated π-electron system. The probes (**41**) and (**42**) are examined for metal binding studies in HEPES buffer solution. The addition of Mg^{2+} ion produced ratiometric changes in the absorption spectra of (**41**) and (**42**). The titration experiment revealed that addition of Mg^{2+} results into enhancement at 445 nm and a decrease in the absorbance intensity at 425 nm with an isosbestic point at 423 nm. The binding of Mg^{2+} ions also influenced the emission spectra of (**41**) and (**42**). The emission maxima showed a bathochromic shift along with enhancement in the intensity of probes (**41**) and (**42**) in the presence of Mg^{2+} ions. These changes are attributed to

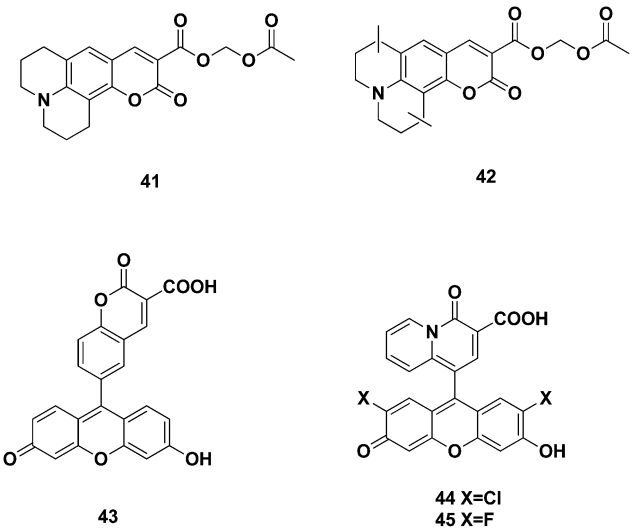

Fig. 18 Structure of (**41–45**).

the binding of Mg^{2+} ions with β-diketone group, which results into an increase of the electron density and polarity of the coumarin group.

The stability of the complexes formed between probes (**41**) or (**42**) and Mg^{2+} ion depends upon the basicity of the oxygen atom that depends on the ability of the ligand molecule to delocalize the charge borne by the metal ion. Both probes (**41**) and (**42**) formed a complex with an Mg^{2+} ion in a 1 : 1 ratio.

Komatsu *et al.* synthesized magnesium-selective fluorescent probes (**43**, **44** and **45**) as shown in Fig. 18.[118] These probes have a fluorescein residue as the fluorophore and showed high selectivity towards Mg^{2+} ions. The binding site consists of charged β-diketone groups which are attached to the 9′-position of xanthene to induce a PET-type response. To increase the resistivity towards pH, halogen substituted derivatives (**44** and **45**) have been synthesized and fluorine substituted fluorescein has more photostability. All probes (**43**, **44** and **45**) showed enhancement in the emission intensity upon binding with Mg^{2+} ions. However, probe (**44**) has an 11.1 fold enhancement in the emission intensity, probe (**45**) has an 8.18 fold enhancement and a 2.73 fold for probe (**43**) in the presence of 100 mM of Mg^{2+} ions. The photoinduced electron transfer (PET) is mainly responsible of the enhancement in the emission intensity. In the case of probe (**44**) and (**45**), HOMO levels are higher in energy, which results into more efficient photoinduced electron transfer in the

Published on 14 April 2016. Downloaded by Fail Open on 7/23/2025 9:06:09 AM.

absence of Mg^{2+} ions and more enhancement upon binding with Mg^{2+} ions. The Benesi–Hildebrand plot depicts that probes (**44**) and (**45**) have higher affinity for Mg^{2+} ions compared to probe (**43**).

6. Sensors for Ca^{2+} ions

Calcium ions play a significant role in physiological and biochemical processes like skeletal mineralization, excitation of skeletal and cardiac muscles, and cofactor and stimulus-mediated hormone secretion.[119,120] Imbalance in Ca^{2+} levels may become the reason of hyperparathyroidism, malignant tumors and hyperthyroidism.[121,122] Liu *et al.* designed and synthesized a naphthalimide-based fluorescent calcium ion sensor (**46**) as shown in Fig. 19.[123] The fluorescent probe was immobilized onto a hydrophilic polymer support like amino-cellulose and most fluorescence signal changes were observed around 10 mM of concentration of the calcium ion. The enhancement in emission as well as excitation intensity of the immobilized sensor (**46**) was observed upon binding with Ca^{2+} ions. The sensor (**46**) has an emission maximum at 470 nm along with a weak green color emission at 540 nm. The addition of Ca^{2+} ions caused a 5-fold enhancement in the emission intensity. The probe (**46**) selectively sense Ca^{2+} ions even in the presence of Mg^{2+}, Sr^{2+} and H^{+} ions. Therefore, probe (**46**) was also utilized for detection of Ca^{2+} ions in sea water. The probe (**46**) responds to Ca^{2+} ions very quickly (less than 2 min).

He *et al.* reported a naphthalimide based fluorescent sensor (**47**) for direct determination of ionized calcium ions at an extracellular concentration found in whole blood, serum or plasma.[124] The resultant sensor (**47**) was assembled through immobilization of fluorescent receptor (**48**) onto amino-functionalized cellulose embedded in a hydrophobic polymer matrix as shown in Fig. 19.

He *et al.* synthesized various ionophores to obtain the desired features. Finally, ionophore (**49**) was selected for binding and has a binding constant in the range of 1.2 nM with high storage selectivity. Another important part of the sensor is the fluorophore and 4-amino-1,8-naphthalimide was selected as the fluorophore because of its excellent thermal and photochemical stability against hydrolysis and photobleaching. The resultant sensor has high affinity towards Ca^{2+} ions. The addition of Ca^{2+} ions results into enhancement in the emission and excitation spectra of the sensor in HEPES buffer solution. The possible reason behind this enhancement was the binding of the cation to the ionophore, which results into cancellation of photoinduced electron transfer (PET) from the anisidine donor. The sensor (**47**) took less than 1 min to produce a stable response for Ca^{2+} ions.

Kim *et al.* developed a calsequestrin (CSQ) functionalized GNPs based calorimetric calcium sensor (**50**) that has high specificity, visual change in color upon interacting with Ca^{2+} ions and worked under physiological environment as shown in Fig. 20.[125] The calsequestrin (CSQ) functionalized GNPs have an approximate size of 13 nm and formed aggregates in the presence of the appropriate concentration of Ca^{2+} ions, which results into a change in color. CSQ is an endogenous Ca^{2+} binding protein in the sarcoplasmic reticulum. It undergoes conformational changes as a function of Ca^{2+} ion concentration. It has an unfolded form in the absence of Ca^{2+} ions and a compact manner in the concentration range of 10 μM to 0.01–1 mM, which subsequently undergoes dimerization and then polymerization (Fig. 20). Kim *et al.* genetically engineered human cardiac muscle CSQ to contain two cysteine residues at the C terminus. The genetically engineered CSQ was immobilized onto GNPs and uncapped CSQ was removed through washing and centrifugation. The resulting GNPs are well dispersed in aqueous medium due to the negative charge of CSQ. The addition of Ca^{2+} into the solution of CSQ GNPs led to a change in color and a precipitate appeared. The plasmon band in the UV/Vis spectrum is shifted from 530 to 575 nm due to formation of aggregates. These aggregates are formed due to change in the conformation of CSQ on the surface of the GNPs. These aggregates are dispersed upon addition of EDTA and an original red-colored solution

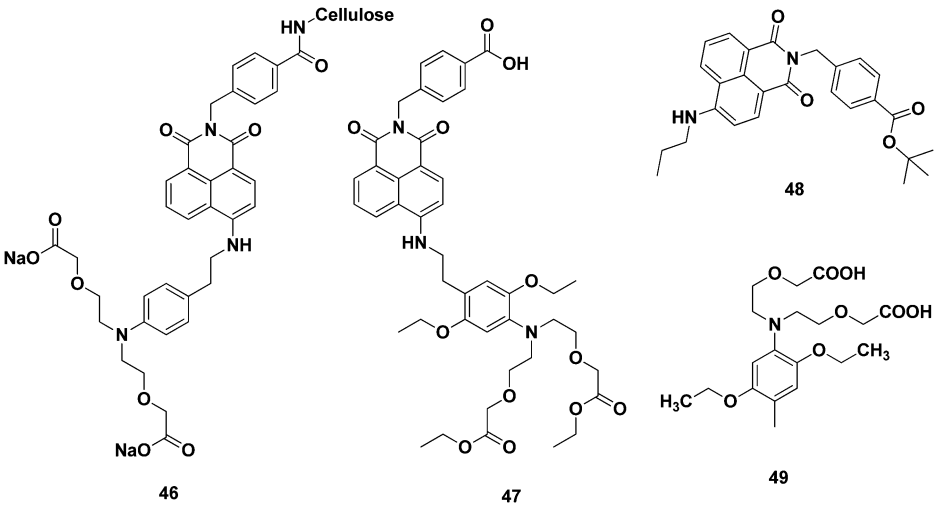

Fig. 19 Structure of (**46–49**).

 This journal is © The Royal Society of Chemistry 2016

Published on 14 April 2016. Downloaded by Fail Open on 7/23/2025 9:06:09 AM.

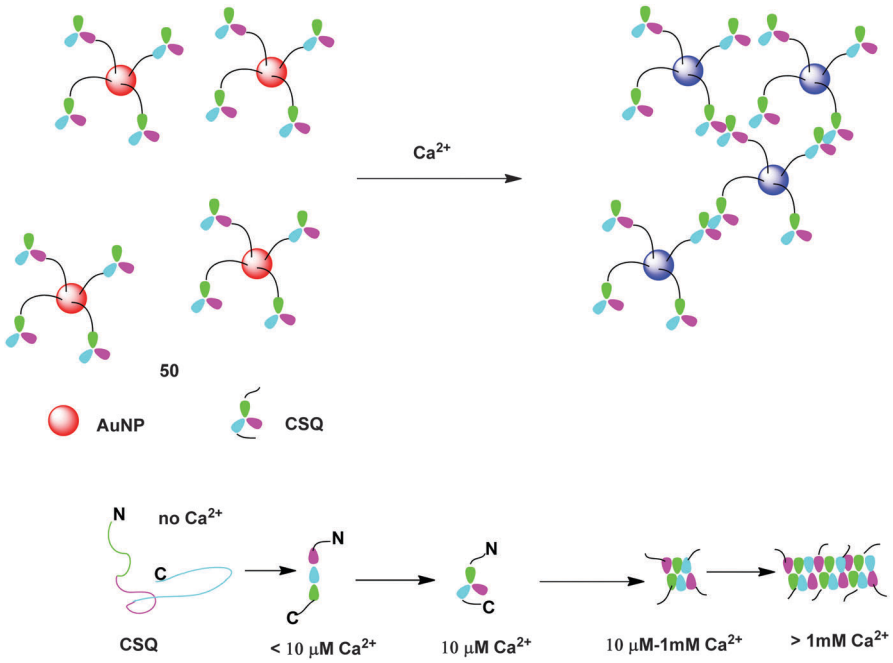

Fig. 20 Proposed mechanism of Ca^{2+} binding and Ca^{2+} dependent conformational changes of CSQ.

having a plasmon peak at 530 nm is observed, which represents the reversibility of Ca^{2+} binding. The metal binding test revealed that probe (**50**) has high selectivity for Ca^{2+} ions and other cations (Mg^{2+}, Zn^{2+}, Cu^{2+}, Mn^{2+}, Ni^{2+}, Hg^{2+}, Cd^{2+}, Ba^{2+}, K^{+} and Na^{+}) and did not produce any color change. The probe (**50**) has a linear detection range of 1–4 mM, which is well matched with the physiological concentration range of Ca^{2+} ions. CSQ–GNPs (**50**) are also utilized to distinguish between normal and abnormal levels of Ca^{2+} ions in serum through characteristic change in color from red to purple.

Grynkiewicz *et al.* reported six sensors (**51–56**) for the detection of Ca^{2+} ions as shown in Fig. 21.[126] These sensors have a strong fluorescence response and higher selectivity over Mg^{2+} and heavy metal ions. They have stilbene as the fluorophore with the a tetracarboxylate pattern of liganding group characteristic of EGTA (ethylene glycol bis(β-aminoethyl ether)-*N*,*N*,*N*′,*N*′-tetraacetic acid)

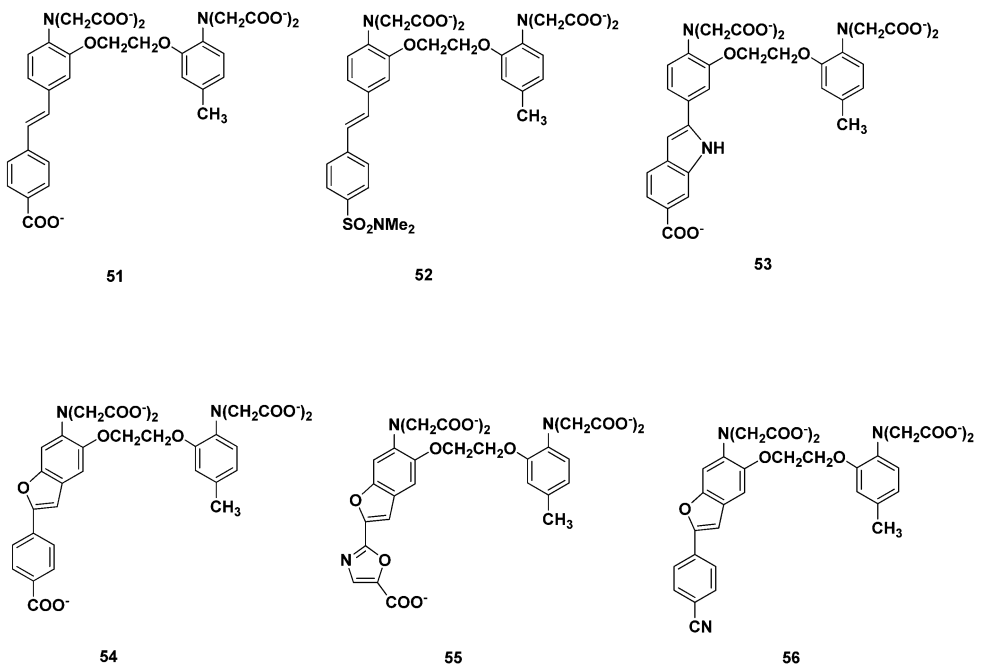

Fig. 21 Structure of (**51–56**).

Published on 14 April 2016. Downloaded by Fail Open on 7/23/2025 9:06:09 AM.

and BAPTA (1,2-bis-(2-aminophenoxy)ethane-*N*,*N*,*N*′,*N*′-tetraacetic acid). The probe (**53**) and (**55**) has extra heterocyclic bridges to strengthen the ethylenic bond of stilbene and to decrease hydrophobicity. The absorbance spectra of the fluorophores arise due to stilbene moiety. The spectra have maxima in the UV region which are shifted towards lower wavelengths upon binding with Ca^{2+} ions. These properties of particular wavelength sensitivity to Ca^{2+} ions make these probes a perfect fluorescent sensor for intracellular applications.

7. Sensors for Cr^{3+}/Cr^{6+} ions

Chromium is a one of the toxic heavy metal ions and mainly exists in the hexavalent and trivalent forms.[127,128] Cr^{6+} is a more toxic form of chromium metal. Trace amount of Cr^{3+} ion is required to maintain normal physiological activities.[129] However, a deficiency of Cr^{3+} may cause alterations in cell signaling and high concentration leads to genotoxic DNA lesions.[128,130,131] Elavarasi *et al.* reported silver nanoparticles (AgNPs) for the detection of Cr^{3+} ions in aqueous solution.[132] Upon interacting with Cr^{3+} ions, the emission maximum shifted toward a higher wavelength (420 to 684 nm) and an intense color change (yellow to purple) was observed. It was noticed that the binding of Cr^{3+} ions cause the aggregation of AgNPs, which is confirmed through SEM and DLS analysis. Elavarasi *et al.* proposed that AgNPs were stabilized in an aqueous system due to the electrostatic repulsion between negatively charged citrate ligands on their surface. Cr^{3+} ions chelate with the citrate ions through hydroxyl and carboxyl groups. Therefore, Cr^{3+} ions can act as cross-linkers between citrate coated AgNPs and induce the aggregation of AgNPs. The electrostatic field generated between cross-linked nanoparticles is much stronger than that of single silver nanoparticles, which caused enhancement in the emission intensity. A linear relationship was observed between the fluorescence intensity at 684 nm against the concentration of Cr^{3+} ions in the range of 1×10^{-3} to 2×10^{-9} M and has a low detection limit of about 2 nM. The sensor can sufficiently detect Cr^{3+} ions in ground water and fresh water. The sensor has high selectivity for Cr^{3+} ions even in the presence of other heavy metal ions (Zn^{2+}, Fe^{3+}, Mn^{2+}, Pb^{2+}, Cu^{2+}, or Hg^{2+}). The color change was observed only in the case of Cr^{3+} ions.

Saha *et al.* described the method to incorporate a rhodamine B derivative onto the alginate backbone and employed the modified polymer (**57**) for detection of toxic and biological active Cr^{3+} ions in aqueous medium (1 mM HEPES buffer, pH ~ 7.1).[133] The water soluble alginate has the ability to form a gel in the presence of Ca^{2+} and acts as a self-indicating sponge for the detection of Cr^{3+} in aqueous buffer as shown in Fig. 22. The binding affinity of sensor (**57**) was examined *via* UV-Visible and fluorescence

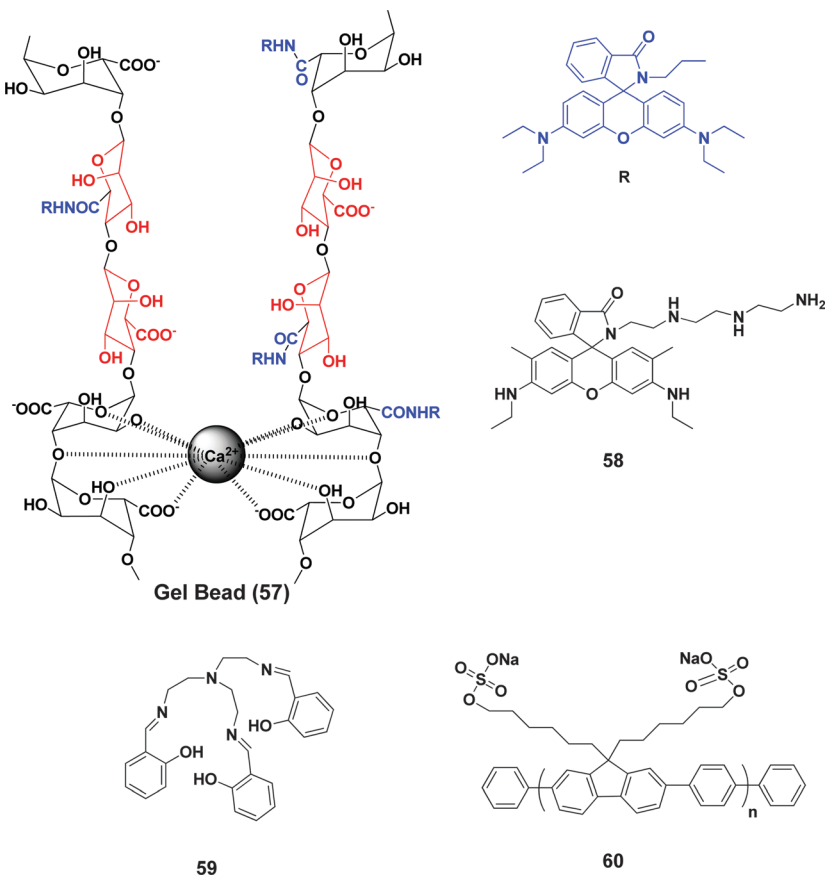

Fig. 22 Structure of (**57–60**).

 This journal is © The Royal Society of Chemistry 2016

Published on 14 April 2016. Downloaded by Fail Open on 7/23/2025 9:06:09 AM.

spectroscopy using various metal ions. The sensor (**57**) has a weak absorbance band at ~560 nm and emission band at ~580 nm indicating the rhodamine moiety in the spirolactam form. The addition of Cr^{3+} ions leads to a strong absorbance band at 560 nm and an emission band at 580 nm as well as a visual color change from pink to red. The change in absorbance and the emission spectra of sensor (**57**) upon binding with Cr^{3+} indicated the formation of acyclic xanthene. The reversibility of the sensor (**57**) was confirmed through addition of EDTA.

Mao *et al.* developed a rhodamine based fluorescent probe (**58**) for the selective determination of Cr^{3+} ions in aqueous system as shown in Fig. 22.[134] The probe (**58**) has no fluorescence signal in the range of 520 to 600 nm, which indicates the existence of a spirocyclic ring. However, the addition of Cr^{3+} ions produced an enhancement in the fluorescence signal at 552 nm and the intensity of this band is a function of the Cr^{3+} ion concentration. The probe (**58**) can selectively bind to Cr^{3+} ions even in the presence of other competing cations. The absorbance spectrum also followed the same pattern; the addition of Cr^{3+} ions produced a band at 527 nm. The binding of Cr^{3+} leads to an opening of the spirolactam ring and a highly delocalized π-conjugated system was formed. The Job plot confirmed the 1 : 1 stoichiometry of the complex between (**58**) and Cr^{3+} and has a binding constant of 4.16×10^4 mol^{-1}.

Elavarasi *et al.* developed a method to recognize Cr^{3+} ions in aqueous medium using gold nanoparticles (AuNPs) without any surface functionalization.[135] These citrate capped AuNPs undergo aggregation in the presence of Cr^{3+} ions and showed red shift in the surface plasmon resonance (SPR) peak from 526 nm to 714 nm and a visual color change from wine red to blue was observed. The formation of aggregates was confirmed through DLS and SEM studies. The AuNPs have good stability in aqueous medium due to strong electrostatic repulsion between negatively charged citrate ions. The Cr^{3+} ion chelates with the oxygen atoms of the citrate ion and binds in a 1 : 2 stoichiometry (Cr^{3+}·citrate), which results into cross-linking and subsequent aggregation of AuNPs. The aggregation may significantly affect the surface plasmon oscillation in the metallic nanoparticles and an enhancement in the emission spectrum was observed. The probe can successfully detect Cr^{3+} ions even in the presence of other competing cations like Cd^{2+}, Co^{2+}, Mg^{2+}, Hg^{2+}, Mn^{2+}, Ni^{2+}, Fe^{2+}, Zn^{2+}, Al^{3+}, Cu^{2+}, and Pb^{2+}. Furthermore, the probe can selectively bind to Cr^{3+} ions even in the presence of Cr^{6+} ions and it did not show any selectivity towards Cr^{6+} ions. A linear relationship was observed between the absorbance ratio ($A_{714/526}$) and the concentration of Cr^{3+} ions over a range of 10^{-3} to 10^{-6} M. The probe has a limit of detection of 1.06×10^{-7} M.

Elavarasi *et al.* reported a colorimetric method for the detection of chromium species *i.e.* Cr^{3+} and Cr^{6+} ions in an aqueous system using citrate capped silver nanoparticles.[136] Two types of silver nanoparticles were prepared through varying the amount of reducing agents (AgNP-I and AgNP-II). The AgNP-I nanoparticles interacted with Cr^{3+} ions and the plasmon resonance peak was shifted from 329 to 526 nm indicating the aggregation of AgNP-I induced by the Cr^{3+} ions. The aggregation formation was checked through SEM analysis. As per the Lewis acid–base theory, Cr^{3+} ions coordinate with oxygen-donating chelates in a 1 : 2 stoichiometry. Similarly, AgNP-II particles interacted with Cr^{3+} and showed a shift in the peak from 392 to 526 nm along with a color change from yellow to red. The SEM studies confirmed the formation of the aggregates. However, AgNP-II particles were also interacted with Cr^{6+} ions and showed a peak shift from 329 to 526 nm. The linear calibration curve was plotted and showed a linear relationship between the Cr^{6+} ion concentration and absorbance at 526 nm. Elavarasi *et al.* proposed that excess amount of $NaBH_4$ in the reaction mixture reduced Cr^{6+} ions to Cr^{3+} ions, which suggests that AgNP-II could estimate both Cr^{6+} and Cr^{3+} in aqueous solution.

8. Sensors for Fe^{2+}/Fe^{3+} ions

Iron is an important transition metal ion in the human body. It acts as a cofactor for many enzymes, is involved in oxygen transport, electron transport and oxidoreductase catalysis.[137] Excess amount of iron can initiate the formation of reactive oxygen species (ROS) through the Fenton reaction. These ROSs interact with lipids, nucleic acids and proteins, which results into the damage of their structures and a deviation from normal functioning. Several disorders like Alzheimer's, Huntington's, Parkinson's diseases, anaemia and low blood pressure are linked with iron.[138–140] Wu *et al.* reported pyrophosphate coated AuNPs for the selective detection of Fe^{3+} ions.[141] The AuNPs were prepared through reduction of $HAuCl_4$ with $NaBH_4$ in the presence of $Na_4P_2O_7$. The IR spectrum confirmed the coating of pyrophosphate on the surface of the AuNPs. These pyrophosphate AuNPs showed aggregation in the presence of Fe^{3+} ions, which results in a change in color and an SPR peak of $P_2O_7^{4-}$–AuNPs. Kim *et al.* reported a tripodial cap-type Schiff base (**59**) for the chromogenic detection of Fe^{2+} ion in aqueous solution (Fig. 22).[142] The binding of Fe^{2+} ions produced a color change from yellow to red. The probe (**59**) could discriminate Fe^{2+} from Fe^{3+} in aqueous medium. The probe (**59**) has an absorption peak at 400 nm and the addition of Fe^{2+} ions produced a new peak at 509 nm, which is attributed to the metal to ligand charge transfer and the red color of the solution. The titration experiment revealed that addition of Fe^{2+} led to a gradual decrease in absorbance at 272 nm and 400 nm; simultaneously, new bands at 257 nm, 325 nm and 509 nm appeared. The four isosbestic points were observed at 267 nm, 290 nm, 359 nm and 442 nm. The Job plot indicates a 1 : 1 stoichiometry between (**59**) and the Fe^{2+} complex and has a binding constant of $\log K_a = 4.30$. The detection limit was found to be in the micro-molar range (1.3 μM). The selectivity experiment showed only Cu^{2+} interference in the binding of Fe^{2+} ions.

Dwivedi *et al.* reported a novel anionic polyfluorene derivative, poly(9,9-bis(60-sulfate)hexyl) fluorene-*alt*-1,4-phenylene sodium salt (**60**) for the selective detection of Fe^{3+} ions under physiological conditions as shown in Fig. 22.[143] The binding of Fe^{3+} produced quenching in the emission spectrum of (**60**). The addition of Fe^{3+} caused a >97% reduction in fluorescence intensity. The possible reasons behind this robust quenching in emission

Published on 14 April 2016. Downloaded by Fail Open on 7/23/2025 9:06:09 AM.

intensity of (**60**) by Fe^{3+} are electron transfer, delocalization of excitons and competent energy migration along the polymer chain. These factors facilitate the efficient transfer of the excited states from the polymer (**60**) to Fe^{3+} and lead to a decrease in the emission intensity of (**60**). It was observed that during titration of (**60**) with Fe^{3+}, a blue shift along with quenching was also observed. The Stern–Volmer plot (K_{sv}) was plotted to calculate the binding constant and it was about 1.98×10^6 M^{-1}.

Raj *et al.* synthesized pyrene based Biginelli compounds (**61** and **62**) for the detection of Fe^{3+} ions in aqueous medium (Fig. 23).[144] These compounds proceed into organic nanoparticles using a reprecipitation method. The emission spectra of **61** and **62** have one peak at 470 nm representing the excimer and two other peaks at 380 nm and 395 nm corresponding to the monomer. It was observed that an addition of Fe^{3+} ions results into quenching in the emission intensity of **61** and **62**. The possible reason behind this quenching was the inner filter effect. The probes **61** and **62** have detection limits of about 7.94 μM and 6.31 μM, respectively. The probes **61** and **62** have high selectivity towards Fe^{3+} ions and the selectivity remain unchanged even in the presence of other competing cations.

Liu *et al.* synthesized a rhodamine-based chemosensor (**63**) for the detection of Fe^{3+} ions in aqueous solution (Fig. 23).[145] The resulting sensor (**63**) was synthesized through condensation of rhodamine-B hydrazine and 2-(*N*-methylpiperazinylimino)-acetaldehyde. The sensor (**63**) is colorless and has weak fluorescence. The metal binding test revealed that sensor (**63**) has high selectivity toward Fe^{3+} ions, a visual color change from colorless to pink and red emission was observed upon binding with Fe^{3+} ions. The titration experiment was performed using a UV-Visible and fluorescence spectrophotometer. The addition of Fe^{3+} ions produced a new band at 564 nm in the absorbance spectrum and produced a color change from colorless to pink. However, a new band at 588 nm appeared in the emission spectrum upon addition of Fe^{3+} ions. These changes are attributed to the opening of the spirolactam ring. The quantum yield of the (**63**)·Fe^{3+} complex was Φ = 0.303 and (**63**) was Φ = 0.009, approximately 34-fold higher. Probe (**63**) can selectively bind to Fe^{3+} ions even in the presence of other competing cations. Furthermore, Job's plot confirmed the 1 : 1 stoichiometry of the (**63**)–Fe^{3+} complex and the binding constant was about to be 6.90×10^3 M^{-1}.

Midya *et al.* synthesized a novel fluorescent probe (**64**) using Cu(I)-catalyzed Huisgen cycloaddition for the selective detection of Fe^{2+} ions in water at pH 7 as shown in Fig. 23.[146] The sensor (**64**) has a weak emission band at 390 nm and a has binding constant of about 5.3 μM, and titration with Fe^{2+} ions led to quenching in the emission intensity. However, sensor (**64**) did not show any change in the emission spectrum for Fe^{3+} ions. Therefore, sensor (**64**) showed high selectivity between Fe^{2+} and Fe^{3+} ions. The observed fluorescence quenching with Fe^{2+} ions may be due to photoinduced electron-transfer (PET) and excitation energy transfer (EET) phenomena arising from the fluorophore and Fe^{2+} interaction.

Wu *et al.* reported glutathione capped CdTe QDs (GSH-CdTe QDs) for the sensitive and selective detection of trace Fe^{2+}.[147] Both Fe^{2+} and Fe^{3+} could quench the emission intensity of GSH-CdTe QDs, however the kinetics of quenching was different for Fe^{2+} and Fe^{3+}. Therefore, the probe can be utilized for discriminating Fe^{2+} and Fe^{3+}. The emission spectrum of the GSH-CdTe QDs (30 nM) was quenched (18%) upon addition of Fe^{3+} ions (10 μM) and remained unchanged with time. On the other hand, addition of Fe^{2+} (10 μM) decreased the emission intensity (65%) of the GSH-CdTe QDs (30 nM) in the first 5 min and then slowly decreased by 15% in the next 25 min. Other transition metals like Cu^{2+}, Ni^{2+}, Co^{2+}, Zn^{2+} and Mn^{2+} also showed quenching but their

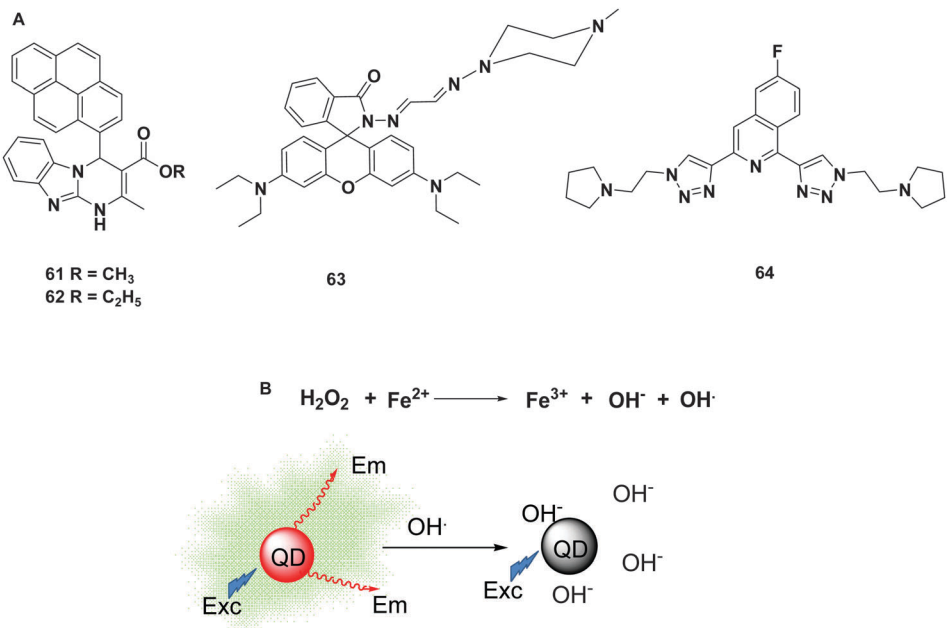

Fig. 23 (A) Structure of (**61–64**) and (B) Fe^{2+} induced hydroxyl generation and QD based sensors for Fe^{2+}.

 This journal is © The Royal Society of Chemistry 2016

Published on 14 April 2016. Downloaded by Fail Open on 7/23/2025 9:06:09 AM.

quenching kinetics are quite different from that of Fe^{2+}. Different capping agents like GSH, thioglycolic acid, and mercaptopropionic acid were employed but the time course of the fluorescence of the QDs for Fe^{2+} or Fe^{3+} remained unchanged. To increase the selectivity of GSH-CdTe QDs for Fe^{2+}, trace amount of H_2O_2 was added to establish a QD–Fenton hybrid system. The Fenton reaction between Fe^{2+} and H_2O_2 produced OH radicals, which can effectively decrease the emission intensity of the QDs through electron transfer from the conduction band of the QDs to a single occupied molecular orbit of a hydroxyl radical as shown in Fig. 23. The detection limit was about 5 nM for Fe^{2+} ions.

9. Sensors for Co^{2+} ions

Cobalt is an essential transition metal ion for the human body.[148] Several biological functions like the metabolism of iron, synthesis of hemoglobin, and synthesis of vitamin B_{12} are directly or indirectly linked with Co^{2+} ions.[149–151] Overdose of Co^{2+} may cause several diseases like asthma, decreased cardiac output, cardiac enlargement, heart diseases, lung infection, dermatitis and vasodilation.[21,152,153] Park *et al.* synthesized a probe (**65**) through the combination of julolidine and quinoline for the selective detection of Co^{2+} ions in aqueous system (bis–tris-MeOH buffer 999 : 1; v/v) as shown in Fig. 24.[154] The addition of Co^{2+} results in a change in color of the solution of (**65**) from yellow to orange. Upon titrating (**65**) with Co^{2+}, the absorption bands at 441 nm and 459 nm decreased and two new bands at 390 nm and 500 nm appeared with two clear isosbestic points at 398 nm and 479 nm. The Job plot analysis illustrated a 2 : 1 stoichiometry for the (**65**)–Co^{2+} complex. Furthermore, EPR spectra confirmed the presence of a 2+ oxidation state of cobalt in the complex. The binding constant was found to be 3.0×10^9 M^{-2} and the detection limit was about 1.28×10^{-6} M. The interference experiment revealed that probe (**65**) can selectivity detects Co^{2+} ions even in the presence of other competing cations. The pH titration results disclosed that sensor (**65**) can be utilized for sensing Co^{2+} ions in the pH range of 4–11.

Ding *et al.* designed a cationic bis-pyrene-based fluorophore (**66**) for the detection of Co^{2+} ions in aqueous solution (Fig. 24).[155] The two charged imidazole groups are introduced into the spacer. These charged imidazole groups could form assemblies with an ionic surfactant having opposite charge moieties. The anionic surfactant like SDS modified the photophysical properties of the bis-pyrene fluorophore. SDS can form supramolecular assemblies like pre-micelles, micelles or vesicles in aqueous solution and provide hydrophobic centers for fluorescent sensors. The addition of SDS increased the intensity of absorption as well as the emission spectra of probe (**66**), which may be due to change in environmental condition of fluorophore such as solvent polarity as the micelles provide hydrophobic local environment to solubilize the probe. Upon interacting with different metal ions, probe (**66**) showed selectivity towards Co^{2+} ions and quenching was observed in the emission spectra. The titration experiment revealed that Co^{2+} induces a remarkable decrease in the emission intensity of the excimer and the Stern–Volmer equation determined the binding constant to be 3.7 ($\pm$0.1) $\times$ 10^5 M^{-1}. The detection limit was found to be 6.0×10^{-8} M. Furthermore, pH studies revealed that sensor (**66**) is stable in the pH range of 7.52–4.89 with slight variations in the emission intensity.

Iniya *et al.* developed a pyridoxal linked aminoethylaminoethanol (PYET) probe (**67**) for the selective binding of Co^{2+} ions in aqueous solution (Fig. 24).[156] The probe (**67**) has good water solubility, optical sensitivity in a buffer medium, dual emission, a low detection limit and visible strong fluorescence under UV light upon binding with guest species. In sensor (**67**), pyridoxal phosphate will act as a signaling moiety because of its low quantum yield and good binding sites. The probe (**67**) has two absorption maxima at 328 nm and 387 nm; the addition of Co^{2+} produced a new band at 369 nm. Upon excitation at 350 nm, two emission peaks were observed at 445 nm and 510 nm, which indicate the possibility of the ESIPT mechanism. The band at 445 nm corresponds to the enol form and band at 510 nm is attributed to the keto form. The addition of Co^{2+} ions produced a ratiometric change in the emission spectrum enhancement at

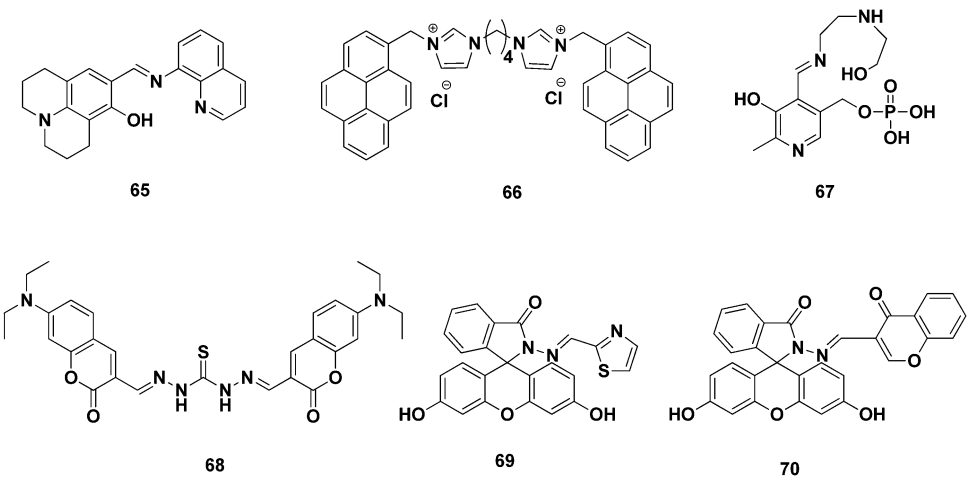

Fig. 24 Structure of (**65–70**).

Published on 14 April 2016. Downloaded by Fail Open on 7/23/2025 9:06:09 AM.

445 nm and simultaneously quenching at 510 nm, which results in the inhibition of the ESIPT phenomena. Job's plot indicated the 1:1 stoichiometry of the (**67**)–Co^{2+} complex. The detection limit and binding constant were found to be 6.42×10^{-7} M and 6.89×10^{4} M^{-1} in an aqueous system, respectively. The interference studies suggested that probe (**67**) can selectively bind to Co^{2+} ions even in the presence of other competing cations.

Maity *et al.* reported a thiocarbanohydrazone probe (**68**) based on coumarin Schiff base derivatives as an efficient colorimetric sensor for Co^{2+} ions in aqueous medium (Fig. 24).[149] The probe (**68**) has an absorption maximum at 470 nm. The addition of Co^{2+} produced a red-shift ($\Delta\lambda$ = 40 nm) in the absorption spectrum along with a color change from yellow to deep pink. The titration studies showed that an addition of Co^{2+} led to a decrease in the intensity of the band at 470 nm along with a red shift and after reaching 2.2 μM, the intensity of the peak started to increase and the maximum overall shifted to 510 nm. The probe (**68**) can selectively bind to Co^{2+} ions even in the presence 5 equiv. of other competing cations. Job's plot and mass analysis are in favor of a 2:1 stoichiometry between (**68**) and the Co^{2+} complex. The binding and signaling subunits are electronically bound to each other to produce the observed color change. The C═S bond is less stale due to poor overlapping between the $2sp^2$ orbital on carbon and the $3sp^2$ orbital on sulfur. Therefore, the thioamide group undergoes conjugation with nitrogen to stabilize the C═S bond and also coordinates to Co^{2+} after deprotonation, which results in a red shift and visible color change in the spectra.

10. Sensors for Ni^{2+} ions

Nickel is an essential micronutrient for animals and plants. It interacts with various amino acids, peptides and nucleic acids[157,158] and is involved as a cofactor for various enzymes like superoxide dismutases, hydrogenases and carbon monoxide dehydrogenases.[159] It may become the reason of various disorders like dermatitis, allergy, carcinogenesis and cell death.[160,161] Abebe *et al.* reported two new fluorescein-based chemosensors (**69**) and (**70**) for the rapid and selective detection of Ni^{2+} ions in an aqueous system (Fig. 24).[162] The probes (**69**) and (**70**) are very weakly fluorescent in solution and did not show any absorption peak in the visible region. The absorption spectra of (**69**) and (**70**) have a weak band above at 400 nm due to trace amount of the open ring form in the DMSO–water (2:98%; v/v) solvent system. However, the addition of Ni^{2+} produced a new peak at 500 nm with a sharp color change from colorless to yellow. The 1:1 stoichiometry of complexes (**69**)·Ni^{2+} and (**70**)·Ni^{2+} was confirmed through Job's plot. The addition of Ni^{2+} also produced enhancement in the emission intensity of (**69**). However, probe (**70**) did not show any change in fluorescence with Ni^{2+} ions.

Li *et al.* reported glutathione-stabilized silver nanoparticles (GSH-Ag NPs, **71**) for the colorimetric detection of Ni^{2+} ions in an aqueous system.[163] The as-synthesized GSH-Ag nanoparticles are very stable at pH > 3 due to strong interparticle electrostatic repulsion between the carboxylate anions of glutathione. Upon interacting with Ni^{2+} ions, the solution color changed from yellow to deep orange. Each Ni^{2+} ion binds to both terminal carboxylate groups of glycine and free-NH_2 group of glutamate as shown in Fig. 25. Therefore, an addition of Ni^{2+} leads to the aggregation of GSH-Ag nanoparticles. It was observed that the addition of 1,2-ethylenediamine can reverse the aggregated silver nanoparticles to a dispersed form. The probe (**71**) has high selectivity towards Ni^{2+} ions even in the presence of other competing cations except Co^{2+} having modest interference. The limit of detection for Ni^{2+} ions using GSH-Ag NPs is 7.5×10^{-5} mol L^{-1}.

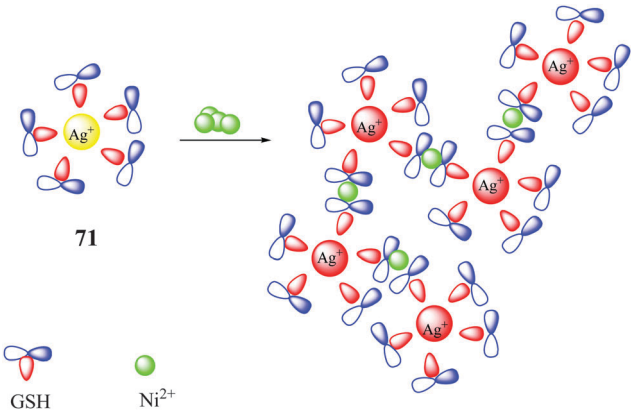

Fig. 25 Proposed mechanism of action of (**71**) (the addition of Ni^{2+} produced a colorimetric change).

Wang *et al.* reported fluorescent copolymer (**72**) for the detection of Ni^{2+} ions in aqueous solution.[164] The fluorescent copolymer is made up of the acrylic monomer Ac-HMPC and the copolymer of AM with Ac-HMPC using an initiator (Fig. 26). The fluorescence intensity of (**72**) increased gradually with a decrease in the pH of the solution and a decrease in intensity upon an increase in the pH of the solution. The piperazine group of coumarin performed two roles: (1) make an intramolecular H-bond between the phenolic OH and the N-1′ of piperazine ring, and (2) PET switch.

Under basic conditions, an intramolecular H-bond was introduced and the lone pair of nitrogen participated in the PET process and quenching was observed. Under acidic conditions, the proton of piperazine can increase the oxidation potential of the receptor and thermodynamically hinder the electron transfer. Upon interaction with different metal ions, probe (**72**) showed significant enhancement in the emission intensity with Ni^{2+} ions. The titration studies disclosed that the fluorescence intensity of probe (**72**) is a function of Ni^{2+} concentration. The coordination of Ni^{2+} ion leads to the involvement of the lone pair of the nitrogen atom of the piperazine group, which results into the cancellation of PET.

Dodani *et al.* reported a BODIPY dye based sensor (**73**) for the detection of Ni^{2+} ions as shown in Fig. 26.[165] The probe (**73**) has an absorption band at 495 nm and an emission maximum at 507 nm. The addition of 50 equiv. of Ni^{2+} enhanced the emission intensity of probe (**73**). The turn-on behavior of probe

 This journal is © The Royal Society of Chemistry 2016

Published on 14 April 2016. Downloaded by Fail Open on 7/23/2025 9:06:09 AM.

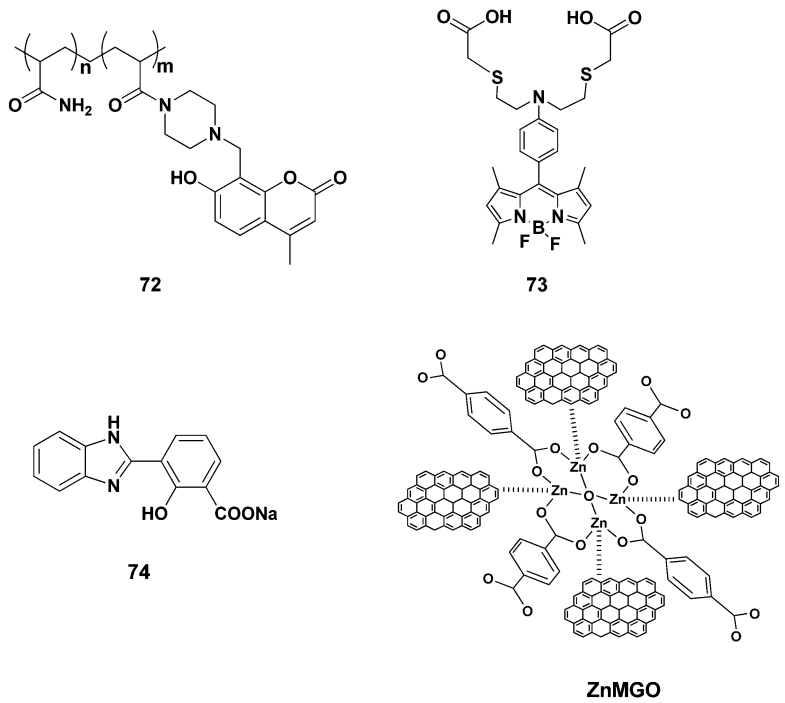

Fig. 26 Structure of (**72–74**) and Zn–MGO.

(**73**) for Ni^{2+} ions is reversible in nature, the addition of TPEN (chelator) restores the original spectrum of probe (**73**). The binding constant was calculated using Hill plot to be 193 ± 5 μM. Probe (**73**) has high selectivity towards Ni^{2+} ions even in the presence of Na^+, K^+, Mg^{2+}, Ca^{2+} and all first row divalent transition metal ions. Only copper ions show interference at 100 μM, but it is minimized at a lower concentration (2 μM).

11. Sensors for Cu^{2+} ions

Copper plays a vital role in normal physiological activities like bone formation, connective tissue development and cellular respiration.[166,167] Overdose of Cu^{2+} could induce neurodegenerative diseases like Menkes and Wilson's diseases, prion disease, familial amyotrophic lateral sclerosis and Alzheimer's disease.[168–170] Fu *et al.* reported a new water soluble fluorescent sensor 3-(1*H*-benzimidazol-2-yl)-2-hydroxy-benzoate sodium (**74**) for the detection of Cu^{2+} ions in aqueous medium (20 mM HEPES buffer, pH 7.4) as shown in Fig. 26.[171] The carboxylic group was introduced to enhance the water-solubility of the sensor. The probe (**74**) has a strong absorption band at 329 nm and the addition of Cu^{2+} ions gradually decreases the absorbance at 329 nm with a simultaneous increase in absorbance at 265 nm. Upon excitation at 243 nm, probe (**74**) gave a strong emission band at 436 nm. The addition of 1 equiv. of Cu^{2+} ions caused a complete quenching in the emission intensity along with a slight shift to 408 nm in the maximum. The probe (**74**) has high selectivity towards Cu^{2+} ions even in the presence of 10 equiv. of most of the competing ions. Job's plot and titration studies confirmed the 2 : 1 stoichiometry of the (**74**)·Cu^{2+} complex. The binding constant was found to be 3.22×10^5 M^{-1} and the detection limit was 2.77×10^{-6} M.

Hao *et al.* reported a graphene oxide (GO) functionalized Zn-based metal–organic framework (ZnMOF) for the selective detection of Cu^{2+} ions in phosphate-buffered saline (PBS) solutions (0.01 M, pH 5.00).[172] The probe has interactions between the carboxyl groups of GO and the metallic centre of ZnMOF as shown in Fig. 26. The absorbance spectra of ZnMGO has one broad band at 243 nm attributed to the $\pi \rightarrow \pi^*$ transition of aromatic carbon bonds. ZnMGO has absorbance maxima towards higher wavelength compared to GO due to the interaction between the carboxyl on the surface of GO and the metal center of ZnMOF. The emission spectra of the ZnMGO composite has a strong band at 442 nm and shows enhancement in the emission intensity upon addition of Cu^{2+} ions. At low pH values, Cu^{2+} addition leads to quenching with low efficiency because of the protonation of carboxyl groups located at the surface of the ZnMGO composite. When the solution is alkaline, the quenching efficiencies are not satisfied either, due to partial hydrolysis of Cu^{2+} ions in alkaline media. However, in weakly acidic medium (pH = 5.00), the quenching efficiency is better, meaning that a weakly acidic solution is suitable for sensing Cu^{2+} ions in aqueous medium. The detection limit was found to be 1.00 μM and the binding constant was found to be 3.07×10^4 M^{-1}. The probe has high selectivity for Cu^{2+} ions even in the presence of alkali, alkaline earth and heavy metal ions. Hao *et al.* speculate the possible luminescence mechanisms due to energy migration (EM) or energy transfer (ET) for the ZnMGO composite. The addition of Cu^{2+} weakened the bonds between the metallic sites and the organic ligands, leading to a collapse of the ZnMGO composite. Therefore, the coordination

Published on 14 April 2016. Downloaded by Fail Open on 7/23/2025 9:06:09 AM.

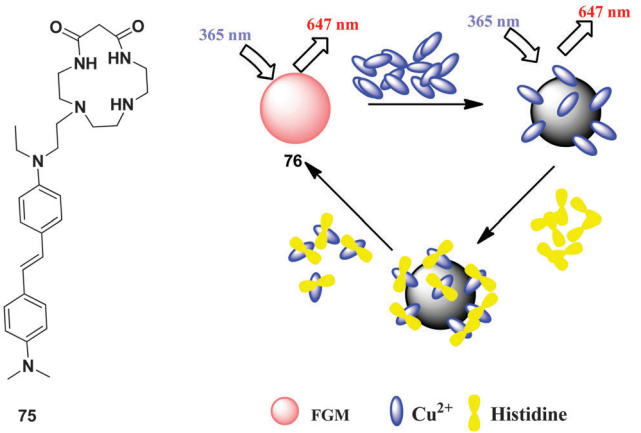

Fig. 27 Chemical structure of (**75**) and schematic representation of Cu^{2+} sensing using a fluorescent gold nanoclusters membrane (**76**).

between Cu^{2+} ions and the carboxyl groups of the ligand hindered the EM or ET process, resulting in fluorescence quenching.

Liu *et al.* designed a two-photon (TP) excited fluorescent chemosensor (**75**) for the detection of Cu^{2+} ion in aqueous medium containing 0.1% TX-100.[173] The probe (**75**) has macrocyclic dioxotetraamine as the Cu^{2+} ion receptor (Fig. 27). The probe (**75**) has an absorbance maximum located at 368 nm. The addition of Cu^{2+} ions results in a blue-shift in the absorption spectra and a gradual decrease in the absorption maxima at 368 nm along with a new absorption peak appearing at 343 nm.

The titration experiment points towards internal charge transfer (ICT) phenomena. The lone pair of the nitrogen atom of the aromatic amine coordinates to the Cu^{2+} ion, which in turn coordinates with the four nitrogen atoms on the macrocyclic dioxotetraamine ring to form a five coordinated complex with Cu^{2+} ions. The blue shift was raised due to the transfer of charge from the amine to the metal center. Thermodynamics studies demonstrated the formation of a 1 : 1 complex between (**75**) and Cu^{2+} ions, having an association constant 1.04×10^5 M^{-1}. The probe (**75**) showed quenching in the emission intensity upon addition of Cu^{2+} ions and the ICT phenomenon is responsible for the observed quenching in the emission spectra. The detection limit was found to be 0.01 μM.

Lin *et al.* reported a fluorescent gold nanoclusters membrane (FGM) as a visual sensor for Cu^{2+} ions in aqueous solution (Fig. 27).[174] The fluorescence of FGM (**76**) can be significantly quenched by Cu^{2+} ions and the emission intensity was recovered through the addition of histidine. The unsupported FGM was immersed into an aqueous solution without and with Cu^{2+} ions. Under UV light, FGM (**76**) emits a bright red light in the absence of Cu^{2+} ions and the fluorescent intensity significantly decreased in the presence of Cu^{2+} ions. The maximum quenching rate was observed at pH 6. It was detected that the fluorescence intensity of FGM (**76**) decreased with increasing interaction time, and their equilibrium values were reached after 10 min. The linear relationship was observed in the concentration range of 30–500 μM. The detection limit was found to be 10 μM and 0.5 μM by naked eyes and a fluorescence spectrophotometer, respectively. The FGM (**76**) sensor has a high selectivity towards Cu^{2+} ions, but the presence of Hg^{2+} ions interferes in the detection of Cu^{2+} ions. The addition of Hg^{2+} ions also caused quenching in the emission intensity of FGM (**76**).

Ahamed *et al.* reported an iminocoumarin based sensor (**77**) having pyridyl and benzothiazolyl moieties for the selective detection of Cu^{2+} ions in 10 mM HEPES buffer (Fig. 28).[175] The probe (**77**) exhibits an absorption band at 482 nm corresponding to the iminocoumarin ring. The addition of 10 equiv. of Cu^{2+} ions shifts the absorbance maximum to a higher wavelength (482 nm to 497 nm) along with a visual color change from yellow to orange. These changes are attributed to LMCT between (**77**) and Cu^{2+} ions through transfer of charge from the lone pair electron on nitrogen to the Cu^{2+} centre. However, the addition of Hg^{2+} ions also produced a negligible peak shift from 482 nm to 485 nm. The titration experiment showed a ratiometric response towards Cu^{2+} ions by (**77**) having two distinct isosbestic points at 454 nm and 534 nm. Job's plot analysis indicated the existence of a biphasic (1 : 1 as well as 2 : 1) (**77**)·Cu^{2+} complex stoichiometry in solution. The binding constant for 1 : 1 complex from UV-Visible titration was found to be 5.975×10^5 M^{-1}. The quenching in the emission intensity of (**77**) was observed upon addition of Cu^{2+} ions. Unlike the UV-Visible experiments, the emission spectra of (**77**) remained unaffected upon addition of Hg^{2+} ions. Job's plot again showed biphasic (1 : 1 and 2 : 1) (**77**)·Cu^{2+}

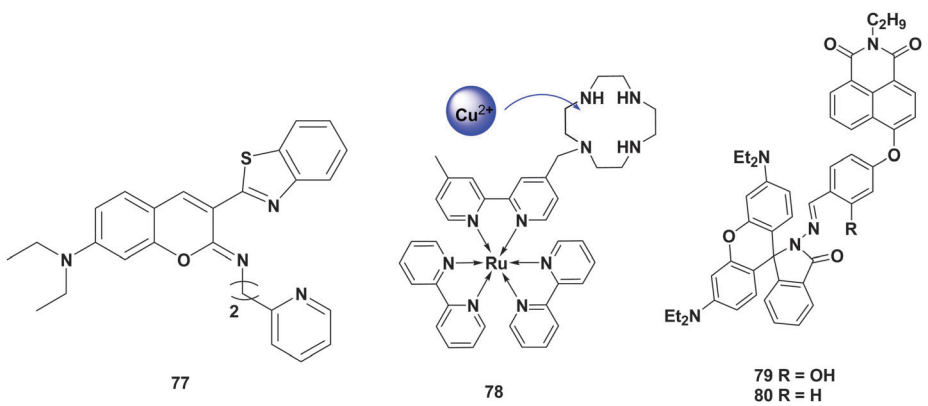

Fig. 28 Chemical structure of (**77–80**).

 This journal is © The Royal Society of Chemistry 2016

Published on 14 April 2016. Downloaded by Fail Open on 7/23/2025 9:06:09 AM.

complex stoichiometry using fluorescence titration data. The naked eye detection limit of Cu^{2+} ions is about 2 μM and 200 nM using emission data.

Li *et al.* reported a novel efficient luminescent chemosensor based on a 1,4,7,10-tetraazacyclododecane (cyclen)-tethered $Ru(bpy)_3^{2+}$ derivative for the detection of Cu^{2+} ions in 100% aqueous solution (Fig. 28).[176] The probe (**78**) has a strong absorbance maximum at 286 nm with two less intense bands at around 244 nm and 450 nm. The addition of Cu^{2+} ions did not produce any change in the absorbance spectra. Upon excitation at 450 nm, a broad emission peak was observed at 604 nm and addition of 1 equiv. of Cu^{2+} led to quenching in the emission intensity of the probe (**78**). Job's plot and ESI-MS analysis confirmed the 1 : 1 stoichiometry between (**78**) and Cu^{2+}. The Benesi–Hildebrand plot was employed to calculate the binding constant ($2.36 \times 10^4\ M^{-1}$).

Yu *et al.* reported a novel Cu^{2+} specific "off–on" fluorescent chemosensor (**79**) of naphthalimide modified rhodamine B for the selective detection of Cu^{2+} ions in aqueous medium [ethanol–water solution (1 : 9, v/v, 50 mM HEPES, pH 7.0)] as shown in Fig. 28.[177] The addition of Cu^{2+} ions raised two new bands in the absorbance spectra at 391 nm and 556 nm with two isosbestic points at 315 nm and 356 nm. Job's plot and ESI-MS analysis confirmed the 1 : 1 stoichiometry between (**79**) and Cu^{2+} ions. The peak above 500 nm was raised due to the rhodamine ring opening process. The detection limit was calculated to be 0.018 μM. However, the emission intensity of probe (**79**) at 450 nm gradually decreased and, simultaneously, a new band was observed at 580 nm. The possible reason behind this phenomenon was the increased fluorescence resonance energy transfer (FRET) from 1,8-naphthalimide to the open form of rhodamine. To confirm the importance of the hydroxyl group, probe (**80**) was synthesized having a hydrogen atom in place of the hydroxyl group. The probe (**80**) did not show any change in the absorption spectra upon binding with Cu^{2+} ions, which shows that the hydroxyl group played a significant role in binding Cu^{2+} ions. Further, addition of Na^+, Ag^+, Zn^{2+}, Pb^{2+}, Co^{2+}, Cd^{2+}, Ni^{2+}, Ca^{2+}, Mg^{2+}, Hg^{2+}, Cr^{3+} and Fe^{3+} did not produce any spectral change of probe (**79**). It means that probe (**79**) has high selectivity for Cu^{2+} ions.

12. Sensors for Zn^{2+} ions

Zinc is the second most abundant essential trace element in the human body. It catalyzes several biological reactions and pathological processes.[178–180] It is linked to severe neurological disorders such as Alzheimer's disease and Parkinson's disease and other diseases like epilepsy, ischemic stroke, and infantile diarrhea.[181–183] Chen *et al.* designed a water-soluble fluorescent sensor (**81**) [2-(2′-aminophenyl)benzoxazole-amide-2-picolylamine] for the detection of Zn^{2+} ions in aqueous solution (Fig. 29).[184] The probe (**81**) has very weak fluorescence in Tris-HCl buffer (10 mM, pH 7.2). The addition of Zn^{2+} ions enhanced the emission intensity of probe (**81**) at 445 nm. The binding constant for Zn^{2+} was found to be $4.3 \times 10^5\ M^{-1}$. Job's plot has a maximum at 0.5, which corresponds to a 1 : 1 stoichiometry of the (**81**)·Zn^{2+} complex. The stoichiometry was also confirmed through ESI-MS analysis. The detection limit and limit of quantification were measured to be 3.66×10^{-8} M and 1.22×10^{-7} M, respectively. The sensor (**81**) can selectively bind to Zn^{2+} ions regardless the effect of other metal ions. The coordination of Zn^{2+} ions induced the conformation restriction as well as cancellation of PET quenching.

Saluja *et al.* reported a chemosensor (**82**) having a long hydrocarbon chain and polar end group for the selective and sensitive detection of Zn^{2+} ions in aqueous 1% Triton-X-100 solution.[185] The probe (**82**) has a chelate ring for effective binding of Zn^{2+} ions and the chelate ring consists of an OH group and sp^2 nitrogen donor (Fig. 29). The probe (**82**) has two emission bands at 355 nm and 440 nm corresponding to the enol and keto forms of (**82**) respectively through excited state intramolecular proton transfer (ESIPT). The addition of Zn^{2+} ions significantly enhanced the emission intensity of probe (**82**) at 440 nm. The binding of Zn^{2+} ions inhibits the ESIPT phenomenon and results in an enhancement in intensity at 440 nm. Job's plot and mass spectra advocate the 1 : 1 stoichiometry of the (**82**)·Zn^{2+} complex. The binding constant was found to be 1.05 (±0.3) × 10^5 and the detection limit was calculated to be 8 nM. The sensor (**68**) has high selectivity for Zn^{2+} ions even in a complex environment.

Kim *et al.* reported a cap-type Schiff base (**83**) for the fluorogenic and chromogenic detection of Zn^{2+} ions in a 10 mM HEPES buffer–CH_3OH (99 : 1; v/v) solvent system as shown in Fig. 29.[142] The addition of Zn^{2+} ions turns on the fluorescence signal of probe (**83**) and is also employed for mapping zinc levels in cells for bioimaging applications. The addition of Zn^{2+} ions produced enhancement in the emission intensity of probe (**83**). The binding of Zn^{2+} ions with probe (**83**) leads to chelation-enhanced fluorescence effects and inhibition of C=N isomerization. Titration was also performed on a UV-Visible spectrophotometer. The addition

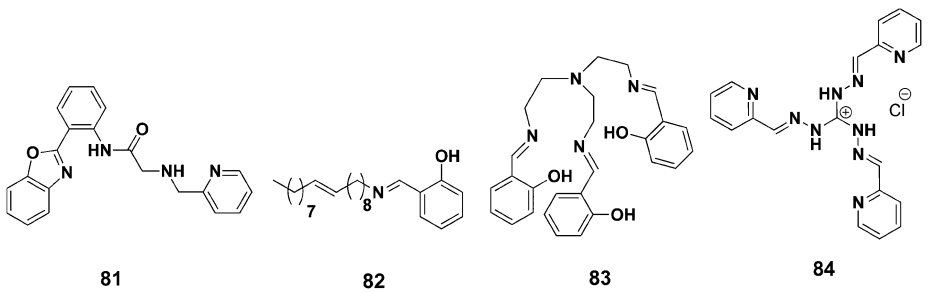

Fig. 29 Structure of (**81–84**).

Published on 14 April 2016. Downloaded by Fail Open on 7/23/2025 9:06:09 AM.

of Zn^{2+} ions leads to a gradual decrease in the absorbance intensity at 272 nm and 400 nm, and a simultaneous enhancement in absorbance at 260 nm and 341 nm with three distinct isosbestic points at 267, 301 and 364 nm. Job's plot and mass analysis advocate the 1 : 1 stoichiometry between (**83**) and Zn^{2+} ions. The binding constant and detection limit were found to be log K_a = 4.52 and 1.1 μM, respectively. The probe (**83**) has high selectivity for Zn^{2+} ions even in the presence of other competing metal ions.

Zhou *et al.* reported a fluorescent chemosensor tris(2-pyridinecarboxaldehyde)triaminoguanidinium chloride (**84**) for the detection of Zn^{2+} ions in aqueous system (10 mM Tris-HCl, pH 7.54) as shown in Fig. 29.[186] The absorbance spectra of probe (**84**) have a broad band at 325 nm. During titration, the intensity of the band at 325 nm decreased with a concomitant gradual increase of a new band at 396 nm with a distinct isosbestic point at 371 nm. Upon excitation at 370 nm, probe (**84**) displayed a weak band in the emission spectra at 483 nm. However, addition of Zn^{2+} led to a prominent enhancement in the emission intensity along with a color change from colorless to dark yellow. The enhancement in the emission spectra may be attributed to the formation of the (**84**)·Zn^{2+} complex, in which C═N isomerization and proton transfer (ESIPT) are inhibited. Upon binding with Zn^{2+} ions, the emission maxima showed a significant bathochromic shift of 97 nm from 483 to 580 nm, indicating the existence of a chelation-enhanced fluorescence (CHEF) mechanism. Job's plot indicates a 1 : 3 stoichiometry for the (**84**)·Zn^{2+} complex, which is also confirmed from single-crystal X-ray spectroscopy. The binding constants of (**84**) with Zn^{2+} were found to be $K_{Zn1} = 1.9 \times 10^5$, $K_{Zn2} = 1.5 \times 10^4$ and $K_{Zn3} = 6.1 \times 10^3$, respectively, and the detection limit was calculated to be 2.5×10^{-6} M. The probe (**84**) has a high selectivity for Zn^{2+} ions even in the presence of other transition metal ions except Cu^{2+} ions.

13. Sensors for Ag^+ ions

Silver metal gained considerable attention due to several possible roles in biological systems, such as: (i) interaction and inactivation of vital enzymes,[187,188] (ii) binding to DNA,[189] (iii) interaction with the cell membrane,[190] and (iv) interference with electron transport[191] and antimicrobial activity.[192] Hatai *et al.* reported the thiocarbamate based sensor (**85**) for the selective detection of Ag^+ ions in aqueous medium (H_2O/DMSO, 99 : 1, v/v) as shown in Fig. 30.[193] The naphthoyl unit worked as a hydrophobic fluorophore. In methanolic solution, sensor (**85**) showed a ratiometric behavior in its absorption spectra upon addition of Ag^+ ions. Likewise, the emission spectra of probe (**85**) showed an enhancement in intensity in the presence of Ag^+ ions. However, the lipophilic ligand (**85**) forms nanoaggregates in the aqueous medium, which is confirmed through dynamic light scattering (DLS) studies.

The addition of Ag^+ ions accelerates the aggregate formation and large aggregates are obtained. Job's plot and mass analysis showed a 1 : 1 stoichiometry between (**85**) and Ag^+ ions. The binding

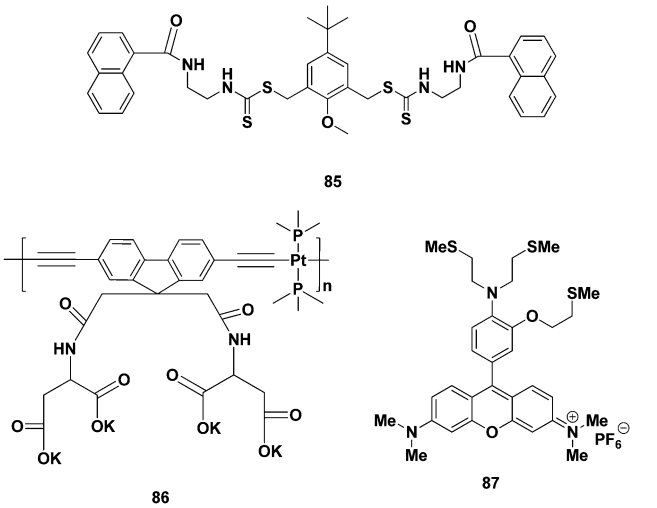

Fig. 30 Structure of (**85–87**).

constant is found to be 1.37 (±0.4) × 10^6 M^{-1}. The probe has high selectivity for Ag^+ ions. The fluorescence response of (**85**) for Ag^+ ions was not altered even in the presence of other competing metal cations.

Qin *et al.*, in 2011, reported a organometallic conjugated polyelectrolyte (**86**) based on an aspartic acid-substituted fluorescence spacer for the detection of silver ions in water (Fig. 30).[194] The probe (**86**) showed a visual color change from colorless to yellow upon addition of Ag^+ ions. The addition of Ag^+ ion produced a large bathochromic shift of 25 nm. Similarly, the emission maxima of probe (**86**) showed a red shift of 40 nm upon addition of Ag^+ ions. The possible reason behind this change was intersystem crossing (ISC). The addition of Ag^+ ions promotes the intersystem crossing from singlet to triplet states. The probe (**86**) has a broad response range from 1 μM to 4 mM, with a detection limit of 0.5 μM. The Stern Volmer (SV) plot was drawn using fluorescence data and the binding constant was found to be 1.9 × 10^5 M^{-1}. The probe (**86**) retained its selectivity for Ag^+ ions even in the presence of other competing metal cations.

Iyoshi *et al.* reported a water soluble rosamine-based fluorescent chemosensor for Ag^+ ions as shown in Fig. 30.[195] The probe (**87**) has an emission maximum at 574 nm and the addition of Ag^+ ions leads to a significant enhancement in the emission intensity in the 50 mM HEPES (pH 7.20 and 0.1 M KNO_3) aqueous system. The fluorescence of probe (**87**) did not show any change above pH 5 and the enhancement in intensity was observed with a decrease in pH, which means cancellation of the PET process through protonation of the aniline nitrogen. However, the fluorescence intensity of the (**87**)·Ag^+ complex remains unchanged in a wide range of pH (from 2 to 12). Job's plot indicates a 1 : 1 stoichiometry for the (**87**)·Ag^+ complex and has a good dissociation constant (K_d = 2.0 μM). ^{1}H NMR titration suggested that aniline nitrogen is bound with the Ag^+ center in the solution state, which inhibits the PET process and results in the enhancement of fluorescence. The probe (**87**) also showed a slight enhancement in the fluorescence intensity for

 This journal is © The Royal Society of Chemistry 2016

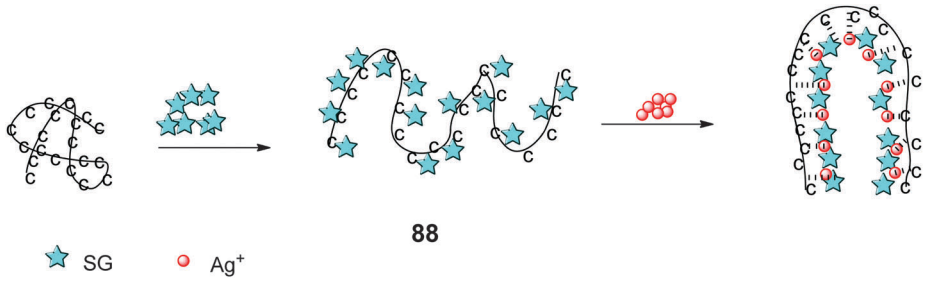

Fig. 31 A schematic representation of recognition of Ag^+ ions using double strand chelating dye SYBR green I (SG).

Published on 14 April 2016. Downloaded by Fail Open on 7/23/2025 9:06:09 AM.

the Cu^+ and Cu^{2+} ions. However, other metals did not produce any change in fluorescence intensity.

Lin *et al.* reported a label-free assay for the highly sensitive and selective detection of Ag^+ ions in aqueous solution (20 mM MOPS and 50 mM $NaNO_3$ at pH 7.0) as shown in Fig. 31.[196] The probe (**88**) consists of repeats of 20 cytosine (C) nucleotides (C_{20}) and a double strand chelating dye SYBR green I (SG). The 20 C nucleotides (C_{20}) have a random coil structure and exhibit weak interaction with SG as shown in Fig. 31.

Due to this weak interaction, probe (**88**) has a weak fluorescence intensity. However, the addition of Ag^+ ions accelerates the formation of C–Ag^+–C complexes and enables C_{20} to change its conformation from a random coil to a folded structure. C_{20} takes 10 min to adopt the folded conformation. However, other DNA probes containing 20-repeat adenosines (A_{20}), 20-repeat thymines (T_{20}) and guanines (G) were prepared but they did not show any particular response toward Ag^+ ions. The binding studies were performed in 3-morpholinopropanesulfonic acid (MOPS) buffer due to the weak interaction between Ag^+ and MOPS. The probe (**88**) has a maximum emission at pH 7. The probe has a detection limit in the nanomolar range (32 nM). The probe can selectively bind to Ag^+ even in the presence of other competing metal ions.

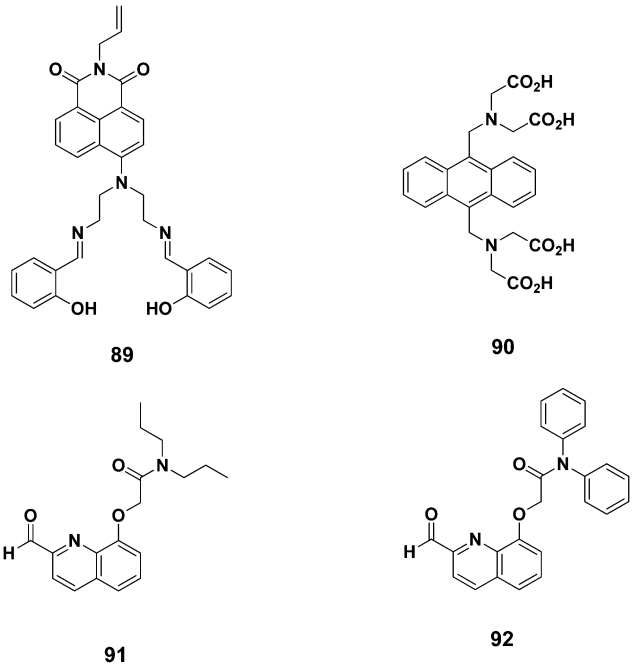

Fig. 32 Chemical structure of (**89–92**).

14. Sensors for Cd^{2+} ions

Cadmium is extensively employed in many products such as the production of nickel–cadmium rechargeable batteries for cellular phones and is also found in phosphate fertilizers.[197,198] The Cd^{2+} ion has a serious toxicological effects on the environment and human beings. It can cause serious injury to human kidneys, bones, lungs and nerve system, which induce renal dysfunction, calcium metabolism disorders and an increased probability of certain forms of cancers.[199,200] Wang *et al.* reported a naphthalimide-based fluorescent sensor (**89**) having *N*,*N*′-bis-(salicylidene)diethylenetriamine for the detection of Cd^{2+} ions in aqueous solution (0.1 M HEPES–NaOH (ethanol–water = 1 : 10, v/v, pH = 7.14)) as shown in Fig. 32.[201] The addition of Cd^{2+} ions leads to a 4-fold enhancement in the fluorescence intensity of probe (**89**), but the absorbance at 445 nm did not change. The fluorescence of probe (**89**) is a function of the concentration of the Cd^{2+} ions. Job's plot exhibited a maximum at 0.5, which corresponds to a 1 : 1 stoichiometry between (**89**) and Cd^{2+} ions. The association constant using fluorescence data was found to be 2.4×10^7 M^{-1} and the detection limit was found to be 5.2×10^{-7} mol L^{-1}. The probe (**89**) has high selectivity towards Cd^{2+} ions even in the presence of other competing cations except Cu^{2+} ions.

Kim *et al.* reported a anthracene based fluorescent PET sensor (**90**) for the detection of Cd^{2+} ions in aqueous medium (0.1 M CAPS, pH 10) as shown in Fig. 32.[202] The addition of Cd^{2+} ions leads to the enhancement in the emission intensity of probe (**90**). The chelation-enhanced fluorescence (CHEF) is responsible of this increase in emission intensity. The association constant was calculated to be 69 100 M^{-1}. The probe (**90**) and Cd^{2+} ions formed complexes in a 1 : 1 stoichiometry which is confirmed through Job's plot. It means that two binding sites at the 9,10-positions of anthracene generate a cooperative binding site for Cd^{2+} ions.

Tian *et al.* utilized 2-(2-formylquinolin-8-yloxy)-*N*,*N*-diisopropylacetamide (FQDIPA) (**91**) and 2-(2-formylquinolin-8-yloxy)-*N*,*N*-diphenylacetamide (FQDPA) (**92**) for the fluorogenic detection of Cd^{2+} ions in 99% aqueous solution as shown in Fig. 32.[203]

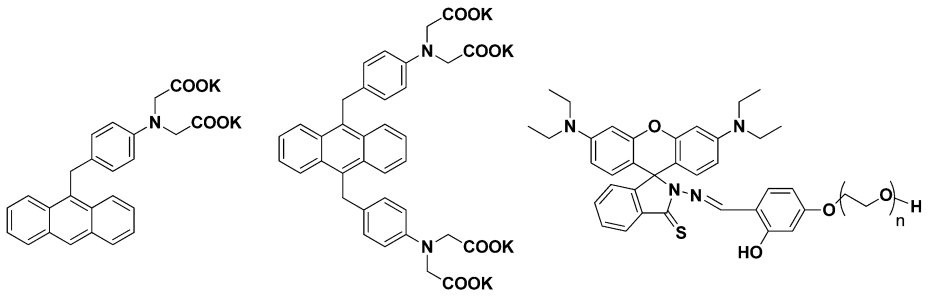

Fig. 33 Structure of (**93–95**).

Published on 14 April 2016. Downloaded by Fail Open on 7/23/2025 9:06:09 AM.

The probes (**91**) and (**92**) have broad absorption spectra centers at 305 nm in 50 mM Tris-HCl (ethanol–H_2O, v/v = 1 : 99, pH = 7.42) solution. The addition of Cd^{2+} produced a red shift in the absorption peak of (**91**) and (**92**). The observed red shift was attributed to the formation of three five-membered chelated rings between Cd^{2+} ion and the quinoline moiety through one nitrogen atom and three oxygen atoms, which results in the extension in conjugation and a reduced energy difference between the n and π^* orbitals. FQDIPA (**91**) showed better selectivity for Cd^{2+} ions under physiological pH conditions. It was observed that the addition of Cd^{2+} ions produced a more significant enhancement in the fluorescence intensity of FQDIPA than for FQDPA. Furthermore, interference study experiments revealed that FQDIPA has better selectivity for Cd^{2+} ions than FQDPA in the presence of other competing cations. The stability constant value of FQDIPA for Cd^{2+} was calculated to be $(1.306 \pm 0.518) \times 10^5\ M^{-1}$ and FQDPA has $(1.068 \pm 0.382) \times 10^5\ M^{-1}$. The Job plot experiment indicates a 1 : 1 stoichiometry for (**91**)·Cd^{2+} and (**92**)·Cd^{2+} complexes. FQDIPA and FQDPA have a 0.6 ppm and 0.8 ppm limit of detection, respectively.

Gunnlaugsson *et al.* reported two fluorescent chemosensor (**93**) and (**94**) for the selective detection of Cd^{2+} ions in water.[204] The anthracene moiety acts as a fluorophore and aromatic iminodiacetate behaves as the receptor (Fig. 33). The photophysical properties of (**93**) and (**94**) are dependent upon the pH of the system and the emission intensity of both was switched off between 3 and 11 in 100% water. The addition of Cd^{2+} ions into the solution of (**94**) produced minor changes in the monomeric emission with the rise of a new band at 500 nm. The probe (**93**) also showed a similar behavior upon addition of Cd^{2+} ions with a narrower band centered at 506 nm. The binding constants were found to be $\log \beta$ 3.9 ± 0.1 and 4.2 ± 0.1 for (**94**) and (**93**) respectively.

15. Sensors for Hg^{2+} ions

Mercury is one of the most dreaded toxins and highly dangerous metals, both the elemental and ionic forms of mercury can be converted into methyl mercury through microorganisms.[205,206] Methyl mercury is a potent neurotoxin and causes several cognitive and motion disorders.[207,208] Mercury enters the environment both from natural sources (oceanic/volcanic emissions) and human activities (industrial effluents and waste incineration).[209,210]

Hazra *et al.* reported a water soluble rhodamine-based chemosensor (**95**) for the detection of Hg^{2+} ions in aqueous system (NaOAc–HOAc, pH 7.2) as shown in Fig. 33.[211] The addition of Hg^{2+} ions to the aqueous solution of the probe (**95**) results into a new band in the emission spectra at 585 nm, corresponding to the ring-opened state of rhodamine. It means that the Hg^{2+} ion triggers the opening of the spirolactam ring. Job's plot analysis indicates a 1 : 1 stoichiometry for the (**95**)·Hg^{2+} complex. Similarly, the absorbance spectra of probe (**95**) showed a new peak at 558 nm upon addition of Hg^{2+} ions. The interference studies indicated that Hg^{2+}-induced fluorescence output of the probe (**95**) was not much affected even in the presence of other metal ions. The detection limit was found to be 7×10^{-7} M.

Singh *et al.* reported a rhodamine-based dipodal framework (**5**) for the detection of Hg^{2+} ions in water (Fig. 19).[82] The rhodamine-based dipodal framework was processed into fluorescent organic nanoparticles (FONs) through a reprecipitation method. The addition of Hg^{2+} ions produced a new emission band in the fluorescence spectra of (**5**) at 547 nm. The fluorescence intensity of probe (**5**) is a linear function of the Hg^{2+} ion concentration range of (0.1 nM to 10 μM) with a detection limit of 0.1 nM. The addition of Hg^{2+} ions produced an intense pink color with a strong band in the absorbance spectra at 530 nm. The possible mechanism behind this color change was the opening of the spirolactam ring, which results into strong fluorescence and intense absorbance at 530 nm. Job's plot and mass analysis confirmed the 1 : 1 stoichiometry of the (**5**)·Hg^{2+} complex and the association constant was determined to be $4.0 \times 10^6\ M^{-1}$. The interference studies conclude that no significant variation in the UV-Visible and fluorescence spectra was found with and without the other competing metal ions.

Liu *et al.* reported a FRET-based ratiometric sensor (**96**) for the recognition of Hg^{2+} ions in water (0.01 M HEPES buffered, pH 7.0) as shown in Fig. 34.[212] The probe (**96**) was fabricated through depositing a multilayered silica structure on a quartz plate followed by three ultrathin functional layers (donor, spacer and receptor).

Upon interaction with an aqueous solution of Hg^{2+}, the non-fluorescent receptor (a spirolactam rhodamine derivative) on the surface could form a complex with Hg^{2+} ions and behave as the acceptor of the energy transfer. Upon excitation, the donor molecule (nitrobenzoxadiazolyl derivative, NBD) transfers its energy to the acceptor molecule *via* the 'through space' energy

 This journal is © The Royal Society of Chemistry 2016

Published on 14 April 2016. Downloaded by Fail Open on 7/23/2025 9:06:09 AM.

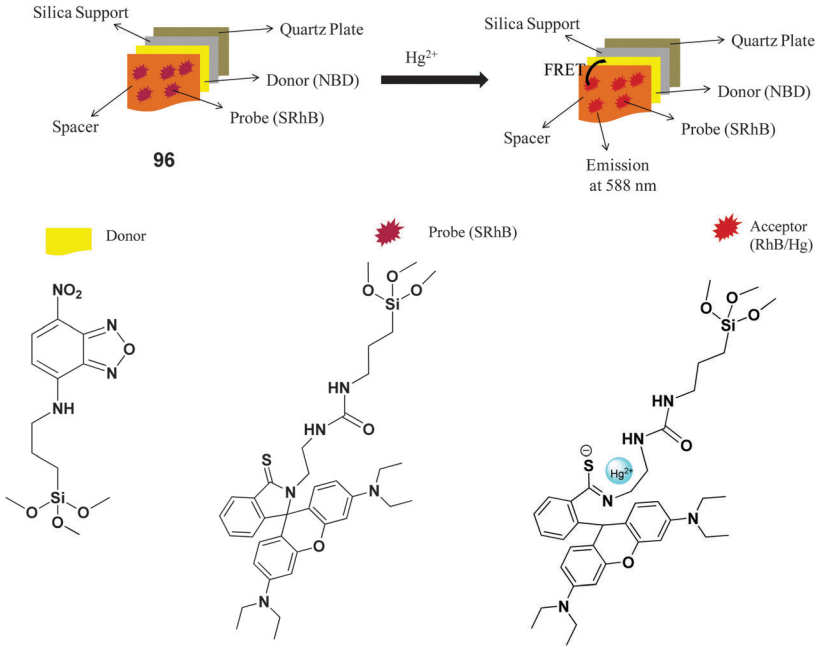

Fig. 34 A schematic representation of FRET-based ratiometric sensor (**96**) and the structure of the donor, probe and acceptor. It was fabricated using a quartz plate followed by deposition of three ultrathin functional layers (donor, spacer and receptor).

transfer process, which results into FRET based sensing of Hg^{2+} ions. The probe (**96**) has a detection limit of 1 μM. Liu *et al.* developed a FRET-based ratiometric sensor (**97**) for Hg^{2+} ion detection in water (HEPES buffer at pH 7.0) using CdTe QDs as the donor fluorophore as shown in Fig. 35.[213] The probe (**97**) was fabricated through doping QDs into specific sites of silica particles and each QD was covered with a positively charged spacer layer followed by covalent binding of a spirolactam rhodamine derivative onto the particle surface.

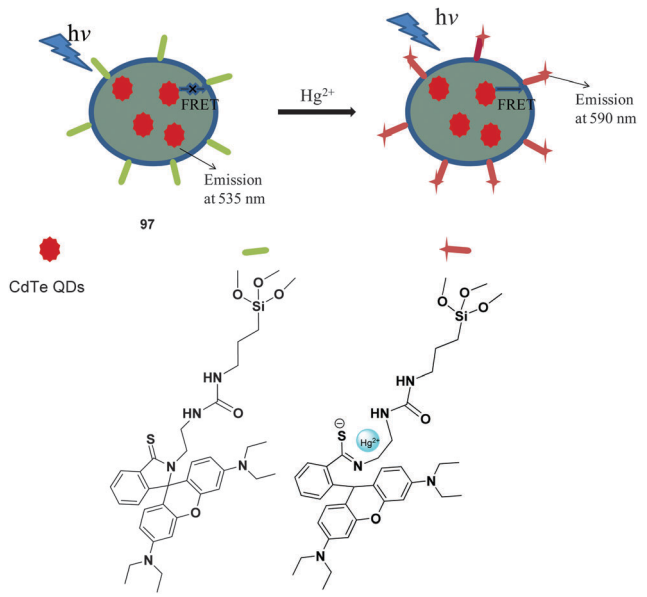

Fig. 35 A schematic representation of FRET-based CdTe QDs (**97**) for the detection of Hg^{2+} ions.

These QDs are optically inert in the absence of Hg^{2+} ions, while the presence of Hg^{2+} ions can induce the ring opening reaction of spirolactam rhodamine and fluorescence enhancement was observed. The probe (**97**) has a detection limit of 260 nM with high selectivity towards Hg^{2+} ions and can be used in a wide pH range.

Li *et al.* reported a hemicyanine-based water soluble chemosensor (**98**) for the detection of Hg^{2+} ions in water (Fig. 36).[214] The probe (**98**) has an intense charge transfer band at 529 nm in water and the addition of 10 equiv. of Hg^{2+} ions results into a change in color from red to colorless. The addition of Hg^{2+} ions produced a new band at 384 nm and a decrease in the intensity of the band at 529 nm. The emission spectra of probe (**98**) showed quenching at 587 nm upon addition of Hg^{2+} ions. No interference was observed in the presence of 50 equiv. of other competing metal ions, which indicates the high selectivity of probe (**98**) for Hg^{2+}. Job's plot and mass analysis indicate a 1 : 1 stoichiometry between (**98**) and Hg^{2+} ions with a binding constant of $4.30 \times 10^5\ M^{-1}$.

16. Sensors for Al^{3+} ions

Aluminum is the third most abundant metal element in the Earth's crust (8.8%) after oxygen and silicon. Due to the widespread use of aluminum such as the treatment of water, food additives, the paper industry, the textile industry, kitchen utensils and also in the production of light alloys,[215,216] accumulation of excessive amounts of aluminum in the human body damages the central nervous system causing Parkinson's disease and kidney diseases; it reduces total bone and matrix causing osteoporosis, and osteomalacia.[217–219] It also hinders plant growth and causes

Published on 14 April 2016. Downloaded by Fail Open on 7/23/2025 9:06:09 AM.

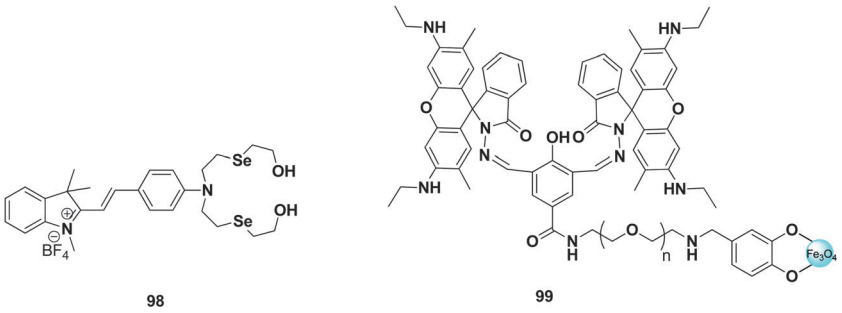

Fig. 36 Structure of (**98**) and (**99**).

acidification of water. Zhi *et al.* employed rhodamine coated Fe_3O_4 nanoparticles for the selective and sensitive detection of Al^{3+} ions in aqueous medium (HEPES buffer) under a physiological pH as shown in Fig. 36.[220] The probe (**99**) showed a weak emission band at 543 nm and the addition of Al^{3+} ions significantly enhanced its intensity. The binding constant was found to be 3.2×10^7 M^{-1}. The 1 : 1 binding mode between (**99**) and Al^{3+} ions was confirmed through ESI-MS spectra. The selectivity of probe (**99**) towards Al^{3+} ions retained even in the presence of other competing metal ions. The detection limit was found to be 0.3 ppb.

Saini *et al.* reported naphthalimide based fluorescent organic nanoparticles for the selective detection of Al^{3+} ions in water (Fig. 37).[221] The probe (**100**) showed dual emission at 390 nm and 494 nm. The addition of Al^{3+} ions leads to an enhancement in intensity at 390 nm. The titration experiment showed a good linear relationship between the fluorescence intensity and concentration of Al^{3+} ions and the detection limit is 677 nM. The coordination of Al^{3+} ions increased the static confirmation through multivalent interactions. The probe (**100**) has high selectivity for Al^{3+} ions. Sen *et al.* reported a chelation enhanced fluorescence (CHEF) type Schiff base probe (**101**) to facilitate the chelation of Al^{3+} ions in aqueous medium (HEPES buffer, DMSO/water: 1/100, v/v at pH 7.4) as shown in Fig. 37. The absorption spectra of probe (**101**) have two peaks centered at 335 nm and 392 nm, which gradually decrease with the addition of Al^{3+} ions and a new peak at 412 nm appeared. The addition of Al^{3+} ions induced a color change from yellow to reddish-yellow. The addition of Al^{3+} ions enhanced the emission intensity of probe (**101**) at 470 nm. The binding constant was calculated to be 0.35×10^5 M^{-1} and the 1 : 1 stoichiometry of the (**101**)·Al^{3+} complex was confirmed through Job's plot. In the absence of Al^{3+} ions, the fluorescence intensity of probe (**101**) is greatly reduced due to the internal charge transfer (ICT) mechanism, while in the presence of metal ions, ICT is hindered and the fluorescence intensity is increased due to rigid chelated complex formation.

17. Sensors for Pb^{2+} ions

Lead is one of the most ubiquitous and toxic heavy metals. The main sources of lead are batteries, gasoline and pigments, which result into a wide distribution in the environment such as the air, soil, and water.[222,223] Owing to its poisonous nature, it may become the reason for several disorders such as anemia, neurological damage, physical growth impairments, nerve disorders, memory loss, kidney disorders, and a reduced IQ.[224–226] Xu *et al.* designed cyclen-functionalized anthracene conjugates (**102**) for the selective and sensitive detection of Pb^{2+} ions in aqueous solution (50 mM HEPES buffer, pH 7.4) as shown in Fig. 37.[227] The pH studies revealed that the fluorescence intensity of (**102**) remained stable in a pH range of 2–10. The addition of 1 equiv. of Pb^{2+} caused a 3-fold enhancement in the fluorescence intensity of probe (**102**). Job's plot indicates a 1 : 1 stoichiometry between (**102**) and Pb^{2+} ions. The interference study showed that probe (**102**) has high selectivity toward Pb^{2+} ions even in the presence of other competing metal ions except Cu^{2+} and Hg^{2+}.

Zhou *et al.* reported cyclen-functionalized perylenediimides (**103**) and (**104**) for the highly sensitive and selective detection of Pb^{2+} ions in aqueous solution (10 mM HEPES buffer, pH 7.2) as shown in Fig. 38.[228] Cyclen (1,4,7,10-tetraazacyclododecane) was employed as an ionophore and introduced into the fluorescent skeleton *via* an alkyl chain. The addition of Pb^{2+} ions results into a change in color from dark red to yellow in an aqueous solution of (**103**) under a UV lamp. However, other metal ions did

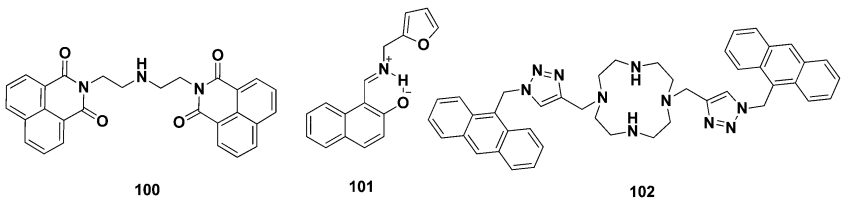

Fig. 37 Chemical structure of (**100–102**).

 This journal is © The Royal Society of Chemistry 2016

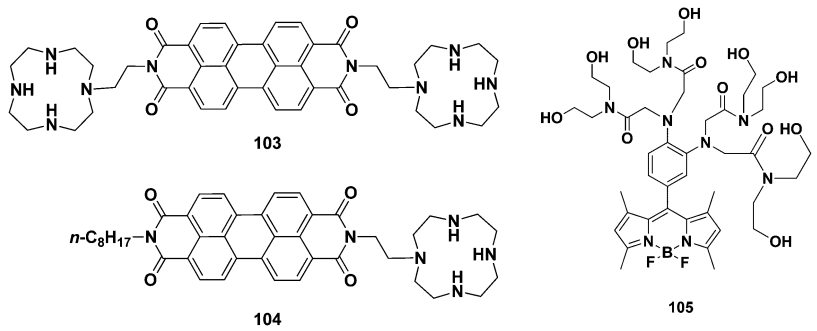

Fig. 38 Structure of (**103–105**).

Published on 14 April 2016. Downloaded by Fail Open on 7/23/2025 9:06:09 AM.

not produce any change in color. The emission spectra of (**103**) showed that the addition of 5 equiv. of Pb^{2+} ion caused enhancement in the fluorescence intensity.

The Job's plot favored the 1 : 2 stoichiometry between (**103**) and Pb^{2+} ions and has a binding constant of ($\log k = 10.6 \pm 0.5$). The 1 : 2 stoichiometry was further confirmed through the ESI-TOF mass spectra of the complex. The interference studies revealed that the Cu^{2+} and Hg^{2+} ions could limit the turn-on Pb^{2+} response of (**103**). However, other metal ions did not produce any change in the response of (**103**) for Pb^{2+} ions. To further improve the selectivity and amphipathicity for cellular uptake and intracellular fluorescent imaging, probe (**104**) was synthesized having an octyl chain. The probe (**104**) has a stable fluorescence intensity in the pH range 6.0–7.9 in 10 mM HEPES/DMSO (90 : 10, v/v). The probe (**104**) has selectivity towards Pb^{2+} ions even in the presence of Cu^{2+} and Hg^{2+} ions. Therefore, probe (**104**) has higher selectivity for Pb^{2+} ions than probe (**104**). Job's plot and ESI-TOF mass spectroscopy confirmed the 1 : 1 stoichiometry between (**104**) and Pb^{2+} and the binding constant is ($\log k = 8.0 \pm 0.3$).

Liu *et al.* reported a BODIPY based sensor (**105**) for Pb^{2+} ions in aqueous medium (0.1 M PBS buffer, pH 7.2) as shown in Fig. 38.[229] The probe (**105**) has an absorption band centered at 497 nm and weak fluorescence at 510 nm due to photoinduced electron transfer (PET). The addition of 2 equiv. of Pb^{2+} ions enhanced the fluorescence intensity (19 times) of probe (**105**), which indicates the blockage of the PET process through coordination of Pb^{2+} ions. Job's plot indicates a 1 : 2 stoichiometry for the (**105**)·Pb^{2+} complex. The association constants K_{11} and K_{21} were determined to be 5.3×10^8 and 8.0×10^6, respectively. No obvious interference was observed in the response of (**105**) toward Pb^{2+} ions even in the presence of other competing cations.

Ganguly *et al.* reported giant Au(I)@Ag_2/Ag_3–thiolate clusters for the selective detection of Pb^{2+} ions in aqueous medium as shown in Fig. 39.[230] The cysteine molecules selectively replace glutathione (GSH) from Au(I)@Ag_2/Ag_3 clusters, which results into the cysteine concentration dependent quenching of fluorescence of the giant clusters (Fig. 39). Upon interacting with Pb^{2+} ions, giant clusters recovered fluorescence. A Pb^{2+} ion binds with a cysteine molecule and GSH takes its original position in the giant clusters. The limit of detection was found to be 15×10^{-8} M.

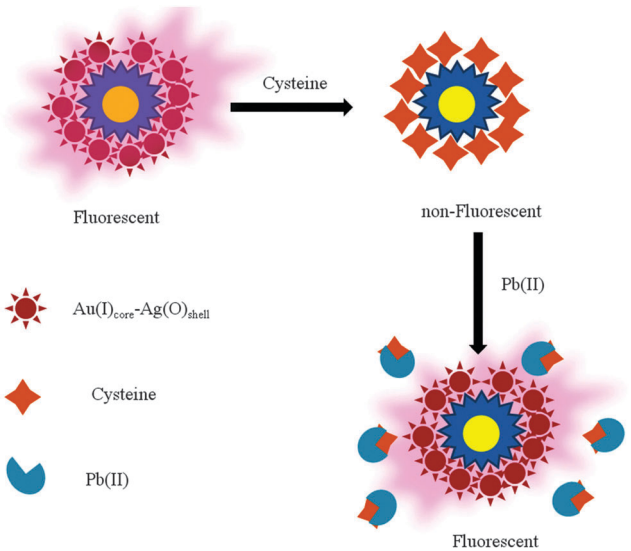

Fig. 39 Proposed mechanism of action of the Au(I)@Ag_2/Ag_3–thiolate clusters for the selective detection of Pb^{2+} ions.

18. Anions and biomolecules

Anion and biomolecule sensing is growing area of research in supramolecular chemistry because of its vast applications in the field of biology, medicine and environment.[231–236] For real time analysis, anion/biomolecule sensor should be work in aqueous medium. However, anion recognition in aqueous medium is a challenging task because water molecules give a tough competition to anions for binding sites.[46,237] Protein molecules captured the anions through multiple hydrogen-bonding interactions. Hydrogen-bonding interactions are not much strong to overcome the high hydration energy of anions.[238,239] Therefore, metal complexes or electrostatic interactions have been used to overcome this problem. Metal displacement from a complex or electrostatic interactions between the metal center of a complex and an anion can cause changes in its photophysical properties.[240–242] Based upon this strategy, several reports are available on anion/biomolecule sensing in aqueous system. In this review, we have divided anion/biomolecule sensors into two categories: (a) nanoparticle based sensors and (b) organic receptor based sensors.

Published on 14 April 2016. Downloaded by Fail Open on 7/23/2025 9:06:09 AM.

18.1 Nanoparticle based sensors

Zhang *et al.* reported a citrate-stabilized core/shell/Cu@Au NPs for selective detection of iodide anion in water.[243] The addition of iodide anion induced colorimetric change in the solution of Cu@Au nanoparticles from purple to red. It also produced blue shift in the gold SPR peak from 536 to 521 nm and the band width dramatically decreased. The limit of detection was found to be 5 μM. The interference tests revealed that no other anions showed a color change with Cu@Au nanoparticles, which means high selectivity towards I^- anion.

Hajizadeh *et al.* reported aqueous colloidal silver nanoparticles (AgNPs) for detection of cyanide (CN^-) anion.[43] The AgNPs has surface plasmon absorption band at 394 nm and addition of cyanide ion leads to decolorization as shown in Fig. 40. Furthermore, the intensity of SPR peak decreased upon increasing the concentration of cyanide ion, which indicates the formation of soluble and colorless complex $Ag(CN)_2^-$. The probe has detection limit of 1.8 μmol L^{-1} with linear dynamic range 16.7 to 133.3 μmol L^{-1}. The probe has high selectivity towards CN^- ion, even the presence of other I^-, Cl^-, Br^-, F^-, NO_3^-, NO_2^-, SO_4^{2-}, SO_3^{2-}, HCO_3^-, CO_3^{2-}, $H_2PO_4^-$, HPO_4^{2-}, $C_2O_4^{2-}$ and SCN^- did not affect the response of AgNPs for cyanide anion.

Zhang *et al.* utilized melamine functionalized gold nanoparticles (**106**) for selective detection of sulfite anion in aqueous system (10 mM Tris-HCl, pH 7.0) as shown in Fig. 40.[45] The modified gold nanoparticles has intense surface plasmon resonance (SPR) peak at 520 nm. The addition of sulfite anion increased the stability of absorption spectra of modified gold nanoparticles in water due to formation of stronger hydrogen bonding network. The probe (**106**) has high selectivity and with linear detection range of 0 to 0.4 μM. The detection limit was calculated using 3σ method and was about (40 nM). The competitive binding experiment revealed that probe (**106**) has high selectivity towards sulfite anion due to stronger hydrogen bonding between melamine and sulfite.

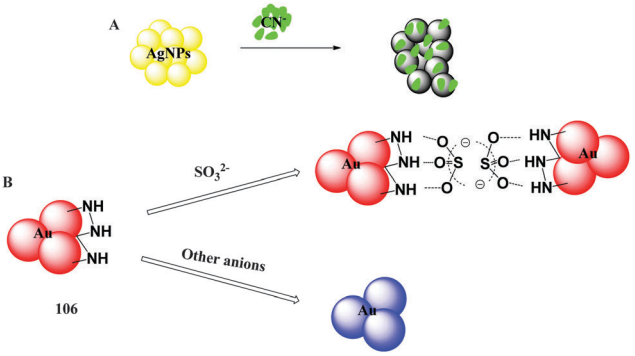

Fig. 40 A schematic representation of (A) CN^- detection using AgNPs and (B) SO_3^{2-} detection using melamine functionalized gold nanoparticles (**106**).

Zhang *et al.* reported a method for the detection of nitrite anion using unmodified citrate-capped gold nanoparticles (Au NPs) in aqueous medium (30 mM phosphate buffer, pH 9.0).[44] The citrate-capped Au NPs are tend to aggregates in the presence of phenylenediamine (PDA), which results into change in color of Au NPs solution from red to blue as shown in Fig. 41 (path A).

However, addition of nitrite anion catalyzed the diazotization of PDA in the presence of phosphoric acid and Au NPs did not aggregates due to weak interaction between the diazonium compound and Au NPs, thus the solution remained red (path B, Fig. 41). This methodology can detect less than 1 ppm of nitrite anion at room temperature without using any instrument. The probe has excellent selectivity towards nitrite anion even in the presence of other competing anions. This excellent selectivity was attributed to nitrous acid-specific diazotization of the aromatic amines.

Zhang *et al.* developed a melamine-modified gold nanoparticle (**107**) for selective detection of sulfite and hypochlorite anions in aqueous medium (10 mM Tris-HCl) as shown in Fig. 42.[244] The addition of sulfite anion decreased the absorbance at 640 nm and simultaneously enhancement at 518 nm, indicating the stability of colloidal solution and prevention of aggregation. The addition of sulfite anion also produced an intense color change from blue through purple to red (Fig. 42). The competitive binding assay indicates toward the high selectivity of probe (**107**) for sulfite anion.

However, addition of hypochlorite leads to oxidation of sulfite to sulfate, which results into aggregation of nanoparticles and color of solution changes from red through purple to blue (Fig. 42). Therefore, aggregation of nanoparticles is indirectly related with concentration of hypochlorite anions. Massue *et al.* reported a gold nanoparticles modified with a heptadentate macrocylic Eu(III) cyclen (**108**) for detection of phosphate anion in water (0.1 M HEPES buffer).[245] The gold nanoparticles are attached to Eu(III) complex through a long alkyl thiol group and form a water soluble gold nanoparticles **AuNP-1·Eu** (Fig. 43).

Furthermore, the β-diketone antenna and **AuNP-1·Eu** form ternary complexes **AuNP-1·Eu-2** (Fig. 43). The ternary complex **AuNP-1·Eu-2** is highly luminescent upon excitation of the antenna. However, addition of biologically relevant phosphate such as flavin

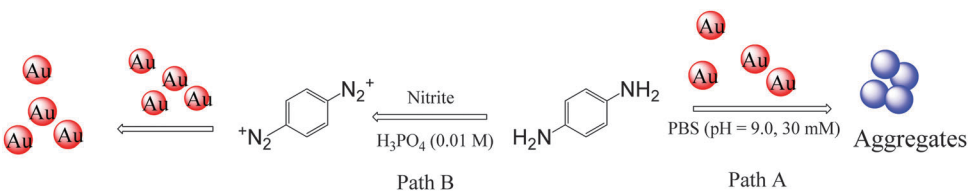

Fig. 41 Proposed mechanism of action of citrate-capped gold nanoparticles (Au NPs). The addition of PDA results into aggregation of Au NPs (path A) and addition of nitrite anion prevent the formation of aggregates (path B).

 This journal is © The Royal Society of Chemistry 2016

Published on 14 April 2016. Downloaded by Fail Open on 7/23/2025 9:06:09 AM.

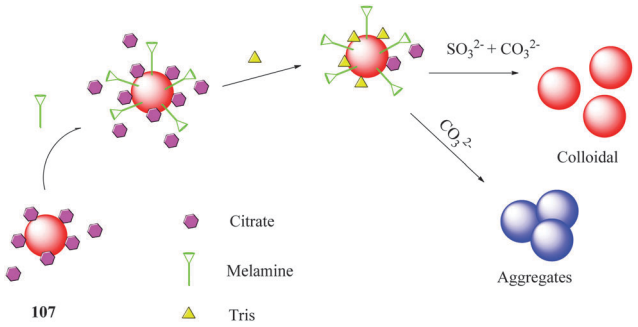

Fig. 42 Proposed mechanism of action of a melamine-modified gold nanoparticle (**107**) for selective detection of sulfite anions.

monophosphate substituted the diketone and resultant complex become non-fluorescent in nature as shown in Fig. 43.

Kaur *et al.* designed a rhodamine based fluorescent organic nanoparticles (**109**) for detection of HSO_4^- anion in water (Fig. 44).[246] The probe (**109**) has emission maxima at 555 nm and addition of HSO_4^- produced 2-fold enhancement in the emission intensity of probe (**109**). The probe (**109**) has linear detection range of 0–37 μM and a detection limit of 108 nM. The interference studies revealed that probe (**109**) selectively recognized the HSO_4^- ion and have no interference from any of the potential interfering anions.

18.2 Organic receptor based sensors

Kumar *et al.* reported a 1-(4-biphenyl)benzimidazolium based dipodal probe (**110**) for the detection of perchlorate anions in aqueous buffer (0.01 M HEPES buffer, 2% DMSO) as shown in Fig. 44.[247] The addition of perchlorate anions produced quenching and a blue shift (Δ = 30 nm) in the emission band of (**110**) at 460 nm. The absorbance spectra of (**110**) showed a ratiometric change upon addition of perchlorate anions with an isosbestic point at 290 nm. The titration was performed on both a UV-Visible and a fluorescence spectrophotometer. The binding constant was calculated using a non-linear regression analysis program (SPECFIT-32) and it was about $\log\beta = 4.24 \pm 0.05$. The 1 : 1 stoichiometry was confirmed through Job's plot and mass spectra. The detection limit was found to be 100 nM. The competitive binding test confirmed the high selectivity of probe (**110**) toward ClO_4^- anions even in the presence of other competing anions.

Iniya *et al.* designed a pyridoxal linked aminoethylethanolamine (PYET) receptor (**111**) for the detection of fluoride anion in aqueous medium (HEPES buffer, pH 7.4) as shown in Fig. 44.[156] The addition of fluoride anion produced a new band at 387 nm along with a decrease in absorbance at 328 nm. The emission spectrum of (**111**) has two maxima at 445 nm and 510 nm, indicating the enol and keto forms of (**111**), respectively. The addition of fluoride anions produced a slight change in the keto emission (510 nm) along with a strong enhancement of the enol emission (445 nm). It represents the inhibition of the ESIPT mechanism. Job's plot advocates the 1 : 1 stoichiometry between (**111**) and fluoride anions. The binding constant was about $1.46 \times 10^5\ M^{-1}$ and the detection limit was 7.77×10^{-8} M. The probe (**111**) has high selectivity towards fluoride anion.

Sen *et al.* reported 5*H*-5,7*a*,12-triaza-dibenzo[*a*,*e*]azulen-6-one (**112**) for the selective detection of hydrogen sulphate anions in aqueous medium (1 mM HEPES buffer, 2% EtOH and pH 7.4) as shown in Fig. 44.[248] The addition of HSO_4^- anions decreased the emission intensity at 430 nm along with the appearance of a new

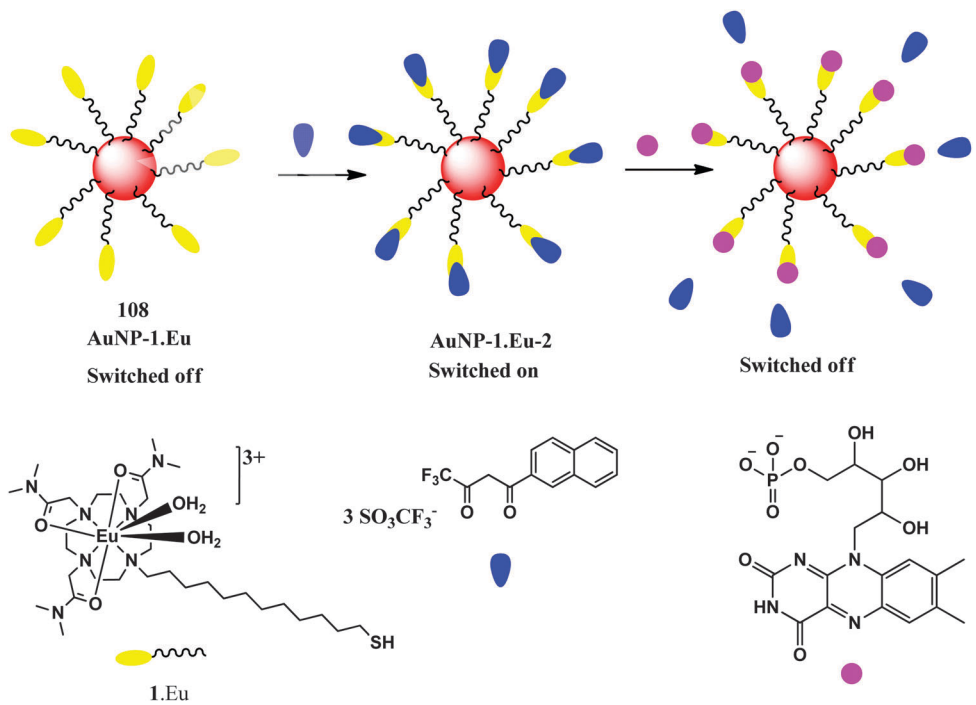

Fig. 43 A schematic representation of phosphate detection using a heptadentate macrocylic Eu(III) cyclen modified gold nanoparticles (**108**).

Published on 14 April 2016. Downloaded by Fail Open on 7/23/2025 9:06:09 AM.

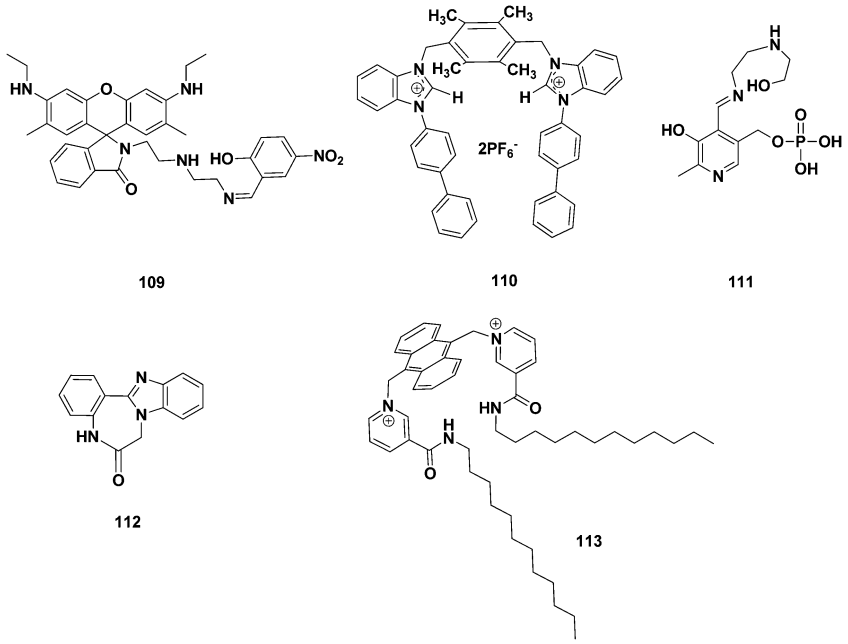

Fig. 44 Structure of (**109–113**).

band at 483 nm through an isosbestic point at 449 nm. The probe (**112**) has a detection limit of 5.5×10^{-7} M^{-1}. Job's plot confirmed the 1:1 stoichiometry between (**112**) and HSO_4^-. The probe (**112**) has high selectivity towards HSO_4^- anions even in the presence of other competing anions.

Saini *et al.* reported a nicotinamide–anthracene conjugate based fluorophore (**113**) for the selective detection of sulfate anions in aqueous system (HEPES buffer, 10% DMSO and pH 7.4) as shown in Fig. 44.[249] The probe (**113**) showed a 16-fold enhancement in the emission intensity at 535 nm upon addition of 1 equiv. of sulfate anions. However, the absorption spectrum of (**113**) showed a small increment in intensity in the region between 360 and 600 nm. The dissociation constant for the (**113**)·SO_4^{2-} complex is 1.20×10^{-5} and the lowest detection limit of 500 nM. The 1:1 stoichiometry was confirmed through Job's plot. The interference studies confirmed the high selectivity of probe (**113**) towards sulfate anions in the presence of other anions.

Xie *et al.* reported a polylysine and tetraphenylethene based probe (**114**) for the detection of sulfite anions in aqueous media (HEPES buffer, pH 7.0) as shown in Fig. 45.[250] The probe (**114**) has excellent water solubility and is non-emissive in the solution state, while it showed enhancement upon aggregation or in the intramolecular rotation-restricted state. Sulfite anions reacts with benzoic aldehyde groups on the polylysine side chains and acquire a negative charge, which results in the an complexation between the polymer chains and the positively charged fluorophore (Fig. 45). It produces enhancement in the emission intensity due to the aggregation induced emission (AIE) effect. The probe (**114**) has high selectivity and sensitivity for sulfite anions with a detection limit of 3.6 μM.

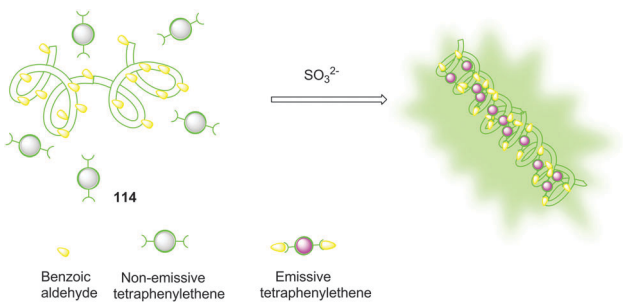

Fig. 45 A schematic representation of sulfite detection using (**114**).

Mahapatra *et al.* reported a carbazole–thiosemicarbazone–Hg^{2+} complex (**115**) for the selective detection of iodide ions in aqueous medium (25 mM HEPES buffer 1% DMSO, pH 7.4) as shown in Fig. 46.[251] The addition of 1 equiv. of iodide anions produced a large fluorescence enhancement in the region of 425 nm. The sensor (**115**) has excellent selectivity toward iodide anions over other competing anions. The probe (**115**) has a linear relationship between the fluorescence intensity at 425 nm and the concentration range of 0.5–8 μM and has a detection limit of 250 nM.

Chung *et al.* reported a fluorescein based Cu^{2+} complex (**116**) for the selective detection of cyanide anions in aqueous medium (0.02 M HEPES buffer, pH 7.4) as shown in Fig. 46.[252] The Cu^{2+} complex (**116**) is non-fluorescent in nature and the addition of CN^- anion revives fluorescence resulting in the "off–on" type sensing of cyanide. However, other anions such as SCN^-, AcO^-, F^-, Cl^-, Br^-, I^-, $H_2PO_4^-$, HSO_4^-, NO_3^-, and ClO_4^- did not produce any change in the emission intensity of probe (**116**). The Cu^{2+} complex has a light pink color attributed to phenolate formation and cyanide addition induced colorimetric change from pink to yellow.

Kim *et al.* reported an iridium(III) complex for the selective detection of $H_2PO_4^-$ anions in 1 mM HEPES buffer at pH 7.4 as

 This journal is © The Royal Society of Chemistry 2016

Published on 14 April 2016. Downloaded by Fail Open on 7/23/2025 9:06:09 AM.

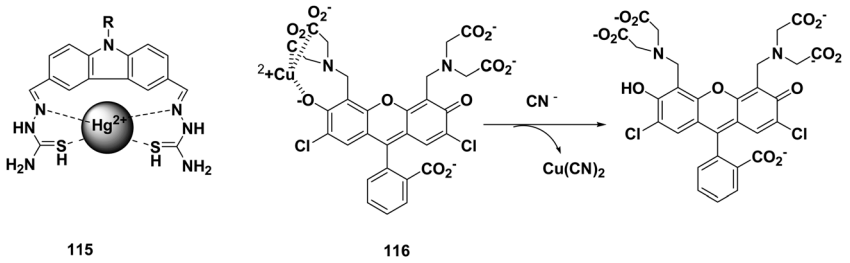

115 116

Fig. 46 Structure of (**115**) and proposed binding mode of (**116**).

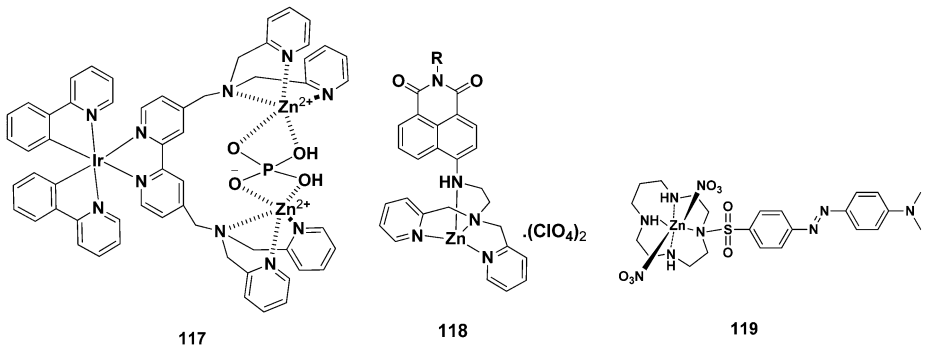

117 118 119

Fig. 47 Proposed mechanism of action of (**117**) for the detection of $H_2PO_4^-$ anions and structures of (**118**) and (**119**).

shown in Fig. 47.[253] The probe (**117**) has two Zn–DPA (dipicolylamine) units cooperatively bound with $H_2PO_4^-$, which produces an enhancement in phosphorescence. Other anions did not induce any particular change in phosphorescence. The stronger interaction between Zn^{2+} and $H_2PO_4^-$ inhibited the ILCT (intraligand charge transfer) and increasing the chance of MLCT (metal-to-ligand charge transfer). The association constant was found to be 9.68×10^4 M^{-1}.

Moro *et al.* reported a fluorescent naphthalimide chemosensor (**118**) for the detection of ATP in aqueous system (0.1 M HEPES buffer, pH 7.4) as shown in Fig. 47.[254] The probe (**118**) was synthesized through the coupling of the dipicolylamine (DPA)–Zn^{2+} complex with naphthalimide using an ethylamine spacer. The addition of ATP produced a significant increase in the fluorescence intensity at 535 nm. Other anions remained silent; even GTP having a similar structure and similar properties compared to ATP has almost no effect on the fluorescence signal of the probe (**118**). However, ADP showed little interaction towards (**118**)·Zn^{2+} but a significant enhancement in the fluorescence intensity was observed with ATP. The second phosphate group of ATP may act as an additional coordinating ligand towards the metal.

Mahato *et al.* reported a Zn^{2+} complex of 1,4,8,11-tetraazacyclotetradecane (**119**) for the detection of ATP in aqueous medium (10 mM HEPES, pH 7.2) as shown in Fig. 47.[255] The complex (**119**) has an absorption maximum at 463 nm attributed to the intercomponent (π–π^*) charge transfer (CT) band. The addition of ATP produced a red shift in the absorption spectra from 463 to 503 nm. However, ADP showed a less prominent response and other anions did not produce any change in the absorption spectra. The binding constant was found to be 978 ± 4 M^{-1}. The 1:1 stoichiometry of (**119**)·ATP was confirmed through ESI-MS spectral studies.

Ahmed *et al.* reported a water soluble imidazolium-anthracene cyclophane (**120**) for the detection of GTP and ATP in aqueous solution (10 mM phosphate buffer at pH 7.4) as shown in Fig. 48.[256] The addition of ATP produced an enhancement in the emission intensity due to a chelation enhancement fluorescence (CHEF) effect. However, a new excimer peak rose at 490 nm along with a chelation-enhanced fluorescence quenching (CHEQ) effect upon addition of GTP. The absorption spectra of (**120**) showed a maximum at 366 nm and the addition of ATP and GTP produced a bathochromic shift of 3 and 6 nm, respectively. Job's plot analysis indicates a 1:1 stoichiometry of the (**120**)·GTP and (**120**)·ATP complexes. The binding constant was calculated using fluorescence data and it was 1×10^6 M^{-1} and 7.4×10^5 M^{-1} for GTP and ATP, respectively. The detection limit for GTP was 9.7×10^{-7} M and 1.4×10^{-6} M for GTP and ATP, respectively.

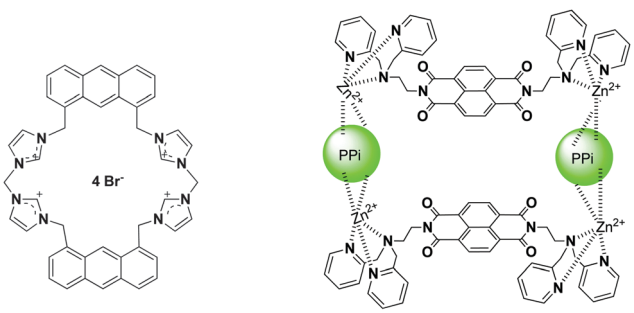

120 121

Fig. 48 Structure of (**120**) and proposed binding mode of (**121**).

Published on 14 April 2016. Downloaded by Fail Open on 7/23/2025 9:06:09 AM.

^{1}H NMR titration and 2D NOESY experiments showed that receptor (**120**) binds with GTP and ATP through the interaction of the imidazolium protons with the O atoms of the phosphate group. The CHEF effect for ATP was observed due to the vertical interaction between H atom at the C-2 position of the adenine base with the plane of the anthracene ring (π–H interaction). However, the excimer emission for GTP binding appeared due to the π–π stacking interaction between the guanine moiety of GTP and the anthracene ring.

Lee *et al.* reported a 1,4,5,8-naphthalenetetracarboxylic dianhydride (**121**) based fluorescent chemosensor for the detection of pyrophosphate (PPi) anions in aqueous medium (0.01 M HEPES, pH 7.4) as shown in Fig. 48.[257] The addition of (PPi) produced a new peak at 490 nm, which is attributed to the excimer formation. However, the absorbance spectra of (**121**) did not show any change upon addition of PPi. The association constant was calculated to be 4.1×10^5 M^{-1}. Moreover, the electrospray ionization experiment also confirmed the excimer formation. It was suggested that (**121**) binds with PPi as a 2+2 complex as shown in Fig. 48.

Ghosh *et al.* reported a pyridinium based tripodal sensor (**122**) for the detection of AMP using the indicator displacement assay (IDA) technique in water (10 mM Tris-HCl buffer, pH 6.4) as shown in Fig. 49.[258] The probe (**122**) showed a ratiometric response with ATP, ADP and AMP having an isosbestic point at 285 nm. The 1 : 1 stoichiometry for (**122**)·ATP, (**122**)·ADP and (**122**)·ADP was confirmed through Job's plot. The binding constant was 6.80×10^2 M^{-1}, 8.85×10^2 M^{-1} and 5.96×10^3 M^{-1} for (**122**) with ATP, ADP and AMP, respectively. The receptor (**122**) showed high affinity toward AMP over ATP and ADP.

Lee *et al.* reported a fluorescent naphthalene–dpa (dpa = bis(2-pyridylmethyl)amine) based sensor (**123**) for the selective detection of PPi ions in aqueous solution (0.01 M HEPES, pH 7.4) as shown in Fig. 49.[259] The complex (**123**) has an absorption maximum at 305 nm and the addition of PPi produced a new band at 316 nm, along with a decrease in intensity at 305 nm. It was observed that an addition of ATP and ADP also showed a small change in the absorbance spectra but the change was less prominent compared to PPi. However, other anions like AMP, HPO_4^{2-}, $CH_3CO_2^-$, F^-, HCO_3^- and Cl^- do not produce any change in the absorption spectra of (**123**). The emission spectra of (**123**) also showed a change upon addition of PPi. The λ_{max} was shifted from 436 nm to 456 nm along with a 9.5 fold fluorescence enhancement. The 1 : 1 stoichiometry was confirmed from Job's plot. The association constant was found to be $(2.9 \pm 0.7) \times 10^8$ M^{-1}.

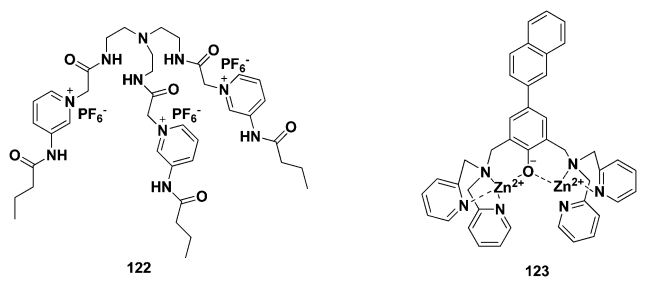

Fig. 49 Structure of (**122**) and (**123**).

19. Conclusions and future perspectives

This review mainly focused on the recognition of analytes (metal, anion and biomolecules) in aqueous medium (≥90% water) and demonstrates that sensing in aqueous medium can be achieved without compromising the selectivity and sensitivity. Yet, detection in aqueous medium is a challenging task due to the solubility of organic moiety, aggregation and competition between water molecules and analytes. However, the sophisticated molecular design of sensors makes the detection of metal ions/anions/biomolecules in aqueous medium feasible. The detailed discussion on the design of chemosensors and mechanism of action has been provided. This review covered sensing of metal ions, anions and biomolecules in aqueous medium reported in 2001–2015. Accordingly, it is divided into three parts. The first section accounts on the recognition of metal ions; 16 metal ions (alkali, alkaline earth and transition metals) have been included. This section described the design of chemosensors for metal ions, recognition conditions and analytical parameters (detection limits and binding constants). From this section, it was concluded that nanoparticle based chemosensors proved to have better sensing moieties for the detection of metal ions in aqueous medium having a low detection limit in the nanomolar range, and a high selectivity and binding constant. The second section focused on the sensing of anions in aqueous medium and further classified into two categories depending upon the type of sensor: (i) nanoparticle based sensors and (ii) organic receptor based sensors. In most cases, Au nanoparticle based chemosensors were employed for the detection of anions in aqueous medium. However, organic receptor based chemosensors focused on the metal complexes and receptors having –NH, –OH and –CH moieties. The last section detailed the detection of biomolecules (ATP, GTP, PPi and AMP) in aqueous medium. The driving force behind the coordination of biomolecules is electrostatic interaction and hydrogen bonding.

We believe that sensing in aqueous medium is still an immature area and requires continuous effort to achieve the targets of Supramolecular Chemistry. The major challenge for future work will be the development of sensors, which are prepared easily and a have broad working pH range, low detection limit, high selectivity, good sensitivity and short response time. The existing sensors required long synthetic procedures for preparation and required particular conditions for working. However, fluorescent organic nanoparticles (FONPs) are new emerging technique, and can detect the analytes up to the nanomolar range and have liberal working conditions. Due to the nano dimensions, FONPs have a small gap between the HOMO and LUMO and can control the band gap by adopting a suitable solvent system. Therefore, even nano-molar detection can be achieved using FONPs. Moreover, FONPs reduced

 This journal is © The Royal Society of Chemistry 2016

Published on 14 April 2016. Downloaded by Fail Open on 7/23/2025 9:06:09 AM.

the use of toxic solvents and detected the analyte in aqueous medium. It is a growing field which has some space for new FONPs.

Abbreviations

A	Adenosines
Apt	Aptamer
AIEE	Aggregation-induced enhanced emission
ATP	Adenosine triphosphate
ADP	Adenosine diphosphate
AMP	Adenosine monophosphate
AgNPs	Silver nanoparticles
AIE	Aggregation induced emission
AuNPs	Gold nanoparticles
BAPTA	1,2-Bis-(2-aminophenoxy)ethane-*N*,*N*,*N*′,*N*′-tetraacetic acid
BODIPY	Boron dipyrromethene difluoride
CdSe	Cadmium selenide
CD	Circular dichroism
CCP	Cationic conjugated polymers
CSQ	Calsequestrin
CHEF	Chelation-enhanced fluorescence
CAPS	*N*-Cyclohexyl-3-aminopropanesulfonic acid
CT	Charge transfer
CHEQ	Chelation-enhanced fluorescence quenching
CdTe	Cadmium telluride
DMAPAM	*N*,*N*-Dimethylaminopropylacrylamide
DBD-AA	*N*-{2-[(7-*N*,*N*-Dimethylaminosulfonyl)-2,1,3-benzoxadiazol-4-yl]-(methyl)amino}ethyl-*N*-methylacrylamide
DCHQ	Diaza-18-crown-6-hydroxyquinoline
DLS	Dynamic light scattering
DPA	Dipicolylamine
dpa	Bis(2-pyridylmethyl)amine
EGTA	Ethylene glycol bis(β-aminoethyl ether)-*N*,*N*,*N*′,*N*′-tetraacetic acid
EET	Excitation energy transfer
ESIPT	Excited state intramolecular proton transfer
ESI-TOF	Electrospray-time of flight
EDTA	Ethylenediaminetetraacetic acid
EM	Energy migration
ET	Energy transfer
ESI-MS	Electrospray-ionization mass spectrometry
EPR	Electron paramagnetic resonance
FAM	6-Carboxyfluorescein
FONPs	Fluorescent organic nanoparticles
FITC	Fluorescein 5(6)-isothiocyanate
FRET	Fluorescence resonance energy transfer
FGM	Fluorescent gold nanoclusters membrane
FQDIPA	2-(2-Formylquinolin-8-yloxy)-*N*,*N*-diisopropylacetamide
FQDPA	2-(2-Formylquinolin-8-yloxy)-*N*,*N*-diphenylacetamide
G	Guanine
GNPs	Gold nanoparticles
GSH	Glutathione
GTP	Guanosine triphosphate
HQ	8-Hydroxyquinoline
HEPES	4-(2-Hydroxyethyl)-1-piperazineethanesulfonic acid
HOMO	Highest occupied molecular orbital
ILCT	Intraligand charge transfer
IDA	Indicator displacement assay
ICT	Intramolecular charge transfer
MPAM	*N*-(3-Morpholin-4-ylpropyl)acrylamide
MOPS	3-Morpholinopropanesulfonic acid
MLCT	Metal-to-ligand charge transfer
NIPAM	*N*-Isopropylacrylamide
NBD	Nitrobenzoxadiazolyl
OG	OliGreen
PSO	Potassium sensing oligonucleotide
PBFI	Potassium-binding benzofuran isophthalate
PF	Poly(9,9-bis(6′-*N*,*N*,*N*-trimethylammonium)hexyl)-fluorenylene phenylene
PPi	Pyrophosphate
PPT	Photoinduced proton transfer
PET	Photo-induced electron transfer
PBS	Phosphate-buffered saline
PDA	Phenylenediamine
PYET	Pyridoxal linked aminoethylethanolamine
QDs	Quantum dots
SEM	Scanning electron microscope
SDS	Sodium dodecyl sulfate
SBFI	Sodium-binding benzofuran isophthalate
SPR	Surface plasmon resonance
SV	Stern Volmer
TEM	Transmission electron microscope
TAMRA	6-Carboxytetramethylrhodamine
TP	Two-photon
TPEN	*N*,*N*,*N*′,*N*′-Tetrakis-(2-pyridylmethyl)ethylenediamine
Tris-HCl	Tris(hydroxymethyl)aminomethane hydrochloride
UV	Ultraviolet
ZnS	Zinc sulfide
ZnMOF	Zn-based metal–organic framework
ZnMGO	Zn-based graphene oxide

References

1 A. W. Czarnik, *Advances in Supramolecular Chemistry*, JAI Press, Greenwich, 1993, vol. 3, pp. 131–157.
2 R. W. Cattral, *Chemical Sensors*, Oxford University Press, Oxford, 1997.
3 J. P. Anzenbacher, P. Lubal, P. Bucek, M. A. Palacios and M. E. Kozelkova, *Chem. Soc. Rev.*, 2010, **39**, 3954–3979.
4 L. J. Fan and W. E. Jones, Jr., *J. Am. Chem. Soc.*, 2006, **128**, 6784.
5 D. T. Quang and J. S. Kim, *Chem. Rev.*, 2010, **110**, 6280–6301.
6 A. P. de Silva, D. B. Fox, A. J. M. Huxley and T. S. Moody, *Coord. Chem. Rev.*, 2000, **205**, 41–57.
7 A. P. de Silva, B. McCaughan, B. O. F. McKinney and M. Querol, *Dalton Trans.*, 2003, 1902–1913.

Published on 14 April 2016. Downloaded by Fail Open on 7/23/2025 9:06:09 AM.

8 V. Amendola, L. Fabbrizzi, C. Mangano and P. Pallavicini, *Acc. Chem. Res.*, 2001, **34**, 488–493.
9 M. Shortreed, R. Kopelman, M. Kuhn and B. Hoyland, *Anal. Chem.*, 1996, **68**, 1414–1418.
10 S. G. Lemos, A. R. A. Nogueira, A. Torre-Neto, A. Parra and J. Alonso, *J. Agric. Food Chem.*, 2007, **55**, 4658–4663.
11 J. Mu, L. Zhang, M. Zhao and Y. Wang, *ACS Appl. Mater. Interfaces*, 2014, **6**, 7090–7098.
12 K. S. Kasprzak, in *Cytotoxic, Mutagenic and Carcinogenic Potential of Heavy Metals Related to Human Environment*, ed. N. Hadjiliadis, Springer Netherlands, 1997, vol. 26, pp. 93–106.
13 C.-H. Ho, Y.-B. Yu and P.-H. Wu, *J. Chin. Med. Assoc.*, 2008, **71**, 119–122.
14 J. Lee, H.-J. Kim and J. Kim, *J. Am. Chem. Soc.*, 2008, **130**, 5010–5011.
15 J. B. Vincent, *Nutr. Rev.*, 2000, **58**, 67–72.
16 P. Cornelis, Q. Wei, S. C. Andrews and T. Vinckx, *Metallomics*, 2011, **3**, 540–549.
17 D. Touati, *Arch. Biochem. Biophys.*, 2000, **373**, 1–6.
18 G. Cairo and A. Pietrangelo, *Biochem. J.*, 2000, **352**, 241–250.
19 D. Maity and T. Govindaraju, *Inorg. Chem.*, 2010, **49**, 7229.
20 S. H. Mashraqui, M. Chandiramani, R. Betkar and K. Poonia, *Tetrahedron Lett.*, 2010, **51**, 1306–1308.
21 Y. Yao, D. Tian and H. Li, *ACS Appl. Mater. Interfaces*, 2010, **2**, 684–690.
22 C. Orvig and M. J. Abrams, *Chem. Rev.*, 1999, **99**, 2201–2204.
23 A. P. de Silva, H. Q. N. Gunaratne, T. Gunnlaugsson, A. J. M. Huxley, C. P. McCoy, J. T. Rademacher and T. E. Rice, *Chem. Rev.*, 1997, **97**, 1515.
24 P. B. Tchounwou, W. K. Ayensu, N. Ninashvili and D. Sutton, *Environ. Toxicol.*, 2003, **18**, 149–175.
25 J. M. Lehn, *Supramolecular Chemistry. Concepts and Perspectives*, VCH, Weinheim, 1995.
26 P. A. Gale, S. E. Garcia-Garrido and J. Garric, *Chem. Soc. Rev.*, 2008, **37**, 151–190.
27 T. Gunnlaugsson, M. Glynn, G. M. Tocci, P. E. Kruger and F. M. Pfeffer, *Coord. Chem. Rev.*, 2006, **250**, 3094–3117.
28 P. A. Gale and R. Quesada, *Coord. Chem. Rev.*, 2006, **250**, 3219–3244.
29 J. P. Gallivan and D. A. Dougherty, *J. Am. Chem. Soc.*, 2000, **122**, 870–874.
30 X. Jiang, D. Zhang, J. Zhang, J. Zhao, B. Wang, M. Feng, Z. Dong and G. Gao, *Anal. Methods*, 2013, **5**, 3222–3227.
31 Y. Zhou, Z. Xu and J. Yoon, *Chem. Soc. Rev.*, 2011, **40**, 2222–2235.
32 N. Singh and D. O. Jang, *Org. Lett.*, 2007, **9**, 1991–1994.
33 H. Sharma, H. J. Guadalupe, J. Narayanan, H. Hofeld, T. Pandiyan and N. Singh, *Anal. Methods*, 2013, **5**, 3880–3887.
34 A. Kaur, H. Sharma, S. Kaur, N. Singh and N. Kaur, *RSC Adv.*, 2013, **3**, 6160–6166.
35 M. Porel, V. Ramalingam, M. E. Domaradzki, V. G. Young, V. Ramamurthy and R. S. Muthyala, *Chem. Commun.*, 2013, **49**, 1633–1635.
36 Y. Shiraishi, S. Sumiya, K. Manabe and T. Hirai, *ACS Appl. Mater. Interfaces*, 2011, **3**, 4649–4656.
37 L. Yang, X. Li, J. Yang, Y. Qu and J. Hua, *ACS Appl. Mater. Interfaces*, 2013, **5**, 1317–1326.
38 P. Anzenbacher, D. S. Tyson, K. Jursíková and F. N. Castellano, *J. Am. Chem. Soc.*, 2002, **124**, 6232–6233.
39 C. Caltagirone and P. A. Gale, *Chem. Soc. Rev.*, 2009, **38**, 520–563.
40 M. E. Moragues, R. Martinez-Manez and F. Sancenon, *Chem. Soc. Rev.*, 2011, **40**, 2593–2643.
41 P. A. Gale, N. Busschaert, C. J. E. Haynes, L. E. Karagiannidis and I. L. Kirby, *Chem. Soc. Rev.*, 2014, **43**, 205–241.
42 H. Sharma, V. K. Bhardwaj, N. Kaur, N. Singh and D. O. Jang, *Tetrahedron Lett.*, 2013, **54**, 5967–5970.
43 S. Hajizadeh, K. Farhadi, M. Forough and R. E. Sabzi, *Anal. Methods*, 2011, **3**, 2599–2603.
44 J. Zhang, C. Yang, X. Wang and X. Yang, *Analyst*, 2012, **137**, 3286–3292.
45 J. Zhang, Y. Yuan, X. Wang and X. Yang, *Anal. Methods*, 2012, **4**, 1616–1618.
46 S. Kubik, *Chem. Soc. Rev.*, 2010, **39**, 3648–3663.
47 T. M. Swager, *Acc. Chem. Res.*, 1998, **31**, 201–207.
48 D. T. McQuade, A. E. Pullen and T. M. Swager, *Chem. Rev.*, 2000, **100**, 2537–2574.
49 Y. Z. Liao, V. Strong, Y. Wang, X.-G. Li, X. Wang and R. B. Kaner, *Adv. Funct. Mater.*, 2012, **22**, 726–735.
50 X.-G. Li, Y. Liao, M.-R. Huang, V. Strong and R. B. Kaner, *Chem. Sci.*, 2013, **4**, 1970–1978.
51 X.-G. Li, Y. Liao, M.-R. Huang and R. B. Kaner, *Chem. Sci.*, 2015, **6**, 2087–2101.
52 S. Huang, P. Du, C. Min, Y. Liao, H. Sun and Y. Jiang, *J. Fluoresc.*, 2013, **23**, 621–627.
53 V. M. Suresh, A. Bandyopadhyay, S. Roy, S. K. Pati and T. K. Maji, *Chem. – Eur. J.*, 2015, **21**, 10799–10804.
54 Z. Li, H. Li, H. Xia, X. Ding, X. Luo, X. Liu and Y. Mu, *Chem. – Eur. J.*, 2015, **21**, 17355–17362.
55 P. Ball, *H_2O: A Biography of Water,* Phoenix, London, 2000.
56 P. Hrdlovic, J. Donovalova, H. Stankovicova and A. Gaplovsky, *Molecules*, 2010, **15**, 8915.
57 J. R. Lakowicz, *Principles of Fluorescence Spectroscopy*, Springer US, US, 3rd edn, 2006.
58 M. Wenzel, J. R. Hiscock and P. A. Gale, *Chem. Soc. Rev.*, 2012, **41**, 480–520.
59 Y. Hu, Y. Liu, G. Kim, E. J. Jun, K. M. K. Swamy, Y. Kim, S.-J. Kim and J. Yoon, *Dyes Pigm.*, 2015, **113**, 372–377.
60 F. Wang, J. H. Moon, R. Nandhakumar, B. Kang, D. Kim, K. M. Kim, J. Y. Lee and J. Yoon, *Chem. Commun.*, 2013, **49**, 7228–7230.
61 S. Park, W. Kim, K. M. K. Swamy, H. Y. Lee, J. Y. Jung, G. Kim, Y. Kim, S.-J. Kim and J. Yoon, *Dyes Pigm.*, 2013, **99**, 323–328.
62 U. Fegade, H. Sharma, K. Tayade, S. Attarde, N. Singh and A. Kuwar, *Org. Biomol. Chem.*, 2013, **11**, 6824–6828.
63 S. Shinoda, K. Yano and H. Tsukube, *Chem. Commun.*, 2010, **46**, 3110–3112.
64 S. Kubik, R. Kirchner, D. Nolting and J. Seidel, *J. Am. Chem. Soc.*, 2002, **124**, 12752–12760.

 This journal is © The Royal Society of Chemistry 2016

Published on 14 April 2016. Downloaded by Fail Open on 7/23/2025 9:06:09 AM.

65 Z. Rodriguez-Docampo, S. I. Pascu, S. Kubik and S. Otto, *J. Am. Chem. Soc.*, 2006, **128**, 11206–11210.
66 M. R. Krause, R. Goddard and S. Kubik, *J. Org. Chem.*, 2011, **76**, 7084–7095.
67 C. Reyheller and S. Kubik, *Org. Lett.*, 2007, **9**, 5271–5274.
68 A. Schaly, R. Belda, E. García-España and S. Kubik, *Org. Lett.*, 2013, **15**, 6238–6241.
69 X. Chen, T. Pradhan, F. Wang, J. S. Kim and J. Yoon, *Chem. Rev.*, 2012, **112**, 1910–1956.
70 X. Zhang, J. Yin and J. Yoon, *Chem. Rev.*, 2014, **114**, 4918–4959.
71 Y. Zhou, J. F. Zhang and J. Yoon, *Chem. Rev.*, 2014, **114**, 5511–5571.
72 J. R. Casey, S. Grinstein and J. Orlowski, *Nat. Rev. Mol. Cell Biol.*, 2010, **11**, 50–61.
73 S. T. Whitten, B. García-Moreno E. and V. J. Hilser, *Proc. Natl. Acad. Sci. U. S. A.*, 2005, **102**, 4282–4287.
74 R. V. Benjaminsen, H. Sun, J. R. Henriksen, N. M. Christensen, K. Almdal and T. L. Andresen, *ACS Nano*, 2011, **5**, 5864–5873.
75 L. Santos, J. P. Neto, A. Crespo, D. Nunes, N. Costa, I. M. Fonseca, P. Barquinha, L. Pereira, J. Silva, R. Martins and E. Fortunato, *ACS Appl. Mater. Interfaces*, 2014, **6**, 12226–12234.
76 Z. Bai, R. Chen, P. Si, Y. Huang, H. Sun and D.-H. Kim, *ACS Appl. Mater. Interfaces*, 2013, **5**, 5856–5860.
77 K. Paek, H. Yang, J. Lee, J. Park and B. J. Kim, *ACS Nano*, 2014, **8**, 2848–2856.
78 Z. Yang, W. Qin, J. W. Y. Lam, S. Chen, H. H. Y. Sung, I. D. Williams and B. Z. Tang, *Chem. Sci.*, 2013, **4**, 3725–3730.
79 Y. Tan, J. Yu, J. Gao, Y. Cui, Z. Wang, Y. Yang and G. Qian, *RSC Adv.*, 2013, **3**, 4872–4875.
80 M. Su, Y. Liu, H. Ma, Q. Ma, Z. Wang, J. Yang and M. Wang, *Chem. Commun.*, 2001, 960–961.
81 H.-H. Lin, S.-Y. Su and C.-C. Chang, *Org. Biomol. Chem.*, 2009, **7**, 2036–2039.
82 V. K. Bhardwaj, H. Sharma, N. Kaur and N. Singh, *New J. Chem.*, 2013, **37**, 4192–4198.
83 A. Singh, S. Kaur, N. Singh and N. Kaur, *Org. Biomol. Chem.*, 2014, **12**, 2302–2309.
84 Y.-L. Yang, Y.-W. Wang, D.-Z. Duan, A.-J. Zhang, J.-G. Fang and Y. Peng, *Org. Biomol. Chem.*, 2013, **11**, 6960–6966.
85 J. Y. Noh, G. J. Park, Y. J. Na, H. Y. Jo, S. A. Lee and C. Kim, *Dalton Trans.*, 2014, **43**, 5652–5656.
86 L. Yin, C. He, C. Huang, W. Zhu, X. Wang, Y. Xu and X. Qian, *Chem. Commun.*, 2012, **48**, 4486–4488.
87 S. Uchiyama and Y. Makino, *Chem. Commun.*, 2009, 2646–2648.
88 J. Li, C. Ji, W. Yang and M. Yin, *Analyst*, 2013, **138**, 7289–7293.
89 X. Chen, X. Cheng and J. J. Gooding, *Analyst*, 2012, **137**, 2338–2343.
90 Y. M. Poronik, G. Clermont, M. Blanchard-Desce and D. T. Gryko, *J. Org. Chem.*, 2013, **78**, 11721–11732.
91 T. Gunnlaugsson, M. Nieuwenhuyzen, L. Richard and V. Thoss, *J. Chem. Soc., Perkin Trans. 2*, 2002, 141–150.
92 T. Gunnlaugsson and J. P. Leonard, *J. Chem. Soc., Perkin Trans. 2*, 2002, 1980–1985.
93 A. T. Harootunian, J. P. Kao, B. K. Eckert and R. Y. Tsien, *J. Biol. Chem.*, 1989, **264**, 19458–19467.
94 T. Gunnlaugsson, H. Q. N. Gunaratne, M. Nieuwenhuyzen and J. P. Leonard, *J. Chem. Soc., Perkin Trans. 1*, 2002, 1954–1962.
95 L. L. del Mercato, A. Z. Abbasi, M. Ochs and W. J. Parak, *ACS Nano*, 2011, **5**, 9668–9674.
96 H. He, M. A. Mortellaro, M. J. P. Leiner, S. T. Young, R. J. Fraatz and J. K. Tusa, *Anal. Chem.*, 2002, **75**, 549–555.
97 J. M. Dubach, D. I. Harjes and H. A. Clark, *J. Am. Chem. Soc.*, 2007, **129**, 8418–8419.
98 J. Kim, D. T. McQuade, S. K. McHugh and T. M. Swager, *Angew. Chem., Int. Ed.*, 2000, **39**, 3868–3872.
99 A. P. de Silva, H. Q. Nimal Gunaratne and K. R. A. Samankumara Sandanayake, *Tetrahedron Lett.*, 1990, **31**, 5193–5196.
100 S. Nagatoishi, T. Nojima, B. Juskowiak and S. Takenaka, *Angew. Chem., Int. Ed.*, 2005, **44**, 5067–5070.
101 E. A. Weitz and V. C. Pierre, *Chem. Commun.*, 2011, **47**, 541–543.
102 H.-C. Kuo, C.-F. Cheng, R. B. Clark, J. J. C. Lin, J. L. C. Lin, M. Hoshijima, V. T. B. Nguyên-Trân, Y. Gu, Y. Ikeda, P.-H. Chu, J. Ross Jr, W. R. Giles and K. R. Chien, *Cell*, 2001, **107**, 801–813.
103 S.-Y. Lin, S.-W. Liu, C.-M. Lin and C.-h. Chen, *Anal. Chem.*, 2001, **74**, 330–335.
104 C.-Y. Chen, C.-T. Cheng, C.-W. Lai, P.-W. Wu, K.-C. Wu, P.-T. Chou, Y.-H. Chou and H.-T. Chiu, *Chem. Commun.*, 2006, 263–265.
105 C.-C. Huang and H.-T. Chang, *Chem. Commun.*, 2008, 1461–1463.
106 H. Ueyama, M. Takagi and S. Takenaka, *J. Am. Chem. Soc.*, 2002, **124**, 14286–14287.
107 H. He, M. A. Mortellaro, M. J. P. Leiner, R. J. Fraatz and J. K. Tusa, *J. Am. Chem. Soc.*, 2003, **125**, 1468–1469.
108 F. He, Y. Tang, S. Wang, Y. Li and D. Zhu, *J. Am. Chem. Soc.*, 2005, **127**, 12343–12346.
109 F. I. Wolf, A. Torsello, S. Fasanella and A. Cittadini, *Mol. Aspects Med.*, 2003, **24**, 11–26.
110 V. Trapani, G. Farruggia, C. Marraccini, S. Iotti, A. Cittadini and F. I. Wolf, *Analyst*, 2010, **135**, 1855–1866.
111 F. I. Wolf and V. Trapani, *Clin. Sci.*, 2008, **114**, 27–35.
112 M. J. S. Nadler, M. C. Hermosura, K. Inabe, A.-L. Perraud, Q. Zhu, A. J. Stokes, T. Kurosaki, J.-P. Kinet, R. Penner, A. M. Scharenberg and A. Fleig, *Nature*, 2001, **411**, 590–595.
113 R. Y. Walder, B. Yang, J. B. Stokes, P. A. Kirby, X. Cao, P. Shi, C. C. Searby, R. F. Husted and V. C. Sheffield, *Hum. Mol. Genet.*, 2009, **18**, 4367–4375.
114 M. Piskacek, L. Zotova, G. Zsurka and R. J. Schweyen, *J. Cell. Mol. Med.*, 2009, **13**, 693–700.
115 H. M. Kim, P. R. Yang, M. S. Seo, J.-S. Yi, J. H. Hong, S.-J. Jeon, Y.-G. Ko, K. J. Lee and B. R. Cho, *J. Org. Chem.*, 2007, **72**, 2088–2096.

Published on 14 April 2016. Downloaded by Fail Open on 7/23/2025 9:06:09 AM.

116 G. Farruggia, S. Lotti, M. Montalti, N. Zaccheroni, P. B. Savage, V. Trapani, P. Sale and F. Wolf, *J. Am. Chem. Soc.*, 2006, **128**, 344.
117 Y. Suzuki, H. Komatsu, T. Ikeda, N. Saito, S. Araki, D. Citterio, H. Hisamoto, Y. Kitamura, T. Kubota, J. Nakagawa, K. Oka and K. Suzuki, *Anal. Chem.*, 2002, **74**, 1423–1428.
118 H. Komatsu, N. Iwasawa, D. Citterio, Y. Suzuki, T. Kubota, K. Tokuno, Y. Kitamura, K. Oka and K. Suzuki, *J. Am. Chem. Soc.*, 2004, **126**, 16353–16360.
119 M. Brini, T. Calì, D. Ottolini and E. Carafoli, in *Metallomics and the Cell*, ed. L. Banci, Springer Netherlands, 2013, vol. 12, pp. 119–168.
120 M. Brini, D. Ottolini, T. Calì and E. Carafoli, in *Interrelations between Essential Metal Ions and Human Diseases*, ed. A. Sigel, H. Sigel and R. K. O. Sigel, Springer Netherlands, 2013, vol. 13, pp. 81–137.
121 T. P. Jacobs and J. P. Bilezikian, *J. Clin. Endocrinol. Metab.*, 2005, **90**, 6316–6322.
122 J. H. Jeong and E. H. Bae, *Electrolyte Blood Pressure*, 2010, **8**, 92–94.
123 D. Liu, J. Qi, Z. Yu, X. Liu, R. Yang, H. Yang, H. Chang, H. He and G. Yang, *Anal. Methods*, 2014, **6**, 3555–3559.
124 H. He, K. Jenkins and C. Lin, *Anal. Chim. Acta*, 2008, **611**, 197–204.
125 S. Kim, J. W. Park, D. Kim, D. Kim, I.-H. Lee and S. Jon, *Angew. Chem., Int. Ed.*, 2009, **48**, 4138–4141.
126 G. Grynkiewicz, M. Poenie and R. Y. Tsien, *J. Biol. Chem.*, 1985, **260**, 3440–3450.
127 N. R. Bishnoi, R. Kumar, S. Kumar and S. Rani, *J. Hazard. Mater.*, 2007, **145**, 142–147.
128 D. G. Barceloux and D. Barceloux, *Clin. Toxicol.*, 1999, **37**, 173–194.
129 A. Levina and P. A. Lay, *Chem. Res. Toxicol.*, 2008, **21**, 563–571.
130 D. A. Eastmond, J. T. MacGregor and R. S. Slesinski, *Crit. Rev. Toxicol.*, 2008, **38**, 173–190.
131 S. A. Katz and H. Salem, *J. Appl. Toxicol.*, 1993, **13**, 217–224.
132 M. Elavarasi, M. L. Paul, A. Rajeshwari, N. Chandrasekaran, A. B. Mandal and A. Mukherjee, *Anal. Methods*, 2012, **4**, 3407–3412.
133 S. Saha, M. U. Chhatbar, P. Mahato, L. Praveen, A. K. Siddhanta and A. Das, *Chem. Commun.*, 2012, **48**, 1659–1661.
134 J. Mao, L. Wang, W. Dou, X. Tang, Y. Yan and W. Liu, *Org. Lett.*, 2007, **9**, 4567–4570.
135 E. M, R. A, N. Chandrasekaran and A. Mukherjee, *Anal. Methods*, 2013, **5**, 6211–6218.
136 M. Elavarasi, A. Rajeshwari, S. A. Alex, D. Nanda Kumar, N. Chandrasekaran and A. Mukherjee, *Anal. Methods*, 2014, **6**, 5161–5167.
137 J. D. Haas and T. Brownlie, *J. Nutr.*, 2001, **131**, 676S–690S.
138 J. Burdo and J. Connor, *BioMetals*, 2003, **16**, 63–75.
139 D. J. Bonda, H.-g. Lee, J. A. Blair, X. Zhu, G. Perry and M. A. Smith, *Metallomics*, 2011, **3**, 267–270.
140 A. S. Pithadia and M. H. Lim, *Curr. Opin. Chem. Biol.*, 2012, **16**, 67–73.
141 S.-P. Wu, Y.-P. Chen and Y.-M. Sung, *Analyst*, 2011, **136**, 1887–1891.
142 K. B. Kim, H. Kim, E. J. Song, S. Kim, I. Noh and C. Kim, *Dalton Trans.*, 2013, **42**, 16569–16577.
143 A. K. Dwivedi, G. Saikia and P. K. Iyer, *J. Mater. Chem.*, 2011, **21**, 2502–2507.
144 T. Raj, P. Saluja and N. Singh, *Sens. Actuators, B*, 2015, **206**, 98–106.
145 S.-R. Liu and S.-P. Wu, *Sens. Actuators, B*, 2012, **171–172**, 1110–1116.
146 G. C. Midya, S. Paladhi, S. Bhowmik, S. Saha and J. Dash, *Org. Biomol. Chem.*, 2013, **11**, 3057–3063.
147 P. Wu, Y. Li and X.-P. Yan, *Anal. Chem.*, 2009, **81**, 6252–6257.
148 C.-Y. Tsai and Y.-W. Lin, *Analyst*, 2013, **138**, 1232–1238.
149 D. Maity and T. Govindaraju, *Inorg. Chem.*, 2011, **50**, 11282–11284.
150 C.-Y. Li, X.-B. Zhang, Z. Jin, R. Han, G.-L. Shen and R.-Q. Yu, *Anal. Chim. Acta*, 2006, **580**, 143–148.
151 Y. Leng, F. Zhang, Y. Zhang, X. Fu, Y. Weng, L. Chen and A. Wu, *Talanta*, 2012, **94**, 271–277.
152 J. Shi, C. Lu, D. Yan and L. Ma, *Biosens. Bioelectron.*, 2013, **45**, 58–64.
153 H.-Y. Luo, X.-B. Zhang, C.-L. He, G.-L. Shen and R.-Q. Yu, *Spectrochim. Acta, Part A*, 2008, **70**, 337–342.
154 G. J. Park, Y. J. Na, H. Y. Jo, S. A. Lee and C. Kim, *Dalton Trans.*, 2014, **43**, 6618–6622.
155 L. Ding, S. Wang, Y. Liu, J. Cao and Y. Fang, *J. Mater. Chem. A*, 2013, **1**, 8866–8875.
156 M. Iniya, D. Jeyanthi, K. Krishnaveni and D. Chellappa, *RSC Adv.*, 2014, **4**, 25393–25397.
157 P. T. Chivers and R. T. Sauer, *Protein Sci.*, 1999, **8**, 2494–2500.
158 N. S. Dosanjh and S. L. J. Michel, *Curr. Opin. Chem. Biol.*, 2006, **10**, 123–130.
159 D. P. Giedroc and A. I. Arunkumar, *Dalton Trans.*, 2007, 3107–3120.
160 M. Costa, T. L. Davidson, H. Chen, Q. Ke, P. Zhang, Y. Yan, C. Huang and T. Kluz, *Mutat. Res., Fundam. Mol. Mech. Mutagen.*, 2005, **592**, 79–88.
161 A. A. Nemec, G. D. Leikauf, B. R. Pitt, K. J. Wasserloos and A. Barchowsky, *Am. J. Respir. Cell Mol. Biol.*, 2009, **41**, 69–75.
162 F. A. Abebe, C. S. Eribal, G. Ramakrishna and E. Sinn, *Tetrahedron Lett.*, 2011, **52**, 5554–5558.
163 H. Li, Z. Cui and C. Han, *Sens. Actuators, B*, 2009, **143**, 87–92.
164 B. Wang, Y. Hu and Z. Su, *React. Funct. Polym.*, 2008, **68**, 1137–1143.
165 S. C. Dodani, Q. He and C. J. Chang, *J. Am. Chem. Soc.*, 2009, **131**, 18020–18021.
166 E. L. Que, D. W. Domaille and C. J. Chang, *Chem. Rev.*, 2008, **108**, 1517–1549.
167 R. Uauy, M. Olivares and M. Gonzalez, *Am. J. Clin. Nutr.*, 1998, **67**, 952S–959S.
168 E. Gaggelli, H. Kozlowski, D. Valensin and G. Valensin, *Chem. Rev.*, 2006, **106**, 1995–2044.

 This journal is © The Royal Society of Chemistry 2016

Published on 14 April 2016. Downloaded by Fail Open on 7/23/2025 9:06:09 AM.

169 G. L. Millhauser, *Acc. Chem. Res.*, 2004, **37**, 79–85.
170 B.-E. Kim, T. Nevitt and D. J. Thiele, *Nat. Chem. Biol.*, 2008, **4**, 176–185.
171 Y. Fu, Q.-C. Feng, X.-J. Jiang, H. Xu, M. Li and S.-Q. Zang, *Dalton Trans.*, 2014, **43**, 5815–5822.
172 L. Hao, H. Song, Y. Su and Y. Lv, *Analyst*, 2014, **139**, 764–770.
173 L. Liu, X. Dong, Y. Xiao, W. Lian and Z. Liu, *Analyst*, 2011, **136**, 2139–2145.
174 Z. Lin, F. Luo, T. Dong, L. Zheng, Y. Wang, Y. Chi and G. Chen, *Analyst*, 2012, **137**, 2394–2399.
175 B. N. Ahamed and P. Ghosh, *Dalton Trans.*, 2011, **40**, 6411–6419.
176 M. Li, Q. Liang, M. Zheng, C. Fang, S. Peng and M. Zhao, *Dalton Trans.*, 2013, **42**, 13509–13515.
177 C. Yu, L. Chen, J. Zhang, J. Li, P. Liu, W. Wang and B. Yan, *Talanta*, 2011, **85**, 1627–1633.
178 P. Jiang and Z. Guo, *Coord. Chem. Rev.*, 2004, **248**, 205–229.
179 W. Maret, C. Jacob, B. L. Vallee and E. H. Fischer, *Proc. Natl. Acad. Sci. U. S. A.*, 1999, **96**, 1936–1940.
180 V. Snitsarev, T. Budde, T. P. Stricker, J. M. Cox, D. J. Krupa, L. Geng and A. R. Kay, *Biophys. J.*, 2001, **80**, 1538–1546.
181 A. I. Bush, *Curr. Opin. Chem.Biol.*, 2000, **4**, 184–191.
182 A. I. Bush, *Trends Neurosci.*, 2003, **26**, 207–214.
183 A. Bush, W. Pettingell, G. Multhaup, M. d Paradis, J. Vonsattel, J. Gusella, K. Beyreuther, C. Masters and R. Tanzi, *Science*, 1994, **265**, 1464–1467.
184 M. Chen, X. Lv, Y. Liu, Y. Zhao, J. Liu, P. Wang and W. Guo, *Org. Biomol. Chem.*, 2011, **9**, 2345–2349.
185 P. Saluja, V. K. Bhardwaj, T. Pandiyan, S. Kaur, N. Kaur and N. Singh, *RSC Adv.*, 2014, **4**, 9784–9790.
186 Y. Zhou, Z.-X. Li, S.-Q. Zang, Y.-Y. Zhu, H.-Y. Zhang, H.-W. Hou and T. C. W. Mak, *Org. Lett.*, 2012, **14**, 1214–1217.
187 K. B. Holt and A. J. Bard, *Biochemistry*, 2005, **44**, 13214–13223.
188 S. Y. Liau, D. C. Read, W. J. Pugh, J. R. Furr and A. D. Russell, *Lett. Appl. Microbiol.*, 1997, **25**, 279–283.
189 S. P. Valappil, D. M. Pickup, D. L. Carroll, C. K. Hope, J. Pratten, R. J. Newport, M. E. Smith, M. Wilson and J. C. Knowles, *Antimicrob. Agents Chemother.*, 2007, **51**, 4453–4461.
190 I. Sondi and B. Salopek-Sondi, *J. Colloid Interface Sci.*, 2004, **275**, 177–182.
191 A. Melaiye, Z. Sun, K. Hindi, A. Milsted, D. Ely, D. H. Reneker, C. A. Tessier and W. J. Youngs, *J. Am. Chem. Soc.*, 2005, **127**, 2285–2291.
192 B. S. Atiyeh, M. Costagliola, S. N. Hayek and S. A. Dibo, *Burns*, 2007, **33**, 139–148.
193 J. Hatai, S. Pal and S. Bandyopadhyay, *RSC Adv.*, 2012, **2**, 10941–10947.
194 C. Qin, W.-Y. Wong and L. Wang, *Macromolecules*, 2010, **44**, 483–489.
195 S. Iyoshi, M. Taki and Y. Yamamoto, *Inorg. Chem.*, 2008, **47**, 3946–3948.
196 Y.-H. Lin and W.-L. Tseng, *Chem. Commun.*, 2009, 6619–6621.
197 F. Beck and P. Rüetschi, *Electrochim. Acta*, 2000, **45**, 2467–2482.
198 C. J. Rydh and B. Svärd, *Sci. Total Environ.*, 2003, **302**, 167–184.
199 M. D. Taylor, *Sci. Total Environ.*, 1997, **208**, 123–126.
200 A. S. Amin and A. A. Gouda, *Food Chem.*, 2012, **132**, 518–524.
201 W. Wang, Q. Wen, Y. Zhang, X. Fei, Y. Li, Q. Yang and X. Xu, *Dalton Trans.*, 2013, **42**, 1827–1833.
202 S. K. Kim, J. H. Lee and J. Yoon, *Bull. Korean Chem. Soc.*, 2003, **24**, 1032–1034.
203 H. Tian, B. Li, J. Zhu, H. Wang, Y. Li, J. Xu, J. Wang, W. Wang, Z. Sun, W. Liu, X. Huang, X. Yan, Q. Wang, X. Yao and Y. Tang, *Dalton Trans.*, 2012, **41**, 2060–2065.
204 T. Gunnlaugsson, T. C. Lee and R. Parkesh, *Org. Lett.*, 2003, **5**, 4065–4068.
205 A. Renzoni, F. Zino and E. Franchi, *Environ. Res.*, 1998, **77**, 68–72.
206 M. Suresh, S. Mishra, S. K. Mishra, E. Suresh, A. K. Mandal, A. Shrivastav and A. Das, *Org. Lett.*, 2009, **11**, 2740–2743.
207 H. H. Harris, I. J. Pickering and G. N. George, *Science*, 2003, **301**, 1203.
208 E. M. Nolan and S. J. Lippard, *Chem. Rev.*, 2008, **108**, 3443–3480.
209 A. Franzblau, H. d'Arcy, M. B. Ishak, R. A. Werner, B. W. Gillespie, J. W. Albers, C. Hamann, S. E. Gruninger, H.-N. Chou and D. M. Meyer, *Neurotoxicology*, 2012, **33**, 299–306.
210 T. Rush, J. Hjelmhaug and D. Lobner, *Neurotoxicology*, 2009, **30**, 47–51.
211 S. Hazra, S. Balaji, M. Banerjee, A. Ganguly, N. N. Ghosh and A. Chatterjee, *Anal. Methods*, 2014, **6**, 3784–3790.
212 B. Liu, F. Zeng, Y. Liu and S. Wu, *Analyst*, 2012, **137**, 1698–1705.
213 B. Liu, F. Zeng, G. Wu and S. Wu, *Analyst*, 2012, **137**, 3717–3724.
214 Y. Li, S. He, Y. Lu and X. Zeng, *Org. Biomol. Chem.*, 2011, **9**, 2606–2609.
215 W. S. Miller, L. Zhuang, J. Bottema, A. J. Wittebrood, P. De Smet, A. Haszler and A. Vieregge, *Mater. Sci. Eng., A*, 2000, **280**, 37–49.
216 R. E. Doherty, *Environ. Forensics*, 2000, **1**, 83–93.
217 E. Altschuler, *Med. Hypotheses*, 1999, **53**, 22–23.
218 L. Tomljenovic, *J. Alzheimer's Dis.*, 2011, **23**, 567–598.
219 C. Exley, *Environ. Sci.: Processes Impacts*, 2013, **15**, 1807–1816.
220 L. Zhi, J. Liu, Y. Wang, W. Zhang, B. Wang, Z. Xu, Z. Yang, X. Huo and G. Li, *Nanoscale*, 2013, **5**, 1552–1556.
221 A. Saini, J. Singh, R. Kaur, N. Singh and N. Kaur, *New J. Chem.*, 2014, **38**, 4580–4586.
222 C. Winder, N. G. Carmichael and P. D. Lewis, *Trends Neurosci.*, 1982, **5**, 207–209.
223 S. Araki, H. Sato, K. Yokoyama and K. Murata, *Am. J. Ind. Med.*, 2000, **37**, 193–204.
224 D. W. Domaille, E. L. Que and C. J. Chang, *Nat. Chem. Biol.*, 2008, **4**, 168–175.
225 R. Turpeinen, J. Salminen and T. Kairesalo, *Environ. Sci. Technol.*, 2000, **34**, 5152–5156.
226 Y. Erel, T. Axelrod, A. Veron, Y. Mahrer, P. Katsafados and U. Dayan, *Environ. Sci. Technol.*, 2002, **36**, 3230–3233.

Published on 14 April 2016. Downloaded by Fail Open on 7/23/2025 9:06:09 AM.

227 H.-R. Xu, K. Li, Q. Liu, T.-M. Wu, M.-Q. Wang, J.-T. Hou, Z. Huang, Y.-M. Xie and X.-Q. Yu, *Analyst*, 2013, **138**, 2329–2334.
228 R. Zhou, B. Li, N. Wu, G. Gao, J. You and J. Lan, *Chem. Commun.*, 2011, **47**, 6668–6670.
229 J. Liu, K. Wu, S. Li, T. Song, Y. Han and X. Li, *Dalton Trans.*, 2013, **42**, 3854–3859.
230 M. Ganguly, J. Jana, C. Mondal, A. Pal and T. Pal, *Phys. Chem. Chem. Phys.*, 2014, **16**, 18185–18197.
231 R. Martínez-Máñez and F. Sancenón, *Chem. Rev.*, 2003, **103**, 4419–4476.
232 P. D. Beer and P. A. Gale, *Angew. Chem., Int. Ed.*, 2001, **40**, 486–516.
233 P. A. Gale, *Coord. Chem. Rev.*, 2001, **213**, 79–128.
234 C. R. Wade, A. E. J. Broomsgrove, S. Aldridge and F. P. Gabbaï, *Chem. Rev.*, 2010, **110**, 3958–3984.
235 F. P. Schmidtchen and M. Berger, *Chem. Rev.*, 1997, **97**, 1609–1646.
236 H. T. Ngo, X. Liu and K. A. Jolliffe, *Chem. Soc. Rev.*, 2012, **41**, 4928–4965.
237 L. E. Santos-Figueroa, M. E. Moragues, E. Climent, A. Agostini, R. Martinez-Manez and F. Sancenon, *Chem. Soc. Rev.*, 2013, **42**, 3489–3613.
238 T. Gunnlaugsson, M. Glynn, G. M. Tocci, P. E. Kruger and F. M. Pfeffer, *Coord. Chem. Rev.*, 2006, **250**, 3094–3117.
239 F. Wurthner, C.-C. You and C. R. Saha-Moller, *Chem. Soc. Rev.*, 2004, **33**, 133–146.
240 L.-Y. Yao, L. Qin, T.-Z. Xie, Y.-Z. Li and S.-Y. Yu, *Inorg. Chem.*, 2011, **50**, 6055–6062.
241 C. R. Bondy, P. A. Gale and S. J. Loeb, *J. Am. Chem. Soc.*, 2004, **126**, 5030–5031.
242 M. H. Lee, D. T. Quang, H. S. Jung, J. Yoon, C. H. Lee and J. S. Kim, *J. Org. Chem.*, 2007, **72**, 4242.
243 J. Zhang, X. Xu, C. Yang, F. Yang and X. Yang, *Anal. Chem.*, 2011, **83**, 3911–3917.
244 J. Zhang, X. Xu and X. Yang, *Analyst*, 2012, **137**, 3437–3440.
245 J. Massue, S. J. Quinn and T. Gunnlaugsson, *J. Am. Chem. Soc.*, 2008, **130**, 6900–6901.
246 R. Kaur, J. Singh, A. Saini, N. Singh and N. Kaur, *RSC Adv.*, 2014, **4**, 48004–48011.
247 R. Kumar, S. Kumar, P. Singh, G. Hundal, M. S. Hundal and S. Kumar, *Analyst*, 2012, **137**, 4913–4916.
248 B. Sen, M. Mukherjee, S. Pal, S. K. Mandal, M. S. Hundal, A. R. Khuda-Bukhsh and P. Chattopadhyay, *RSC Adv.*, 2014, **4**, 15356–15362.
249 R. Saini and S. Kumar, *RSC Adv.*, 2013, **3**, 21856–21862.
250 H. Xie, F. Zeng, C. Yu and S. Wu, *Polym. Chem.*, 2013, **4**, 5416–5424.
251 A. K. Mahapatra, J. Roy, P. Sahoo, S. K. Mukhopadhyay and A. Chattopadhyay, *Org. Biomol. Chem.*, 2012, **10**, 2231–2236.
252 S. Y. Chung, S. W. Nam, J. Lim, S. Park and J. Yoon, *Chem. Commun.*, 2009, 2866–2868.
253 H.-b. Kim, Y. Liu, D. Nam, Y. Li, S. Park, J. Yoon and M. H. Hyun, *Dyes Pigm.*, 2014, **106**, 20–24.
254 A. J. Moro, P. J. Cywinski, S. Korsten and G. J. Mohr, *Chem. Commun.*, 2010, **46**, 1085–1087.
255 P. Mahato, A. Ghosh, S. K. Mishra, A. Shrivastav, S. Mishra and A. Das, *Chem. Commun.*, 2010, **46**, 9134–9136.
256 N. Ahmed, B. Shirinfar, I. S. Youn, A. Bist, V. Suresh and K. S. Kim, *Chem. Commun.*, 2012, **48**, 2662–2664.
257 H. N. Lee, Z. Xu, S. K. Kim, K. M. K. Swamy, Y. Kim, S. J. Kim and J. Yoon, *J. Am. Chem. Soc.*, 2007, **129**, 3828–3829.
258 K. Ghosh, S. S. Ali, A. R. Sarkar, A. Samadder, A. R. Khuda-Bukhsh, I. D. Petsalakis and G. Theodorakopoulos, *Org. Biomol. Chem.*, 2013, **11**, 5666–5672.
259 D. H. Lee, S. Y. Kim and J.-I. Hong, *Angew. Chem., Int. Ed.*, 2004, **43**, 4777–4780.

 This journal is © The Royal Society of Chemistry 2016